MATERIALS CHARACTERIZATION AND ANALYSIS OF THE MARQUETTE INTERCHANGE HMA PERPETUAL PAVEMENT

Project 08-08
August 2008

Midwest Regional University Transportation Center
College of Engineering
Department of Civil and Environmental Engineering
University of Wisconsin, Madison

Authors: James A. Crovetti, Hani Titi, Aaron Coenen, Mohammed Elias R. Christopher Williams & Xinjun Li;
Marquette University, the University of Wisconsin-Milwaukee and Iowa State University

Principal Investigator: James A. Crovetti
Associate Professor, Marquette University

Co-Principal Investigators: Hani Titi & R. Christopher Williams
Associate Professors, University of Wisconsin–Milwaukee & Iowa State University

Technical Report Documentation Page

1. Report No. **MRUTC 08-08**	2. Government Accession No. Aaron Coenen	3. Recipient's Catalog No. **CFDA 20.701**
4. Title and Subtitle Materials Characterization and Analysis of the Marquette Interchange HMA Perpetual Pavement		5. Report Date August, 2008 6. Performing Organization Code
7. Author/s James A. Crovetti, Hani Titi, R. Christopher Williams, Aaron Coenen, Mohammed Elias & Xinjun Li		8. Performing Organization Report No. **MRUTC 08-08**
9. Performing Organization Name and Address **Midwest Regional University Transportation Center** **University of Wisconsin-Madison** **1415 Engineering Drive, Madison, WI 53706**		10. Work Unit No. (TRAIS) 11. Contract or Grant No. **0092-07-13**
12. Sponsoring Organization Name and Address **Wisconsin Department of Transportation** **Hill Farms State Transportation Building** **4802 Sheboygan Avenue** **Madison, WI 53707**		13. Type of Report and Period Covered **Final Report [05//01/07 – 08/31/08]** 14. Sponsoring Agency Code
15. Supplementary Notes **Project completed for the Midwest Regional University Transportation Center with support from the Wisconsin Department of Transportation.**		

16. Abstract

This project focused on the characterization of materials used to construct the Hot Mix Asphalt (HMA) perpetual pavement within the Marquette Interchange and on the analysis of collected pavement response data to investigate the interactions between materials, environment, and traffic loadings. While these pavements are designed for a service life in excess of 50 years, to date there is insufficient field data to confirm this performance expectation. To help bridge this knowledge gap, this study included a mechanistic-empirical appraisal of the HMA perpetual pavement to provide predictions of key performance indicators over a fifty year service period. Laboratory testing was conducted following appropriate AASHTO testing protocols to provided valuable data to characterize the HMA, unbound aggregate and unbound soil pavement layers. This data was used to develop Level 1 HMA inputs to the current version 1.003 of the Mechanistic-Empirical Pavement Design Guide (MEPDG) and to better characterize the unbound aggregates and soils during Level 3 analysis. Weigh-In-Motion (WIM) data obtained as part of WHRP Project 0092-06-01 was analyzed to develop site-specific inputs characterizing the heavy axle loading spectra using this pavement facility.

Pavement performance predictions were developed using the MEPDG v1.003 and stand-alone KENPAVE software. Consideration was given to both free flow (55 mph) and congested (15 mph) traffic conditions. Using a combined traffic approach, pavement distress at the 90% reliability level were projected to 50 years of trafficking. Only top-down fatigue cracking, which should be confined within the uppermost 0.5 inches of the pavement surface, is projected to exceed typical design limits. This projected distress will easily be corrected using the standard practice of mill and relay. Furthermore, after 50 years of service the 90% reliability level for bottom-up fatigue damage is expected over 15% of the total lane area, or 30% of the loaded wheel paths, which is well below typical design limits of 25% and 50%, respectively. All analysis results indicate the constructed HMA perpetual pavement should meet or exceed performance expectations.

17. Key Words HMA Perpetual Pavement, Pavement Instrumentation, Dynamic Modulus, Resilient Modulus, Mechanistic-Empirical Design, Fatigue Analysis, Weigh-In-Motion	18. Distribution Statement **No restrictions. This report is available through the Transportation Research Information Services of the National Transportation Library.**		
19. Security Classification (of this report) **Unclassified**	20. Security Classification (of this page) **Unclassified**	21. No. Of Pages	22. Price **-0-**

Form DOT F 1700.7 (8-72) **Reproduction of form and completed page is authorized.**

SI* (MODERN METRIC) CONVERSION FACTORS

APPROXIMATE CONVERSIONS TO SI UNITS

Symbol	When You Know	Multiply By	To Find	Symbol
	LENGTH			
(none)	mil	25.4	micrometers	µm
in	inches	25.4	millimeters	mm
ft	feet	0.305	meters	m
yd	yards	0.914	meters	m
mi	miles	1.61	kilometers	km
	AREA			
in^2	square inches	645.2	square millimeters	mm^2
ft^2	square feet	0.093	square meters	m^2
yd^2	square yard	0.836	square meters	m^2
ac	acres	0.405	hectares	ha
mi^2	square miles	2.59	square kilometers	km^2
	VOLUME			
fl oz	fluid ounces	29.57	milliliters	mL
gal	gallons	3.785	liters	L
ft^3	cubic feet	0.028	cubic meters	m^3
yd^3	cubic yards	0.765	cubic meters	m^3
NOTE: volumes greater than 1000 shall be shown in m^3				
	MASS			
oz	ounces	28.35	grams	g
lb	pounds	0.454	kilograms	kg
T	short tons (2000 lb)	0.907	megagrams (metric tons)	Mg (or t)
	TEMPERATURE (exact degrees)			
°F	Fahrenheit	5 (F-32)/9 or (F-32)/1.8	Celsius	°C
	ILLUMINATION			
fc	foot-candles	10.76	lux	lx
fl	foot-Lamberts	3.426	candela/m^2	cd/m^2
	FORCE and PRESSURE or STRESS			
lb	pounds	4.45	Newtons	N
lb/in^2 (psi)	pounds per square inch	6.89	kiloPascals	kPa
k/in^2 (ksi)	kips per square inch	6.89	megaPascals	MPa
	DENSITY			
lb/ft^3 (pcf)	pounds per cubic foot	16.02	kilograms per cubic meter	kg/m^3

APPROXIMATE CONVERSIONS FROM SI UNITS

Symbol	When You Know	Multiply By	To Find	Symbol
	LENGTH			
µm	micrometers	0.039	mil	(none)
mm	millimeters	0.039	inches	in
m	meters	3.28	feet	ft
m	meters	1.09	yards	yd
km	kilometers	0.621	miles	mi
	AREA			
mm^2	square millimeters	0.0016	square inches	in^2
m^2	square meters	10.764	square feet	ft^2
m^2	square meters	1.195	square yards	yd^2
ha	hectares	2.47	acres	ac
km^2	square kilometers	0.386	square miles	mi^2
	VOLUME			
mL	milliliters	0.034	fluid ounces	fl oz
L	liters	0.264	gallons	gal
m^3	cubic meters	35.71	cubic feet	ft^3
m^3	cubic meters	1.307	cubic yards	yd^3
	MASS			
g	grams	0.035	ounces	oz
kg	kilograms	2.202	pounds	lb
Mg (or t)	megagrams (metric tons)	1.103	short tons (2000 lb)	T
	TEMPERATURE (exact degrees)			
°C	Celsius	1.8C+32	Fahrenheit	°F
	ILLUMINATION			
lx	lux	0.0929	foot-candles	fc
cd/m^2	candela/m^2	0.2919	foot-Lamberts	fl
	FORCE and PRESSURE or STRESS			
N	Newtons	0.225	pounds	lb
kPa	kiloPascals	0.145	pounds per square inch	lb/in^2 (psi)
MPa	megaPascals	0.145	kips per square inch	k/in^2 (ksi)
	DENSITY			
kg/m^3	pounds per cubic foot	0.062	kilograms per cubic meter	lb/ft^3 (pcf)

*SI is the symbol for the International System of Units. Appropriate rounding should be made to comply with Section 4 of ASTM E380. (Revised September 1993)

DISCLAIMER

This research was funded by the Midwest Regional University Transportation Center. The contents of this report reflect the views of the authors, who are responsible for the facts and the accuracy of the information presented herein. This document is disseminated under the sponsorship of the Department of Transportation, University Transportation Centers Program, in the interest of information exchange. The U.S. Government assumes no liability for the contents or use thereof. The contents do not necessarily reflect the official views of the Midwest Regional University Transportation Center, the University of Wisconsin, the Wisconsin Department of Transportation, or the USDOT's RITA at the time of publication.

The United States Government assumes no liability for its contents or use thereof. This report does not constitute a standard, specification, or regulation.

The United States Government does not endorse products or manufacturers. Trade and manufacturers names appear in this report only because they are considered essential to the object of the document.

ACKNOWLEDGEMENTS

This research was performed under MRUTC 08-08 by Marquette University Transportation Research Center (MU-TRC – prime contractor), in association with the University of Wisconsin-Milwaukee (UW-M) and Iowa State University (ISU). Dr. James Crovetti (MU-TRC) was the principal investigator and Dr. Hani Titi (UW-M) and Dr. R. Christopher Williams (ISU) were the co-principal investigators. The coauthors of this report were Mr. Aaron Coenen and Mohammed Elias (UW-M), and Mr. Xinjun Li (ISU).

We are grateful to the Midwest Regional University Transportation Center (MRUTC) at the University of Wisconsin--Madison for generously taking the lead in providing funding for this project. The work would not have been possible without a grant from MRUTC. We would like to thank our project oversight committee who assisted us and gave us feedback:

Wesley Shemwell, *Federal Highway Administration*
Leonard Makowski, *Wisconsin Department of Transportation*
Deborah Schwerman, *Wisconsin Department of Transportation*
Judith Ryan, *Wisconsin Department of Transportation*
Thomas Brokaw, *Wisconsin Department of Transportation*
Irene Battaglia, *Wisconsin Department of Transportation*
Signe Richelt, *Payne & Dolan, Inc.*
Ervin Dukatz, *Mathy Construction*
Ceci Pieroni, *CH2M Hill, Inc.*
Scot Schwandt, *Wisconsin Asphalt Pavement Association*
Robert Schmitt, *University of Wisconsin-Platteville*

EXECUTIVE SUMMARY

Project Summary

This project focused on the characterization of materials used to construct the Hot Mix Asphalt (HMA) perpetual pavement within the Marquette Interchange and on the analysis of collected pavement response data to investigate the interactions between materials, environment, and traffic loadings. HMA perpetual pavements are relatively new in Wisconsin. While these pavements are designed for a service life in excess of 50 years, to date there is insufficient field data to confirm this performance expectation. To help bridge this knowledge gap, this study included a mechanistic-empirical appraisal of the HMA perpetual pavement to provide predictions of key performance indicators over a fifty year service period.

Background

The design and construction of long-life pavements is gaining momentum across the United States as limited owner/agency budgets are facilitating longer lasting highways systems. The HMA perpetual pavement design concept provides an improved opportunity for asset management as this design represents an enhanced life-cycle cost basis over traditional pavement designs. The Wisconsin Department of Transportation (WisDOT) recently constructed their first mainline HMA perpetual pavement in the highly urbanized area of Milwaukee. The HMA perpetual pavement is located along Interstate 43, commonly referenced as the North Leg of the Marquette Interchange reconstruction project. Concurrent with the construction of this HMA perpetual pavement was a highly advanced instrumentation of the pavement system collecting climatic, loading characteristics, and loading responses. The instrumentation, combined with laboratory characterization of materials used to construct this HMA perpetual pavement, represents a unique opportunity to evaluate the newly completed Mechanistic-Empirical Pavement Design Guide and provide insight for local calibration of the guide to Wisconsin conditions. This project serves as a supplement to Wisconsin Highway Research Program (WHRP) Study 0092-06-01 *Perpetual Pavement Instrumentation for the Marquette Interchange Project*.

Process

The objectives of this study are to characterize the materials used to construct the HMA perpetual pavement and to analyze the collected pavement response data to investigate the interactions between materials, environment, and traffic loadings. Dynamic and resilient modulus testing was conducted at Iowa State University and the University of Wisconsin-Milwaukee, respectively, using construction materials obtained during paving operations. Key personnel from WisDOT and Payne & Dolan, Inc. provided invaluable support during materials sampling and subsequent storage.

The lab testing was conducted following appropriate AASHTO testing protocols and provided valuable data to characterize the HMA, unbound aggregate and unbound soil pavement layers. This data was used to develop Level 1 HMA inputs to the current version 1.003 of the Mechanistic-Empirical Pavement Design Guide (MEPDG) and to better characterize the unbound aggregates and soils during Level 3 analysis. Weigh-In-Motion (WIM) data obtained as part of WHRP Project 0092-06-01 was analyzed to develop site-specific inputs characterizing the heavy axle loading spectra using this pavement facility.

Findings and Conclusions

Pavement performance predictions were developed using the MEPDG v1.003 and stand-alone KENPAVE software. For both analyses, the baseline material properties determined via laboratory testing were used to estimate monthly variations in response to changes in environmental conditions (i.e., temperature, moisture). Critical pavement stresses and strains resulting from applied traffic loadings were used to develop estimates of accumulated cracking, rutting and roughness over time. Consideration was given to both free flow (55 mph) and congested (15 mph) traffic conditions. Using a combined traffic approach, pavement distress at the 90% reliability level were projected after 16 and 22 years of trafficking as follows:

Pavement Distress 90% Reliability Level	At End of Year 16	At End of Year 22	Design Limit
Heavy Truck Applications	26.4 million	36.8 million	n.a.
Top-Down Fatigue Cracking, ft/mi	1,058	1,199	1,000
Bottom-Up Fatigue Cracking, % Area	2.3	2.8	25
Thermal Cracking ft/mi	84.5	84.5	1,000
Total Rutting, in	0.45	0.48	0.50
IRI, in/mi	138	157	175

The predicted distress levels after 16 and 22 years of trafficking were selected to coincide with the typical initial service life expectations for HMA perpetual pavements in Wisconsin. As shown, only top-down fatigue cracking, which is confined within the uppermost 0.5 inches of the pavement surface, is projected to exceed typical design limits. This projected distress will easily be corrected using the standard practice of mill and relay. Furthermore, after 50 years of service the 90% reliability level for bottom-up fatigue damage is expected over 15% of the total lane area, or 30% of the loaded wheel paths, which is well below typical design limits of 25% and 50%, respectively. All analysis results indicate the constructed HMA perpetual pavement should meet or exceed performance expectations.

Recommendations for Further Action

The pavement analyses conducted for the Marquette Interchange HMA perpetual pavement, using the MEPDG v.1003 and KENPAVE programs, yielded acceptable long-term performance expectations. This pavement was constructed in September, 2006 and to date, there is insufficient field performance data available to confirm or deny these expectations (i.e., no pavement distress measured to date). To augment these results, it is recommended that the monitoring of pavement performance be continued through at least the first 10 years to provide comparative values of measured versus predicted pavement distress. This will provide valuable data for calibrating mechanistic-empirical performance models for local conditions.

Furthermore, analyses of this type should be extended to existing aged HMA pavement structures in Wisconsin, preferably built using paving materials and construction practices which reflect current conditions. For practical applications, this will likely include pavements constructed from 1996 – 2002. Comparative analyses between the field performance data of these pavements to MEPDG predicted levels of distress will further validate the use of the MEPDG for designing HMA pavements in Wisconsin.

This page intentionally left blank

TABLE OF CONTENTS

TABLE OF CONTENTS (Cont.)

LIST OF FIGURES

LIST OF FIGURES (Cont.)

LIST OF TABLES

LIST OF TABLES (Cont.)

CHAPTER 1.0
INTRODUCTION

The design and construction of long-life pavements is gaining momentum across the United States as limited owner/agency budgets are facilitating longer lasting highways systems. The Hot Mix asphalt (HMA) perpetual pavement design concept provides an improved opportunity for asset management as this design represents an improved "life" cycle cost basis over traditional pavement designs. The Wisconsin Department of Transportation (WisDOT) recently constructed their first mainline HMA perpetual pavement in the highly urbanized area of Milwaukee. The HMA perpetual pavement is located along the North Leg of the Marquette Interchange reconstruction project. Concurrent with the construction of this HMA perpetual pavement was a highly advanced instrumentation of the pavement system collecting climatic, loading characteristics, and loading responses. The instrumentation combined with additional characterization of materials used to construct this HMA perpetual pavement represents a unique opportunity to evaluate the newly completed Mechanistic-Empirical Pavement Design Guide (MEPDG) and provide insight for local calibration of the guide to Wisconsin conditions.

1.1 Research Objectives

The objectives of this study are to characterize the materials used to construct the HMA perpetual pavement and to analyze the collected pavement response data to investigate the interactions between materials, environment, and traffic loadings. This study included an examination of the predictive equations and sub-routines which are part of the mechanistic-empirical design procedures developed under NCHRP Project 1-37A and 1-40D to determine how well these reflect the actual response measures. The conclusions of this study provide guidance for WisDOT as it performs mechanistic empirical pavement designs which are validated for local conditions.

The MEPDG software analysis provides insight into the expected pavement performance as quantified by the accumulation of pavement distress and surface roughness. The MEPDG utilizes state-of-the-practice mechanistic-based pavement analysis and distress prediction algorithms. The distress prediction models were developed based on the field performance of in-service pavements located throughout the United States and monitored as part of the Long Term Pavement Performance (LTPP) project.

The MEPDG integrates climate conditions and material properties of all paving materials and uses mechanistic principles to compute critical pavement responses to applied traffic loads. The critical responses are then used to compute accumulated damage based on Miner's hypothesis. The MEPDG software may be used for the analysis of new or reconstructed HMA pavements, jointed concrete pavements, and continuously reinforced concrete pavements as well as for pavement rehabilitations with HMA or concrete overlays.

This project focused on the analysis of one particular HMA perpetual pavement in Wisconsin. Research is also being conducted by WisDOT under Project # 1009-03-35 to develop a catalogue of inputs to MEPDG software which are specific to conditions, materials and construction practices used throughout the State of Wisconsin.

1.2 Report Organization

This report is divided into four chapters. Following this introductory chapter is a presentation of the laboratory testing conducted at Iowa State University and the University of Wisconsin-Milwaukee in chapter 2.

Chapter 3 presents an analysis of the HMA perpetual pavement using both the current version of the mechanistic-empirical pavement design guide and stand-alone software programs KENLAYER and EVERSTRESS. Chapter 4 presents a summary of the findings and recommendations for future work.

CHAPTER 2.0
LABORATORY TESTING

2.1 Introduction

Laboratory testing was conducted at Iowa State University and the University of Wisconsin-Milwaukee using paving materials which were sampled and stored during construction. Bulk samples of each material layer were obtained at the production sites and subsequently stored at the Wisconsin Department of Transportation Southeast Region facilities prior to testing. Figure 2.1 provides an illustration of the HMA perpetual pavement cross section used within the Marquette Interchange.

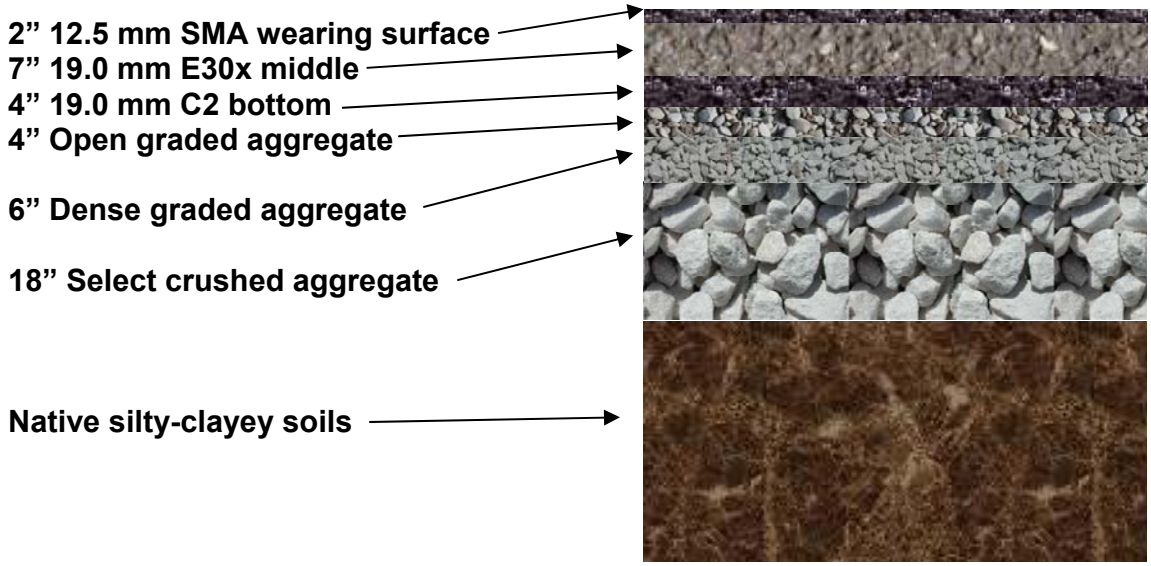

Figure 2.1 HMA Perpetual Pavement Structure

The primary focus of the laboratory testing was the development of material characterization inputs for the mechanistic-empirical appraisal of projected pavement performance. In some cases, these inputs are direct outputs of laboratory tests while in others, further analysis of the laboratory test data is necessary to developed the needed input values.

2.2 HMA Dynamic Modulus Testing

2.2.1. Sample Preparation

Cylindrical hot mixed asphalt (HMA) specimens 100-mm by 150-mm were compacted in the Iowa State laboratory using a Pine gyratory compactor. Adjustments were made to the number of gyrations during laboratory compaction to achieve the designated air voids, which were targeted to average compacted values measured by the paving contractor using a nuclear gauge. This sample preparation procedure was followed to prepare five samples for each of the three HMA mixtures used for paving within the Marquette Interchange. Table 2.1 summarizes the parameters obtained during laboratory sample preparation, including compaction temperature, number of gyrations, air voids and height of the specimens.

Table 2.1. Sample Preparation Data

Sample ID	Compact Temp, °C	Number of Gyrations	Air voids, %	Height, Mm
C2-1	145	27	5.73	149.1
C2-2	145	22	6.42	149.3
C2-3	145	21	6.02	149.0
C2-5	145	23	5.99	149.1
C2-6	145	23	6.80	149.0
E30x-1	145	42	7.53	149.0
E30x-2	145	57	6.95	148.9
E30x-3	145	46	6.85	149.1
E30x-4	145	48	6.96	149.7
E30x-5	145	52	7.40	149.1
SMA-1	145	41	11.91	148.8
SMA-2	145	29	11.61	148.9
SMA-3	145	42	11.01	148.8
SMA-4	145	35	11.74	148.8
SMA-5	145	38	11.74	148.9

2.2.2 Testing Equipment

All tests were performed on a Cooper servo-hydraulic testing system. Flat, circular load platens were used to apply the cyclic compressive load to the specimens. The vertical deformation measurements were obtained using four Cooper extensometers with a 100-mm gage length. They were attached to specimens by aluminum buttons which were glued on the specimen's surface using epoxy glue. One average strain measurement was obtained from the four extensometers and this average strain was then used to control the testing. The test setup is shown in Figure 2.2.

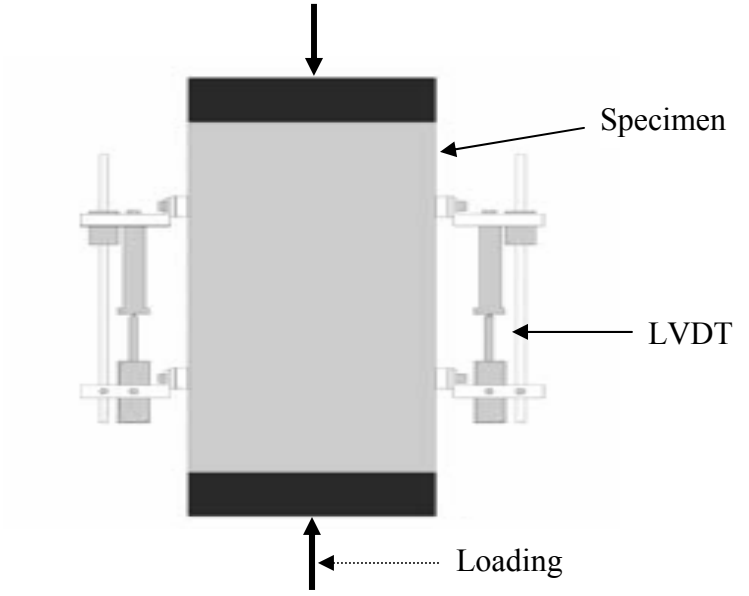

Figure 2.2 Dynamic Modulus Test Setup (NCHRP Report 547)

All tests were performed inside an environmental chamber. Mechanical cooling and heating was used for the test temperatures. The temperature was controlled by a temperature controller and verified using an independent platinum thermometer.

2.2.3 Testing Procedures

The testing procedure was based on AASHTO TP 62: *Standard Method of Test for Determining Dynamic Modulus of Hot-Mix Asphalt Concrete Mixtures* [1]. The procedure describes performing tests at several different temperatures and loading frequencies. Tests were performed at temperatures of 4, 21 and 37°C and frequencies of 25, 15, 10, 5, 3, 1, 0.5, 0.3 and 0.1 Hz. Each specimen was tested for 27 combinations of temperature and frequency. Testing began with the lowest temperature and proceeded to the highest. At a given temperature, the testing began with the highest frequency of loading and proceeded to the lowest.

On the morning of testing, specimen were placed in the environmental test chamber at the desired temperature and allowed to equilibrate for three hours. To begin testing, a minimal contact load was applied to the specimen. A sinusoidal axial compressive load was applied to the specimen without impact in a cyclic manner. The load was adjusted in each case to attempt to achieve an axial strain with an amplitude of 80 με with the aim to avoid accumulated damage to the specimen. It should be noted that the strain used for the testing control is an average strain from the four extensometers. The axial compressive load was adjusted in each test in an attempt to maintain the 80 με level of axial strain.

The first step was to apply a preconditioning load to the specimen with 200 cycles at 25 Hz. Testing continued with varying load cycles for each frequency as shown in Table 2.2. A two minutes rest period was set between two continuous frequencies for all tests. The data acquisition system was programmed to record the last seven cycles for analysis at each frequency with about 200 points per cycle.

Table 2.2 Cycles for Test Sequence

Frequency, Hz	Number of Cycles
Preconditioning (25)	200
25	200
15	200
10	200
5	100
3	20
1	20
0.5	15
0.3	15
0.1	15

A total of five replicates were tested for each mixture for the same testing condition. After the entire cycle of testing was complete at the lower temperature, the environmental chamber was set to the next temperature. After another three hours conditioning, the above steps were repeated until the entire sequence of temperatures and frequencies was completed.

2.2.4 Data Analysis and Discussion

The test variables obtained from the data acquisition system include the time, axial force, axial displacement and the displacements from the four extensometers. The variable time is the time period from the test start to the time a data point is recorded. The axial force is the vertical load on the specimen, and axial displacement is the vertical displacement of the load piston. The axial displacement for each extensometer was recorded. After the axial force and displacement for each extensometer was recorded, the actual stress and strain was calculated for the analysis.

For any given test temperature, one data file was created for each frequency for each specimen. The data file starts from 25 Hz and ends at 0.1 Hz for each of the test temperatures. At 25 Hz, 15 Hz, 10Hz, the test data is obtained from the 194^{th} cycle to the 200^{th} cycle, and there are 400 data points in each cycle. For 5 Hz, the test data is from the 94^{th} cycle to the 100^{th} cycle, and there are about 400 data points in each cycle. For 3 Hz and 1 Hz, the data is from the 14^{th} cycle to the 20^{th} cycle, and there are about 400 data points in each cycle. For 0.5 Hz, 0.3 Hz and 0.1 Hz, the data is from the 9^{th} cycle to 15^{th} cycle and about 400 points in each cycle.

For asphalt concrete, the complex dynamic modulus and phase angle change with temperature and load duration time or frequency of loading. At lower temperatures, the modulus for asphalt concrete is large, so it is easy to control the applied axial force in order to obtain small displacements. At higher temperatures, such as 37°C, the material becomes soft and it is more difficult to control the axial force to obtain small displacements. Figure 2.3 is a typical plot of the raw test data, in which the stress curve is sinusoidal shape whereas the curve for strain has an upward drift with time.

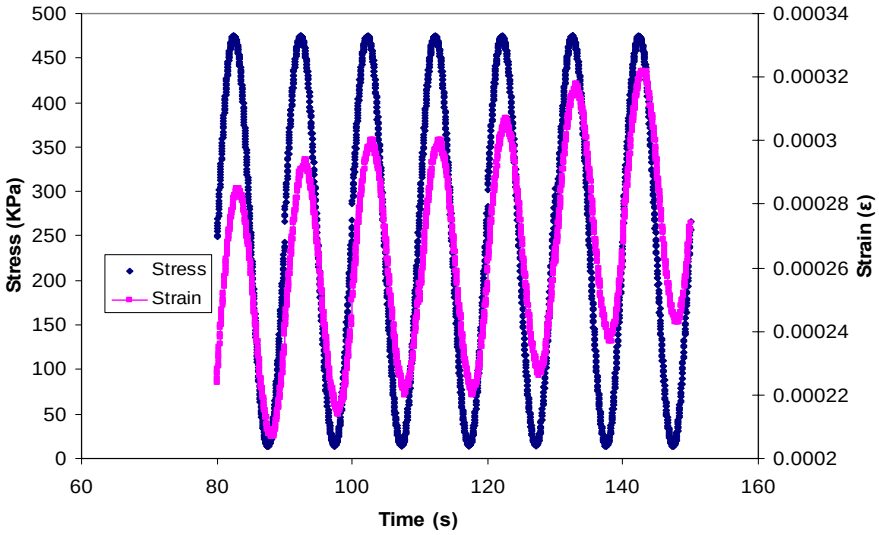

Figure 2.3 Typical Stress, Strain vs. Time Plot at Lower Temperature (4°C)

From the above plot, it can be seen that the displacement curves are not sinusoidal but increase with time, due to the drift in the displacement. This is especially obvious for higher temperatures. The following equations generally represent the load and displacement.

$$F = A_{0F} + C_{1F} * \sin(2\pi f * t + \theta_F) \tag{2.1}$$

$$D = A_{0D} * t + C_{1D} * \sin(2\pi f * t + \theta_D) \tag{2.2}$$

where: F and D = load and displacement, respectively;
A_{0F} = mean value for the load;
A_{0D} = slope of the drift curve for the displacement;
C_{1F} and C_{1D} = amplitude specifies the height of the oscillation for the load and displacement, respectively;
f = frequency for the test; and
θ_F and θ_D = phase angle for the load and displacement, respectively.

One can invoke the trigonometric identity for equations (2.1) and (2.2):

$$C_{1F} \sin(2\pi ft + \theta_F) = C_{1F}\left[\sin(2\pi ft)\cos(\theta_F) + \cos(2\pi ft)\sin(\theta_F)\right] \tag{2.3}$$

$$F = A_{0F} + C_{1F} * \sin(2\pi f * t + \theta_F) = A_{0F} + A_{1F}\cos(2\pi ft) + B_{1F}\sin(2\pi ft) \quad (2.4)$$

where

$$A_{1F} = C_{1F}\sin(\theta_F) \quad \text{and} \quad B_{1F} = C_{1F}\cos(\theta_F) \quad (2.5)$$

The phase angle and amplitude for the load are obtained as follows [2]:

$$\theta_F = \arctan(\frac{A_{1F}}{B_{1F}}) \quad (2.6)$$

$$C_{1F} = \sqrt{A_{1F}{}^2 + B_{1F}{}^2} \quad (2.7)$$

Using the least-square fit of a sinusoid, the goal is to determine coefficient values that minimize [2]:

$$S_r = \sum_{i=1}^{N}\{y_i - [A_0 + A_1\cos(2\pi ft_i) + B_1\sin(2\pi ft_i)]\}^2 \quad (2.8)$$

The solutions for the equation (2.8) are [2]:

$$A_0 = \frac{\sum Y}{N}, \quad A_1 = \frac{2}{N}\sum Y\cos(2\pi ft) \quad \text{and} \quad B_1 = \frac{2}{N}\sum Y\sin(2\pi ft) \quad (2.9)$$

Here, Y is the centered load from the actual load value and N is the data point. The four parameters are used to characterize the sinusoidal function for the load.

Maximum and minimum values were obtained for every cycle for the displacement. The slope was then calculated for the maximum and minimum values, respectively. The average of these two slopes was interpreted as the drift rate.

Equation 2.9 could be used to calculate the parameters for the displacement. It should be noted that Y should be the corrected displacement. The method for this correction is given by the following equation:

$$Y_c = (Y_0 - E) - R * t \quad (2.10)$$

where: Y_C = Corrected displacement;
Y_0 = actual displacement;
E = Average of all the actual displacements;
(Y_0-E) = centered displacement;
R = displacement drift rate; and
t = time.

After the corrected displacement was obtained, equation 2.9 was used to calculate A_0, A_1 and B_1. From these parameters, equations 2.4, 2.5, and 2.6 were used to calculate the amplitude and phase angle for the displacement curve.

Once all the parameters for the load and displacement curve are obtained, it is straightforward to calculate the complex dynamic modulus and phase angle for the asphalt mixture:

$$\left|E^*\right| = \frac{C_{1F}}{C_{1D}} * \frac{L_G}{A} \tag{2.11}$$

$$\theta = \theta_F - \theta_D \tag{2.12}$$

where $|E^*|$ and θ = complex modulus and phase angle for the material, respectively;
C_{1F} and C_{1D} = amplitude for the load and displacement curve as described above;
L_G = gage length;
A = specimen area; and
θ_F and θ_D = phase angle for the load and displacement, respectively.

One analysis file was obtained for each load frequency. In this analysis file, the complex dynamic modulus in GPa and the phase angle in degrees were obtained for the given test temperature and frequency. Five replicate specimens were tested for each asphalt mixture. After all the complex dynamic modulus and phase angle values were calculated for each specimen under the same test conditions, the average value for both of these parameters was calculated. The coefficients of variation for both dynamic modulus and phase angle were also calculated for each mixture. The average values from the five specimens for the three asphalt mixtures are shown in Table 2.3, 2.4, 2.5, respectively.

Table 2.3 Average Dynamic Modulus and Phase Angle for the SMA Mixture

Temperature (ºC)	Frequency (Hz)	Dynamic Modulus, GPa			Phase Angle, degrees		
		Mean	Standard Deviation	Coefficient of Variation (%)	Mean	Standard Deviation	Coefficient of Variation (%)
4	25	14.86	0.93	6.25	7.16	0.43	5.97
	15	13.92	0.79	5.67	8.98	0.35	3.89
	10	13.02	0.75	5.76	10.60	0.59	5.54
	5	11.92	0.64	5.35	11.36	0.38	3.33
	3	10.92	0.69	6.36	12.32	0.33	2.66
	1	9.40	0.64	6.77	14.16	0.23	1.63
	0.5	8.56	0.50	5.88	16.58	0.30	1.83
	0.3	7.80	0.47	6.01	18.12	0.36	1.97
	0.1	6.26	0.37	5.93	21.08	0.48	2.26
21	25	6.16	0.25	4.07	16.88	0.35	2.07
	15	5.50	0.21	3.86	18.56	0.89	4.80
	10	5.00	0.24	4.90	20.50	1.41	6.89
	5	4.26	0.21	4.87	19.20	0.46	2.40
	3	3.32	0.18	5.39	20.32	0.62	3.06
	1	2.64	0.15	5.74	21.48	0.38	1.75
	0.5	2.28	0.16	7.21	26.82	0.42	1.55
	0.3	2.00	0.12	6.12	28.94	0.45	1.55
	0.1	1.38	0.11	7.94	29.54	0.40	1.36
37	25	2.22	0.11	4.93	22.02	0.61	2.78
	15	1.92	0.08	4.36	22.98	0.62	2.69
	10	1.72	0.08	4.86	22.38	2.79	12.47
	5	1.46	0.05	3.75	18.58	1.49	8.00
	3	1.02	0.04	4.38	17.34	2.01	11.57
	1	0.92	0.08	9.09	16.10	2.36	14.66
	0.5	0.68	0.04	6.58	21.68	0.90	4.15
	0.3	0.60	0.07	11.79	22.24	0.70	3.15
	0.1	0.48	0.04	9.32	20.50	0.98	4.79

Table 2.4 Average Dynamic Modulus and Phase Angle for the E30x Mixture

Temperature (ºC)	Frequency (Hz)	Dynamic Modulus, GPa			Phase Angle, degrees		
		Mean	Standard Deviation	Coefficient of Variation (%)	Mean	Standard Deviation	Coefficient of Variation (%)
4	25	28.32	1.39	4.91	3.14	0.78	24.93
	15	26.34	1.36	5.17	4.84	1.18	24.39
	10	25.14	1.17	4.64	6.80	1.44	21.18
	5	23.62	0.93	3.92	7.28	0.15	2.04
	3	22.46	0.92	4.11	7.98	0.15	1.86
	1	20.26	0.74	3.67	9.36	0.18	1.94
	0.5	18.96	0.72	3.81	10.76	0.24	2.24
	0.3	17.72	0.65	3.64	12.06	0.23	1.91
	0.1	15.02	0.52	3.47	14.54	0.15	1.04
21	25	14.44	1.30	9.04	10.82	1.46	13.45
	15	13.06	0.96	7.38	13.18	0.74	5.58
	10	12.20	0.79	6.51	14.53	1.04	7.18
	5	10.60	0.78	7.37	15.20	0.38	2.50
	3	8.80	0.55	6.28	16.08	0.59	3.68
	1	7.42	0.57	7.65	18.52	0.31	1.69
	0.5	6.62	0.52	7.81	23.14	0.38	1.63
	0.3	5.86	0.48	8.24	25.78	0.40	1.56
	0.1	4.16	0.38	9.25	29.28	0.80	2.74
37	25	5.72	0.54	9.45	21.30	0.98	4.62
	15	4.84	0.34	6.95	23.10	0.91	3.95
	10	4.28	0.30	7.09	24.08	1.69	7.02
	5	3.46	0.21	5.99	23.56	0.36	1.51
	3	2.38	0.24	10.03	22.60	1.76	7.81
	1	1.94	0.15	7.82	22.84	1.54	6.72
	0.5	1.48	0.13	8.81	29.34	1.05	3.57
	0.3	1.22	0.11	8.98	30.10	1.09	3.61
	0.1	0.84	0.09	10.65	27.22	1.28	4.70

Table 2.5 Average Dynamic Modulus and Phase Angle for the C2 Mixture

Temperature (ºC)	Frequency (Hz)	Dynamic Modulus, GPa			Phase Angle, degree		
		Mean	Standard Deviation	Coefficient of Variation (%)	Mean	Standard Deviation	Coefficient of Variation (%)
4	25	29.52	0.83	2.80	2.75	0.82	29.76
	15	29.23	0.91	3.10	4.10	0.56	13.58
	10	27.16	0.23	0.85	5.82	0.49	8.36
	5	25.33	0.43	1.72	6.98	0.25	3.58
	3	24.26	0.40	1.66	7.76	0.47	6.02
	1	21.90	0.36	1.65	9.12	0.43	4.74
	0.5	20.56	0.34	1.63	10.64	0.54	5.09
	0.3	19.14	0.38	2.01	11.90	0.55	4.60
	0.1	16.28	0.40	2.47	14.38	0.58	4.04
21	25	14.55	0.24	1.64	11.06	1.27	11.46
	15	13.08	0.26	1.98	12.88	1.32	10.22
	10	12.24	0.54	4.38	14.64	1.55	10.60
	5	10.74	0.42	3.87	15.14	0.57	3.80
	3	8.94	0.30	3.32	15.94	0.37	2.33
	1	7.48	0.29	3.83	18.66	0.45	2.39
	0.5	6.68	0.29	4.42	23.92	0.47	1.99
	0.3	5.88	0.29	4.87	27.10	0.43	1.60
	0.1	4.08	0.22	5.31	31.34	0.57	1.82
37	25	5.42	0.29	5.44	22.54	0.55	2.42
	15	4.66	0.27	5.80	23.43	0.95	4.05
	10	4.08	0.40	9.71	24.62	3.84	15.61
	5	3.20	0.23	7.33	24.76	0.66	2.67
	3	2.22	0.23	10.27	22.44	1.96	8.75
	1	1.74	0.17	9.62	22.84	1.90	8.31
	0.5	1.34	0.17	12.49	30.96	1.42	4.57
	0.3	1.08	0.18	16.56	32.22	1.27	3.95
	0.1	0.72	0.13	18.11	29.42	1.14	3.88

It can be seen from the experimental data that for all mixtures, most coefficients of variation (COV) for both the dynamic modulus and phase angle under the different test temperatures and frequencies are less than 20%, which means the repeatability of the tests is satisfactory. Figures 2.4 through 2.6 plot the average dynamic modulus data for the SMA, E30x and C2 mixtures, respectively, while Figures 2.7 through 2.9 illustrate the phase angle values for these same three mixtures.

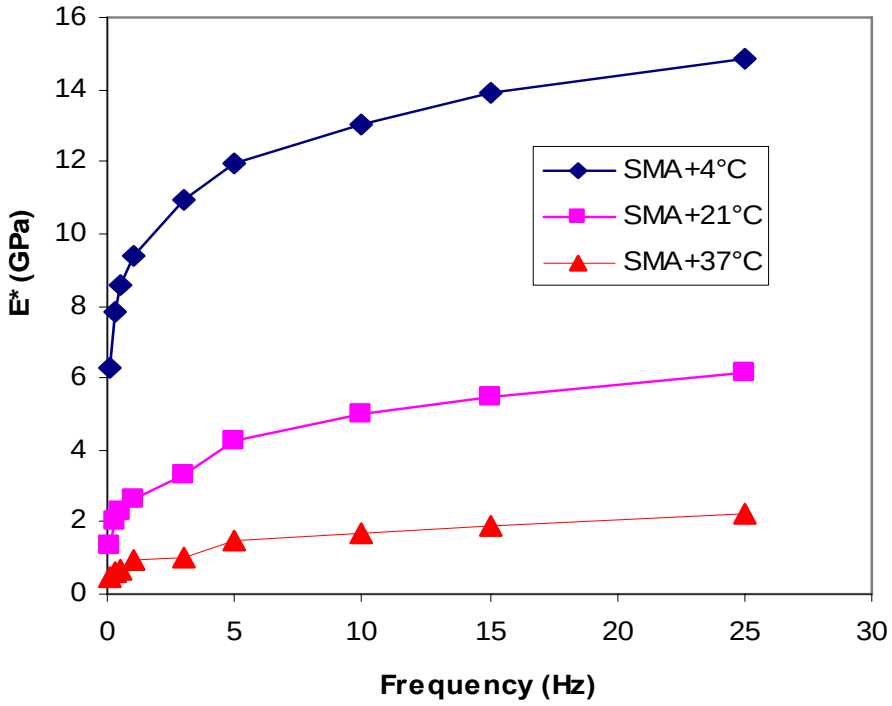

Figure 2.4 Dynamic Modulus Data for the SMA Mixture

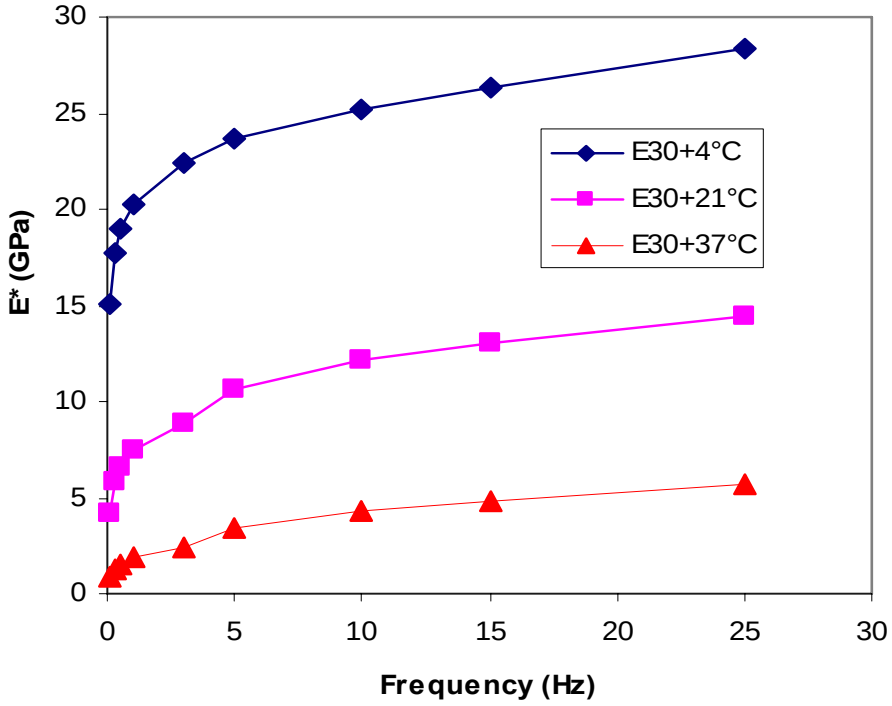

Figure 2.5 Dynamic Modulus Data for the E30x Mixture

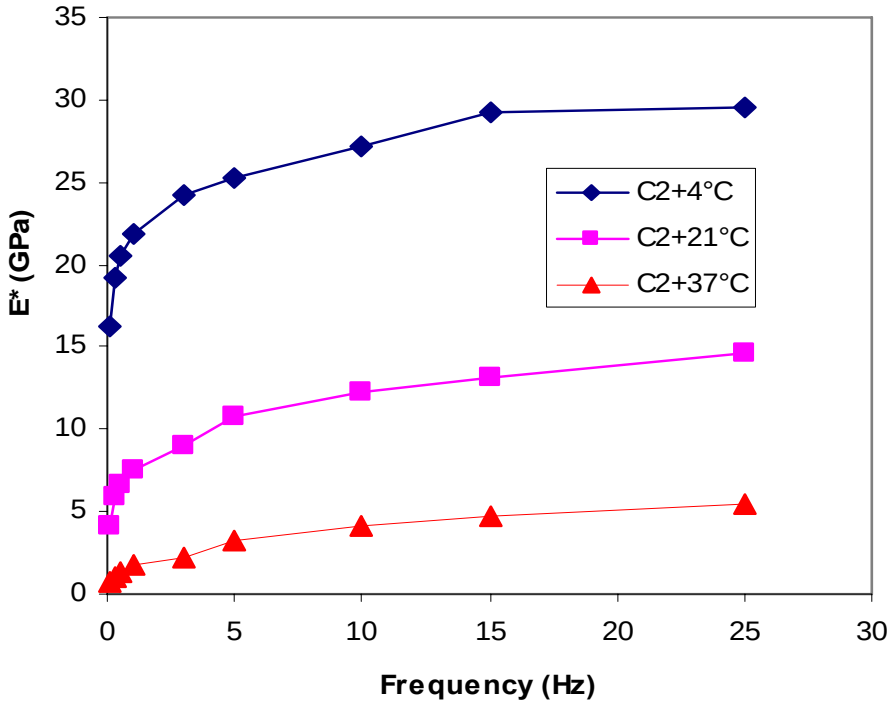

Figure 2.6 Dynamic Modulus Data for the C2 Mixture

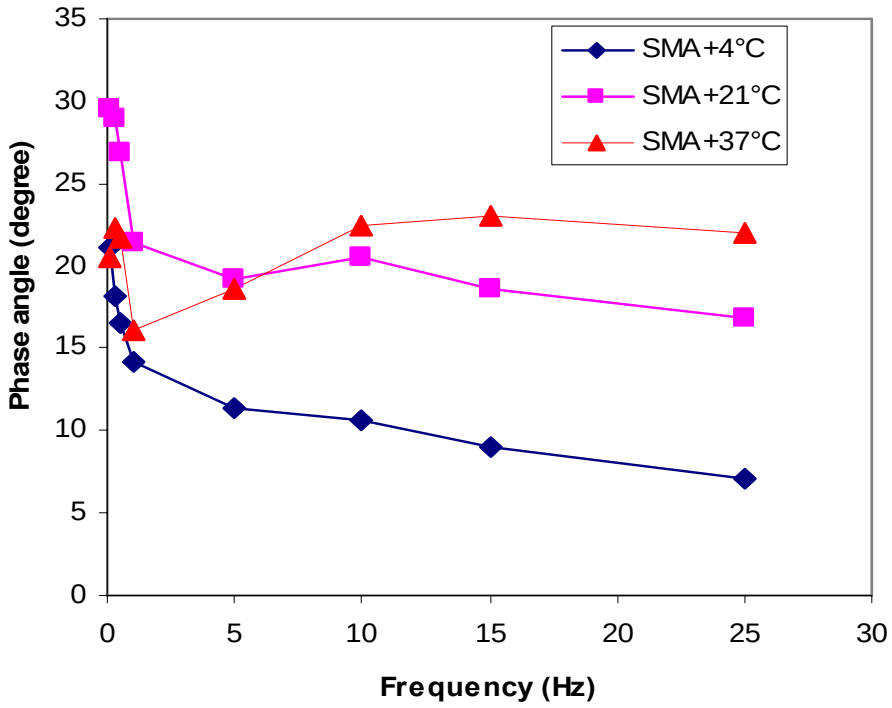

Figure 2.7 Phase Angle Data for the SMA Mixture

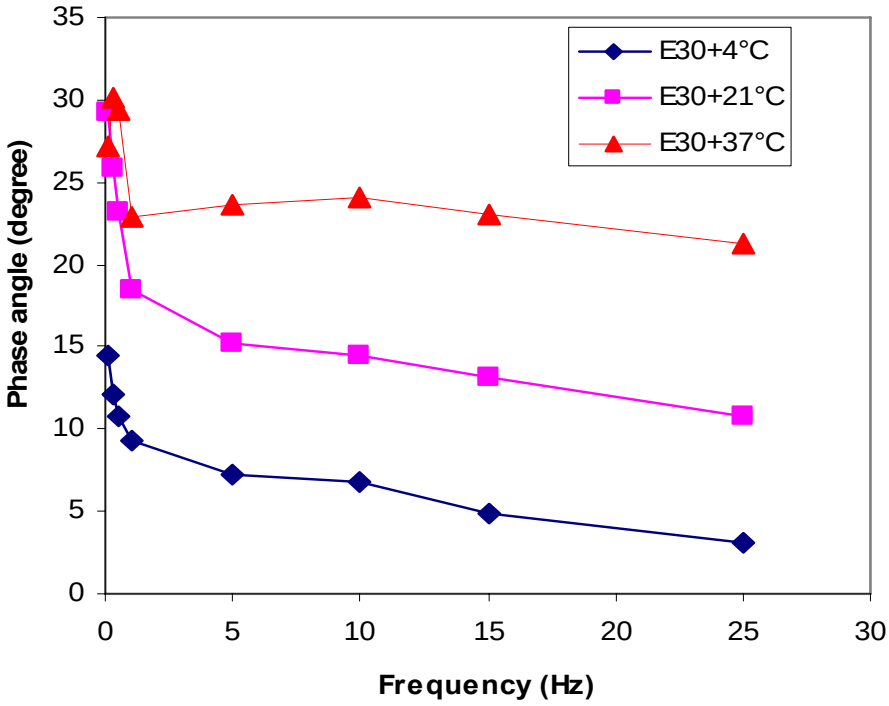

Figure 2.8 Phase Angle Data for the E30x Mixture

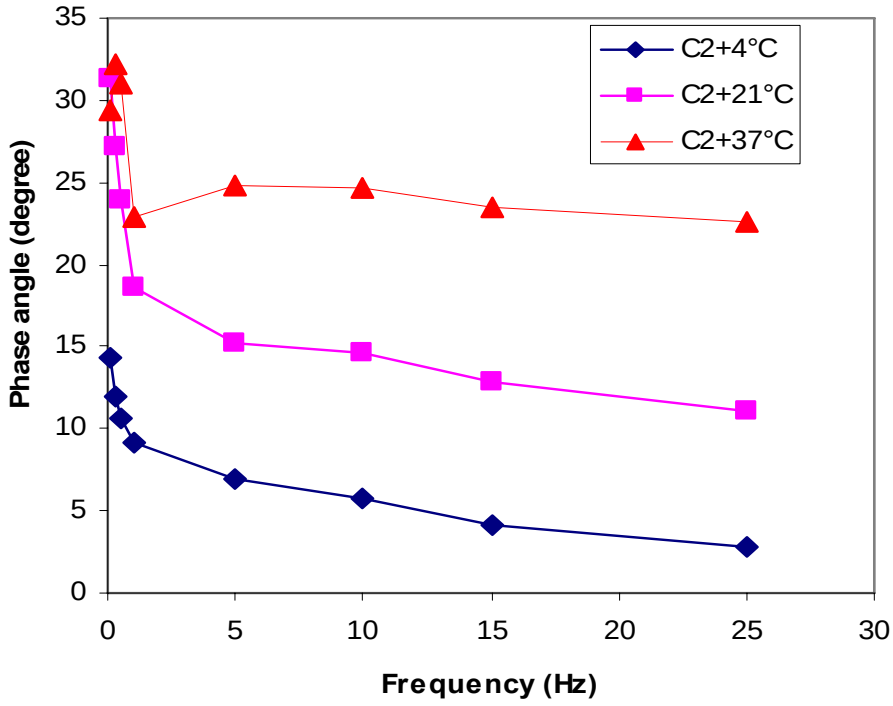

Figure 2.9 Phase Angle Data for the C2 Mixture

From the above figures, it was observed that the dynamic modulus values for all mixtures decrease with the increase of test temperature and increase with the increase of frequency, as is well known for asphalt mixtures. As for the phase angle, it was found that the phase angle increases with the increase of test temperature and decreases with frequency. This is nearly true for all mixtures except for few points at the highest test temperature. It is well documented that asphalt materials are viscoelastic materials and they always demonstrates more viscous properties at higher temperatures, which leads to more difficult accurate measurement of the phase angle at higher temperatures, such as 37º C. This can be used to explain the phase angle values at higher temperature, as shown in Figures 2.7 through 2.9.

In order to compare the dynamic modulus values for different mixtures, the dynamic modulus data is plotted in one figure, as shown in Figure 2.10.

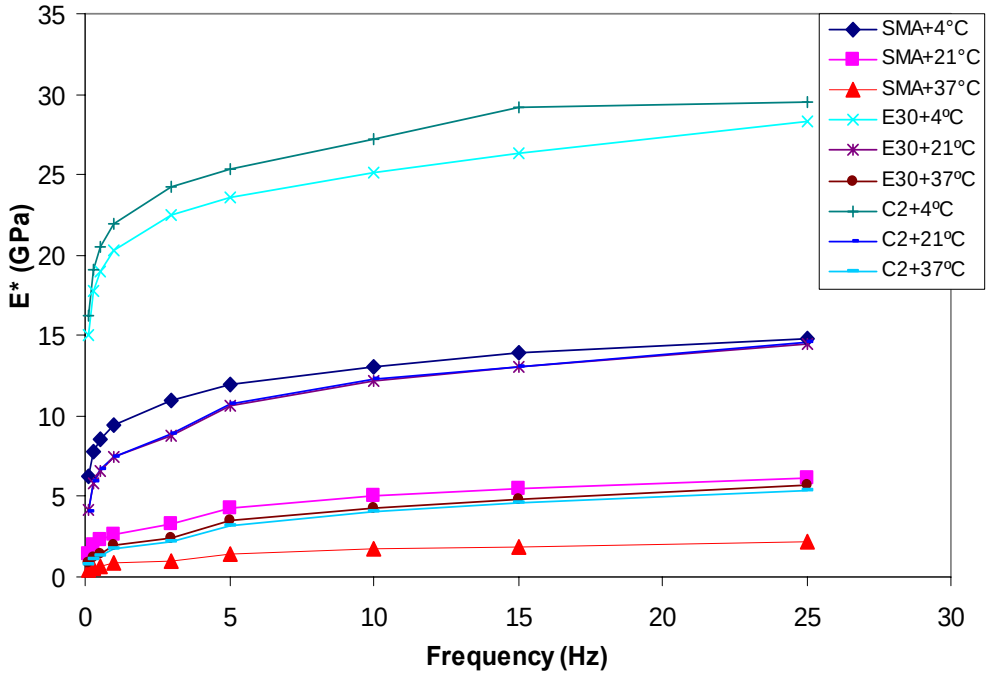

Figure 2.10 Dynamic Modulus Data for all Mixtures

It can be seen from Figure 2.10 that the SMA mixture has substantially lower dynamic modulus value than the other two mixtures, given the same test condition. The E30x and C2 mixtures have very close dynamic modulus values at the two higher test temperatures, whereas at the highest test temperature the C2 mixture has a higher dynamic modulus than the E30x mixture.

2.2.5 Dynamic Modulus Master Curves

The asphalt mixtures are thermorheologically simple materials and the time-temperature superposition principle is applicable in the linear viscoelastic state. The dynamic modulus and phase angle of asphalt mixtures can be shifted along the frequency axis to form single characteristic master curves at a desired reference temperature or frequency.

Typically the shift factors α_T are obtained from the WLF equation [3]:

$$\log \alpha_T = \frac{C_1(T - T_S)}{C_2 + T - T_S} \tag{2.13}$$

where C_1 and C_2 are constants, T_s is the reference temperature, and T is the temperature of each individual test.

A new method of developing the master curve for asphalt mixtures was developed in the research conducted by Pellinen [4] at the University of Maryland. In this study, master curves were constructed fitting a sigmoidal function to the measured compressive dynamic modulus test data using non-linear least squares regression techniques [4]. The shift can be done by solving the shift factors simultaneously with the coefficients of the sigmoidal function. The sigmoidal function is defined by equation 2.14.

$$\log|E^*| = \delta + \frac{\alpha}{1 + e^{\beta - \gamma(\log(f_r) + s_T)}} \tag{2.14}$$

where

$\log|E^*|$ = log of dynamic modulus;
δ = minimum modulus value;
f_r = reduced frequency;
α = span of modulus values;
s_T = shift factor according to temperature; and
β, γ = shape parameters.

The master curve can be constructed using any non-linear curve-fitting technique. The reference temperature for all mixtures is 21°C. The Microsoft Excel Solver was used to fit the master curve for each set of data. This method uses the Generalized Reduced Gradient nonlinear optimization approach to find the parameters that give the "best fit" between the equation and the data. The nonlinear regression algorithm seeks the values of the parameters that minimize the sum of the squared differences between the values of the observed and predicted values of the dynamic modulus. Figure 2.11 shows the dynamic modulus master curve for the three mixtures.

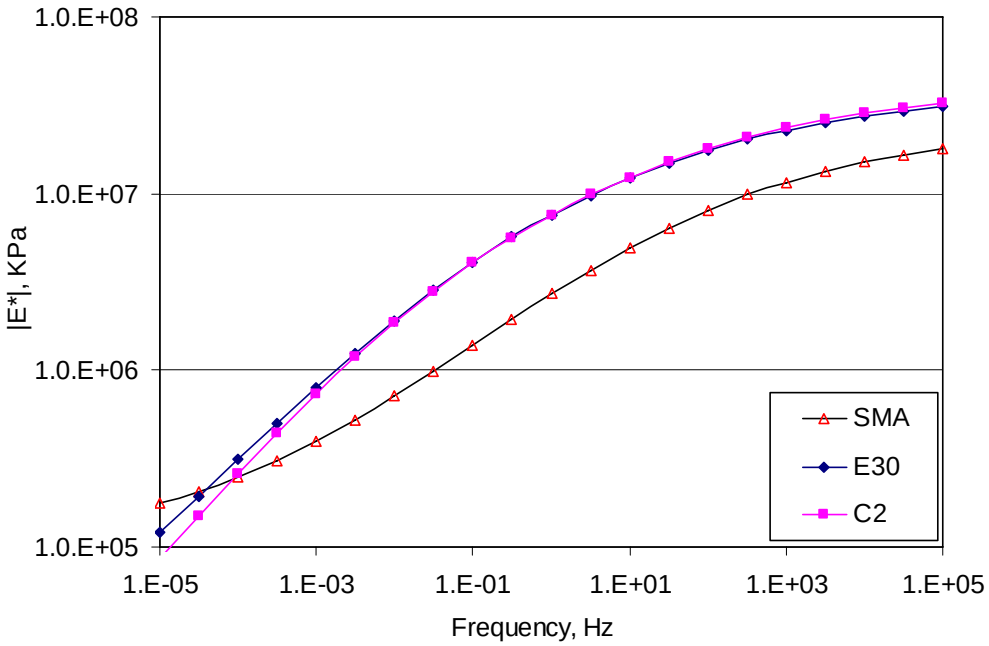

Figure 2.11 Dynamic Modulus Master Curves for the Three Mixtures

From the dynamic modulus master curve, it can be found that the SMA mixture has the lowest dynamic modulus values for the most of the frequency domain except in the low frequency range. It also shows that the E30x and C2 mixtures have very similar dynamic modulus value in most of the frequency domain. However, it was found that the E30x mixture has a higher dynamic modulus values than the C2 mixture at the low frequency domain, whereas the C2 mixture has a slightly higher dynamic modulus values than the E30x mixture at a high frequency domain, which is consistent with the dynamic modulus data shown in Figures 2.4 through 2.6.

2.2.6 HMA Dynamic Modulus Testing Summary

A complex dynamic modulus experimental protocol was developed and three asphalt mixtures were performed the dynamic modulus test at three test temperatures and nine frequencies using this protocol. Dynamic modulus and phase angle was calculated using the axial load and displacements recorded by four extensometers mounted on the specimen surface. The dynamic modulus master curves were constructed by fitting a sigmoidal function to the measured compressive dynamic modulus test data using non-linear least squares regression techniques for each of the three mixtures tested.

As expected, the experimental data shows that dynamic modulus increases with an increase of frequency, but decreases with the increase of test temperature. It is also shown that the phase angle calculated from experimental data increases with the increase of test temperature, but decreases with the increase of frequency. The experimental data also

shows that the mixture of SMA has the lowest dynamic modulus values, given the same test condition. The E30x and C2 mixtures have very similar dynamic modulus values at the two higher test temperatures while at the lowest temperature the C2 mixture has higher dynamic modulus values than E30x. The dynamic modulus master curve confirms that the SMA mixture has the lowest dynamic modulus values for most of the frequency domain. The dynamic modulus master curves also demonstrates that the E30x and C2 mixtures have very similar dynamic modulus values for most of the frequency domain, and only a slight difference was found at the high frequency domain.

2.3 Binder Characterization

Characterization of tank asphalt binders supplied by Marquette University was done in accordance with AASHTO test specifications. The test specifications followed were:

-Dynamic Shear Rheometer: AASHTO T315-06,
-Rolling Thin Film Oven Test: AASHTO T240-06,
-Pressure Aging Vessel: AASHTO R28-06,
-Bending Beam Rheometer: AASHTO T313-06, and
-Rotational Viscometer: AASHTO T316-06.

The test results are summarized in Tables 2.6 through 2.8 below. The A and VTS parameters in Table 2.8 were determined as summarized by Mirza and Witczak (1995) and used in the AASHTO Mechanistic-Empirical Pavement Design Guide (2004).

Table 2.6 Asphalt Binder Dynamic Shear Rheometer Test Results

Asphalt Binder	Temperature, ºC	G*, kPa	Delta (δ), º	G*/sin(δ), kPa[1]
PG64-22	Unaged			
	58	2.501	87.54	2.503
	64	1.135	86.60	1.133
	70	0.561	86.79	0.562
	Rolling Thin Film Oven Aged			
	58	6.277	83.38	6.319
	64	2.681	85.98	2.688
	70	1.236	88.75	1.236
	Pressure Aging Vessel Aged			
	19	12,615	42.88	8,584
	22	8,279	46.19	5,974
	25	5,240	49.69	3,996
PG70-22	Unaged			
	64	2.528	65.55	2.758
	70	1.484	68.38	1.595
	76	0.893	70.08	0.936
	Rolling Thin Film Oven Aged			
	64	4.308	61.90	4.884
	70	2.449	63.37	2.740
	76	1.436	65.35	1.580
	Pressure Aging Vessel Aged			
	16	8432	40.71	5,500
	19	5606	43.61	3,867
	22	3698	45.88	2,655

[1]The calculated values for Pressured Aging Vessel Aged are G*xsin(δ).

Table 2.7 Bending Beam Rheometer Test Results of PAV Aged Asphalt Binders

Asphalt Binder	Temperature, ºC	Stiffness (S), MPa	m-value
PG64-22	-12	244	0.268
PG70-22	-12	112	0.308
	-18	246	0.237

Table 2.8 Rotational Viscometer Test Results (10Hz) and A and VTS Parameters

Asphalt Binder	Temperature, ºC	Viscosity, cP	A	VTS
PG64-22	100	3480	9.773228	3.26367
	121	855		
	135	399		
	165	125		
PG70-22	115	3545	8.458896	2.78133
	135	1120		
	165	330		
	176	230		

2.4 Characterization of Unbound Subgrade and Aggregate Base Course Materials

A laboratory testing program was conducted on subgrade soil and aggregate base course materials obtained from the Marquette Interchange site in Milwaukee, Wisconsin. The testing program was conducted at the Geotechnical and Pavement Research Laboratory at the University of Wisconsin-Milwaukee. Soil and aggregate samples were subjected to different tests to determine their physical properties, compaction characteristics, and resilient modulus.

The samples from the Marquette Interchange Project consist of two soil samples and two aggregate samples. The soil samples are from Location 1 (sta. 385+26.43, off. 64.61 Rt) and Location 2 (sta. 385+40.84, off. 63.67 Rt) herein referred to as Soil 1 and Soil 2, respectively. These sampling locations were selected as representative of the two distinct soil types within the instrumented section (sta. 385+10 to 385+50). Two 5-gallon buckets of each soil were provided, each sampled from different elevations. Soil 1 samples were extracted from elevations 657.0'-656.0' and 656.0'-655.0', representing the top 12 inches and next 12 inches of native soils, respectively. Soil 2 samples were from elevations 656.4'-655.4' and 655.4'-654.4', again representing the top 12 inches and next 12 inches of native soils, respectively. Basic soil characterization tests showed that samples of Soil 1 from each elevation have different properties and as a result different classifications, and will be referred to herein as Soil 1A and Soil 1B. Tests indicated that the two samples of Soil 2 were of the same material and will therefore continue to be grouped as Soil 2. This extended the testing to three soil samples, Soil 1A, Soil 1B, Soil 2, and two aggregate samples: Open-Graded and Dense-Graded.

2.4.1 Laboratory Testing of Subgrade Soils

Collected soils were subjected to standard laboratory tests to determine their physical properties, permeability, and compaction characteristics. Soil testing consisted of the following: grain size distribution (sieve and hydrometer analyses), Atterberg limits (liquid limit, *LL*, plastic limit, *PL*, and Shrinkage Limit, *SL*), specific gravity (G_s), and permeability. Soils were also subjected to Standard Proctor test to determine the optimum moisture content ($w_{opt.}$) and maximum dry unit weight (γ_{dmax}).

Laboratory tests were conducted following the AASHTO standard test procedures. Table 2.9 presents a summary of the standard tests used in this study.

Table 2.9: Standard Tests Used in this Investigation

Soil Property	Standard Test Designation
Specific Gravity	AASHTO T 84/85: Specific Gravity and Absorption of Fine Aggregate/Coarse Aggregate AASHTO T 100: Standard Method of Test for Specific Gravity of Soils
Particle Size Analysis	AASHTO T 88/311: Particle Size Analysis of Soils/Grain-Size Analysis of Granular Soil Materials
Permeability	AASHTO T 215: Permeability of Granular Soils (Constant Head) Falling Head Permeability Test of Cohesive Soils*
Atterberg Limits	AASHTO T 89/90: Determining the Liquid Limit of Soils/Determining the Plastic Limit and Plasticity Index of Soils
Shrinkage Limit	AASHTO T 92: Determining the Shrinkage Factors of Soils
Compaction Tests	AASHTO T 99/180: Moisture-Density Relations of Soils Using a 2.5-kg (5.5-lb) Rammer and a 305-mm (12-in) Drop/4.54-kg (10-lb) Rammer and a 457-mm (18in) Drop
AASHTO Soil Classification	AASHTO M 145-91: Standard Classification of Soils and Soil-Aggregate Mixtures for Highway Construction Purposes
ASTM Soil Classification	ASTM D 2487: Standard Classification of Soils for Engineering Purposes (Unified Soil Classification System)

* Traditional rigid wall permeability test.

2.4.2 Repeated Load Triaxial Test

A repeated loading triaxial test was conducted, to determine the resilient modulus of the investigated soils, following AASHTO T 307*: Standard Method of Test for Determining the Resilient Modulus of Soils and Aggregate Materials*. The test was conducted on compacted soil specimens that were prepared in accordance with the procedure described by AASHTO T 307.

The repeated load triaxial test was conducted using Instron FastTrack 8802 closed loop servo-hydraulic dynamic materials test system at UWM. The system utilizes 8800 Controller with four control channels of 19-bit resolution and data acquisition. A computer with FastTrack Console is the main user interface. This is a fully digital controlled system with adaptive control that allows continuous update of PID terms at 1 kHz, which automatically compensates for the specimen stiffness during repeated load testing. The loading frame capacity of the system is 56 kips with a series 3690 actuator that has a stroke of 6 inches. The system has two dynamic load cells 1.1 and 0.22 kip for measurement of the repeated applied load. The load cells include integral accelerometer to remove the effect of dynamic loading on the moving load cell. Figure 2.12 depicts pictures of the dynamic materials test system used in this study.

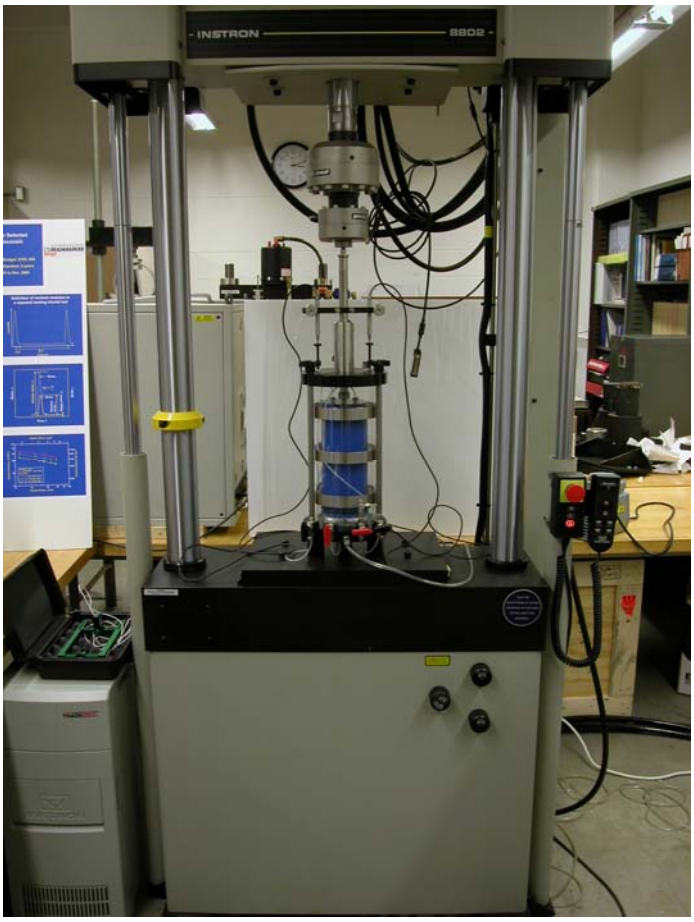

(a) Loading frame

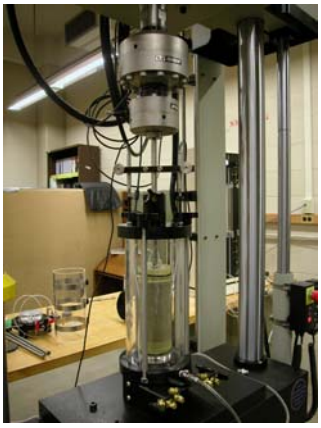

(b) Triaxial cell

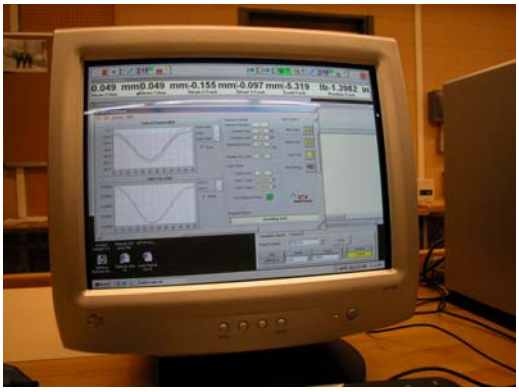

(c) Control software

Figure 2.12 Triaxial Test System

2.4.3 Subgrade Specimen Preparation

Compacted soil specimens were prepared according to the procedure described by AASHTO T 307, which requires five-lift static compaction. Therefore, special molds were designed and used to prepare soil specimens by static compaction of five equal layers. This compaction method provided uniform compacted lifts while using the same weight of soil for each lift. Figure 2.13 depicts pictures of the molds used to prepare soil specimens and pictures of specimen preparation procedure.

For each soil type, compacted soil specimens were prepared at the maximum dry unit weight and optimum moisture content. In order to ensure the repeatability of test results, the repeated load triaxial test was performed on two specimens of each soil at the specified unit weight and moisture content.

After a soil specimen was prepared under a specified unit weight and moisture content, it was placed in a membrane and mounted on the base of the triaxial cell. Porous stones were placed at the top and bottom of the specimen. The triaxial cell was sealed and mounted on the base of the dynamic materials test system frame. All connections were tightened and checked. Cell pressure, LVTD's, load cell, and all other required setup were connected and checked. Figure 2.14 shows pictures of specimen preparation for the repeated load triaxial test.

2.4.4 Subgrade Specimen Testing

The software that controls the materials dynamic test system was programmed to apply repeated loads according to the test sequences specified by AASHTO T 307 based on the material type. Once the triaxial cell is mounted on the system, the air pressure panel is connected to the cell. The required confining pressure (σ_c) is then applied. Figure 2.15 shows pictures of the software used to control and run the repeated load triaxial test.

The soil specimen was conditioned by applying 1,000 repetitions of a specified deviator stress (σ_d) at a certain confining pressure. Conditioning eliminates the effects of specimen disturbance from compaction and specimen preparation procedures and minimizes the imperfect contacts between end platens and the specimen. The specimen is then subjected to different deviator stress sequences according to AASHTO T 307. The stress sequence is selected to cover the expected in-service range that a pavement or subgrade material experiences because of traffic loading.

It is very difficult to apply the exact specified loading on a soil specimen in a repeated load configuration. This is in part due to the controls of the equipment and soil specimen stiffness. However, the closed-loop servo hydraulic system is one of the most accurate systems used to apply repeated loads. In this system, the applied loads and measured displacements are continuously monitored. This is to make sure that the applied loads are within an acceptable tolerance. If there are out of range applied loads or measured displacements, then the system will display warning messages and can be programmed to terminate the test.

(a) Molds of different sizes

(b) Filling mold with one soil layer

(c) Applying static force to compact soil specimen

Figure 2.13 Soil Specimen Preparation

(a) Compacted subgrade soil specimen

(b) Seating a specimen on the cell base and placing the top cap

(c) Mounting the cell on the loading frame

Figure 2.14 Soil Specimen Preparation for Repeated Load Triaxial Testing

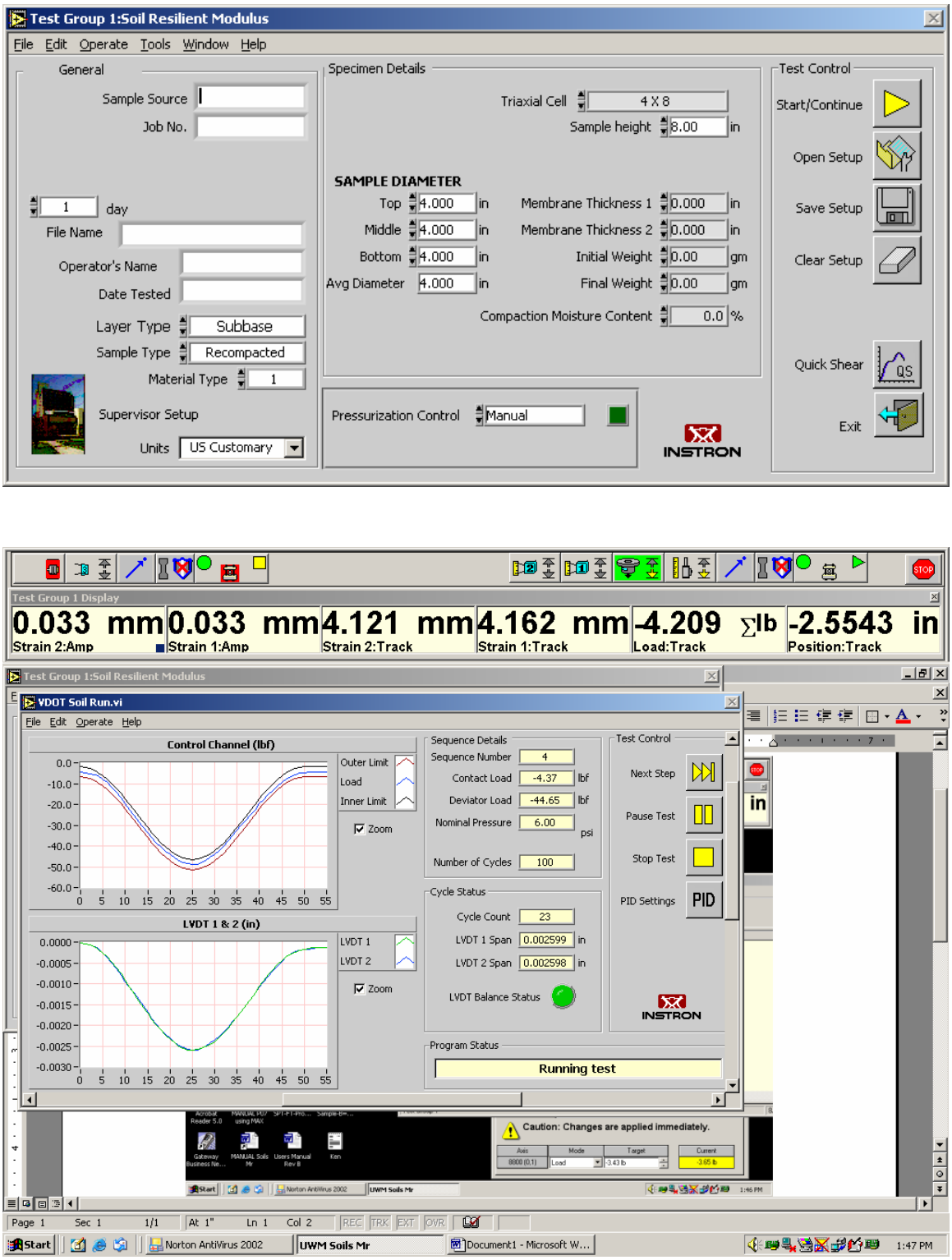

Figure 2.15 Computer Program Used for Triaxial Testing

2.4.5 Results of Testing on Subgrade Soils

The results of laboratory tests conducted to evaluate soil properties are presented in Table 2.10. The data on soil properties consists of particle size analysis (sieve and hydrometer); consistency limits (*LL*, *PL*, *SL*, and *PI*); specific gravity; maximum dry unit weight and optimum moisture content; soil classification using the Unified Soil Classification System (USCS); and soil classification using the AASHTO method including group index (*GI*). The following is a brief description of selected soils.

Soil (1A)

Test results indicated that the soil consists of 78% of fine materials (passing sieve #200) with a plasticity index PI = 2, which was classified as silt with sand (ML) according to the USCS and silty soil (A-4) according to the AASHTO soil classification with a group index GI = 0. Figure 2.16 shows the particle size distribution curve of soil 1A. The results of the Standard Proctor test on soil 1A are depicted in Figure 2.17. Test results showed that the maximum dry unit weight γ_{dmax} =20.1 kN/m^3 and the optimum moisture content $w_{opt.}$ = 10%.

Soil (1B)

Figure 2.18 depicts the particle size distribution curve for soil 1B. This soil consists of 94% passing sieve #200 with plasticity index *PI* = 8, which was classified as lean clay (CL) according to USCS and silty soil (A-4) according to the AASHTO soil classification with *GI*=5. Standard Proctor test results showed that the average maximum dry unit weight γ_{dmax} = 18.9 kN/m^3 and the corresponding average optimum moisture content w_{opt} = 12.5%, as shown in Figure 2.19.

Figure 2.20 shows a comparison of particle distribution curves for soils 1A and 1B.

Soil (2)

The results of particle size analysis of soil 2 are shown in Figure 2.21. Both tests are showing consistent results. Soil consists of about 60% passing sieve #200 with non plastic fines. The soil was classified as sandy silt (ML) according to USCS and silty soil (A-4) according to the AASHTO soil classification with *GI*=0. Standard Proctor test results showed that the average maximum dry unit weight γ_{dmax} = 18.6 kN/m^3 and the corresponding average optimum moisture content $w_{opt.}$ = 10.5%, as shown in Figure 2.22.

The results of the repeated load triaxial test conducted on the investigated soils are shown in Table 2.11. The test was conducted on soil specimens 1 and 2 compacted at γ_{dmax} and optimum moisture content $w_{opt.}$. Table 2.11 presents the mean resilient modulus values, standard deviation, and coefficient of variation for the 15 test sequences conducted according to AASHTO T 307. The mean resilient modulus values, standard deviation and coefficient of variation summarized in Table 2.11 are obtained from the last five load cycles of each test sequence. The coefficient of variation for the test results presented in Table 2.11 ranges between 0.30 and 9.87% for specimen #1 and from 0.16 to 8.56% for

specimen #2. This indicates that each soil specimen showed consistent behavior during each test sequence.

Figure 2.23 shows a graphical representation of the results presented in Table 2.11. Inspection of Figure 2.23 indicates that the resilient modulus (M_r) of soil 1A decreases with the increase of the deviator stress (σ_d) under constant confining pressure (σ_c). Under constant σ_c = 41.4 kPa, the resilient modulus decreased from M_r = 74.88 MPa at σ_d = 13.0 kPa to M_r = 61.91 MPa at σ_d = 61.6 kPa for soil specimen #1. Moreover, the resilient modulus increases with the increase of confining pressure under constant deviator stress, which reflects a typical behavior.

Resilient modulus test results for soils 1B and 2 are summarized in Tables 2.12 and 2.13, respectively. Moreover, these results are shown in Figures 2.24 and 2.25.

The traditional (rigid wall) falling head permeability test was conducted on the investigated subgrade soils. Test results are presented in Table 2.14.

Table 2.10: Properties of the Investigated Soils

Soil ID	Moisture Content (%)	Passing Sieve #200 (%)	Liquid Limit LL (%)	Plastic Limit PL (%)	Plasticity Index PI (%)	Shrinkage Limit SL (%)	Specific Gravity Gs	Optimum Moisture Content W_{opt} (%)	Maximum Dry Unit Weight		Unified Soil Classification System (USCS)	Group Index (GI)	AASHTO Soil Classification
									γ_{dmax} (pcf)	γ_{dmax} (kN/m^3)			
Soil 1A Test-1	15.2	78	17	15	2	14.42	2.69	10	128.0	20.1	ML (Silt w/ Sand)	0	A-4
Soil 1A Test-2	--	77	17	13	4	14.47	2.72	10	127.0	19.96	CL-ML (Silty clay w/sand)	0	A-4
Soil 1B Test-1	19.7	94	23	15	8	2.38	2.86	12.5	120.0	18.9	CL (Lean Clay)	5	A-4
Soil 1B Test-2	--	94	25	18	7	1.62	2.88	12.5	118.0	18.55	CL-ML (Silty clay w/sand	5	A-4
Soil 2A	14.5	65	NP	NP	NP	NP	2.75	10.5	119.3	18.8	ML (Sandy Silt)	0	A-4
Soil 2B	14.6	56	NP	NP	NP	NP	2.70	10.5	117.8	18.5	ML (Sandy Silt)	0	A-4

NP: Non Plastic

Soil 1A: sta. 385+26.43, off. 64.61 Rt Elev. 657.0-656.0
Soil 1B: sta. 385+26.45, off. 64.61 Rt Elev. 656.0-655.0

Soil 2A: sta. 385+40.84, off. 63.67 Rt Elev. 655.4-654.4
Soil 2B: sta. 385+40.84, off. 63.67 Rt Elev. 656.4-655.4

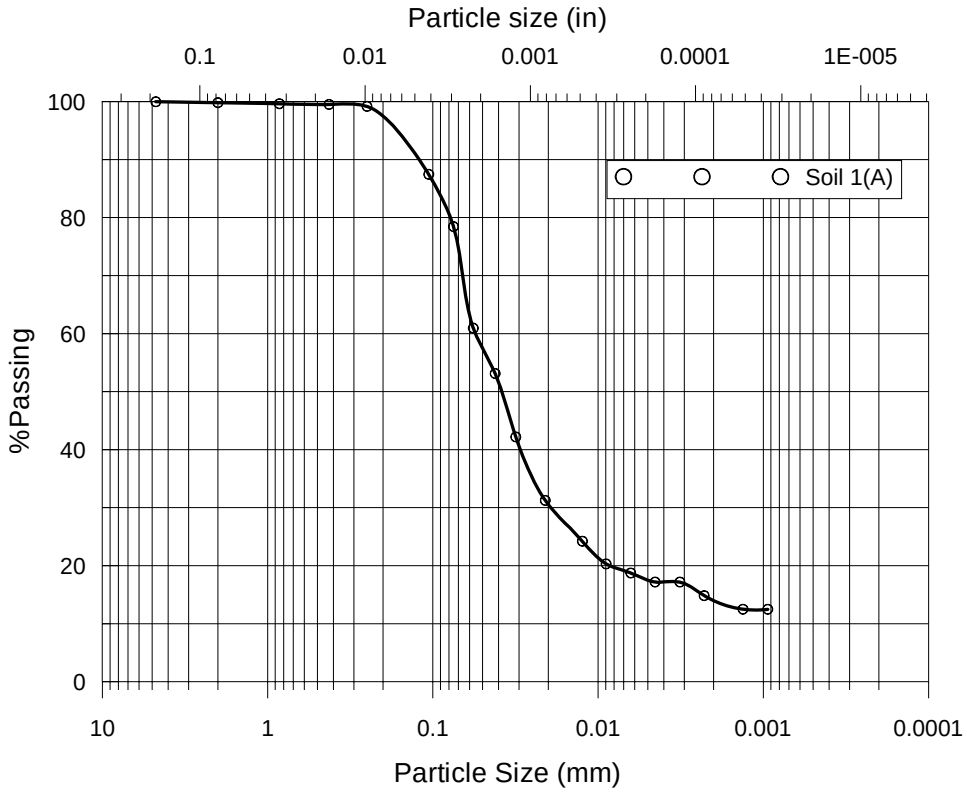

Figure 2.16 Particle Size Distribution of Soil 1(A)

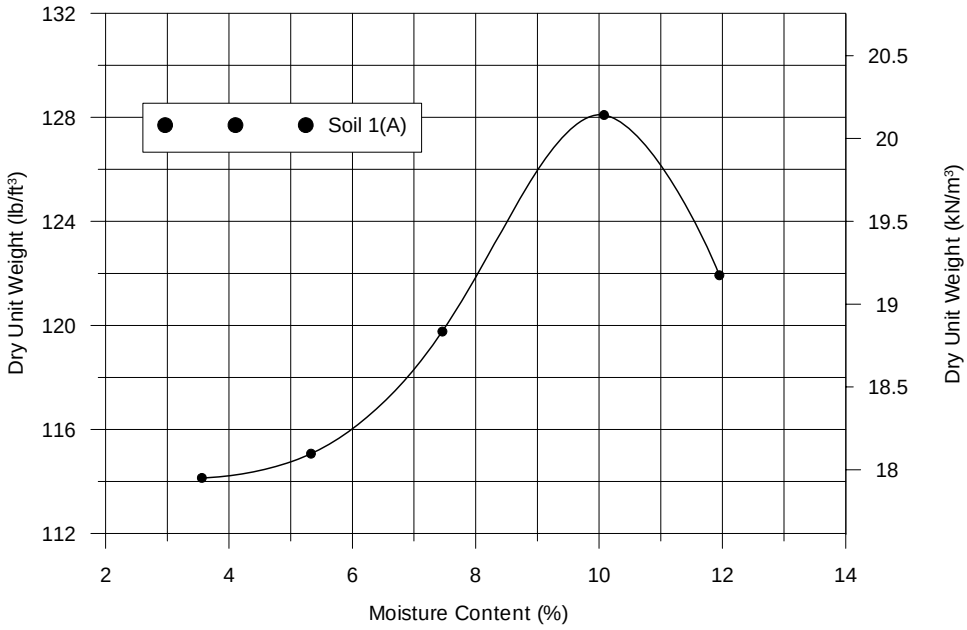

Figure 2.17 Compaction Curve for Soil 1(A)

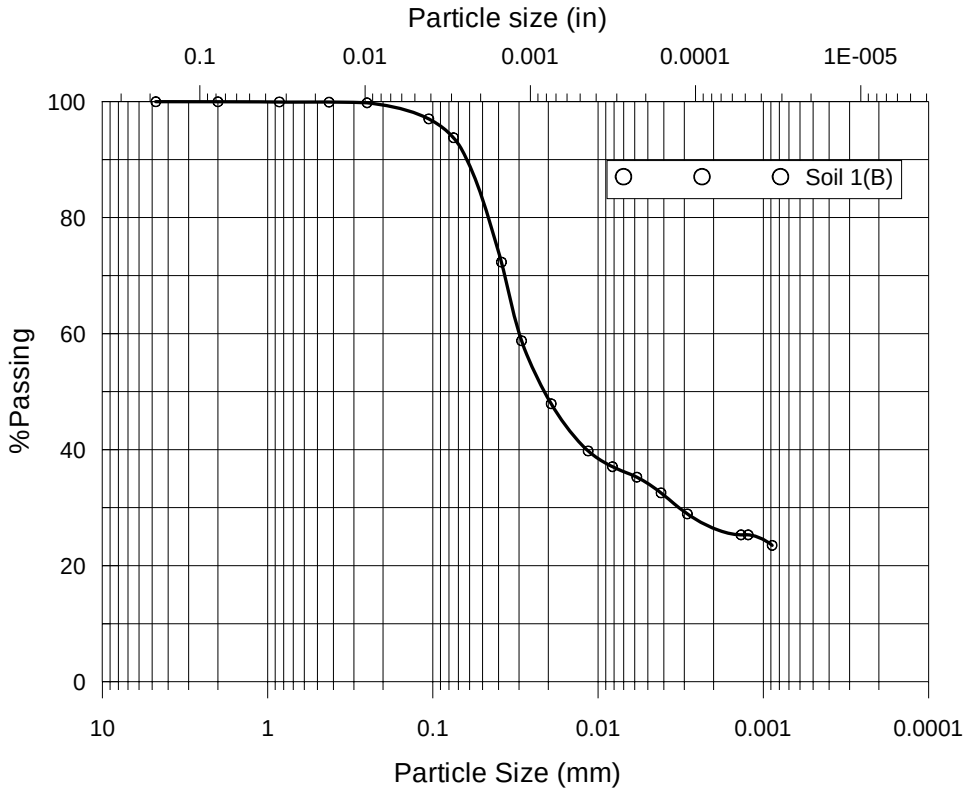

Figure 2.18 Particle Size Distribution of Soil 1(B)

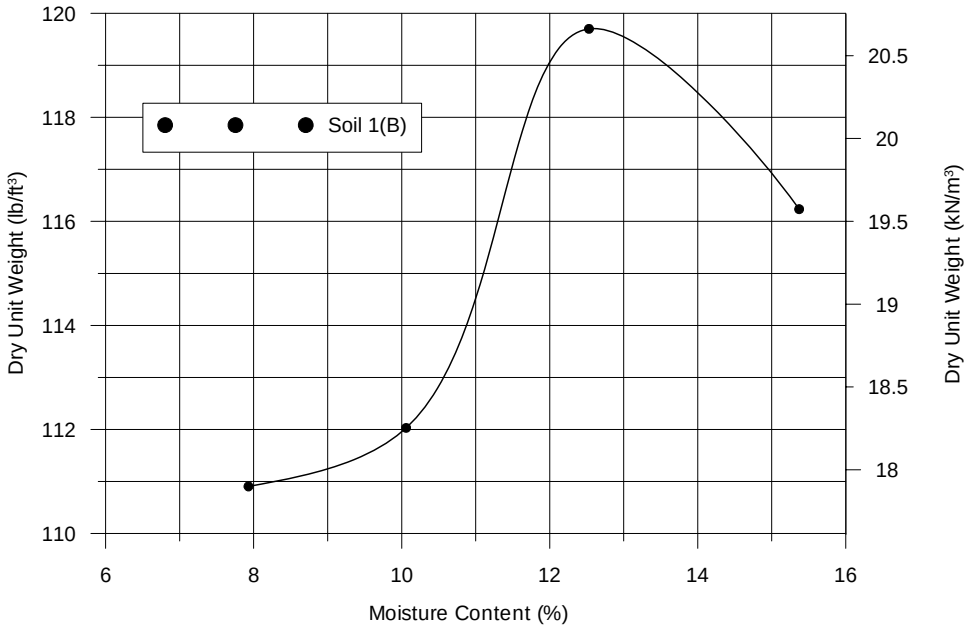

Figure 2.19 Compaction Curve for Soil 1(B)

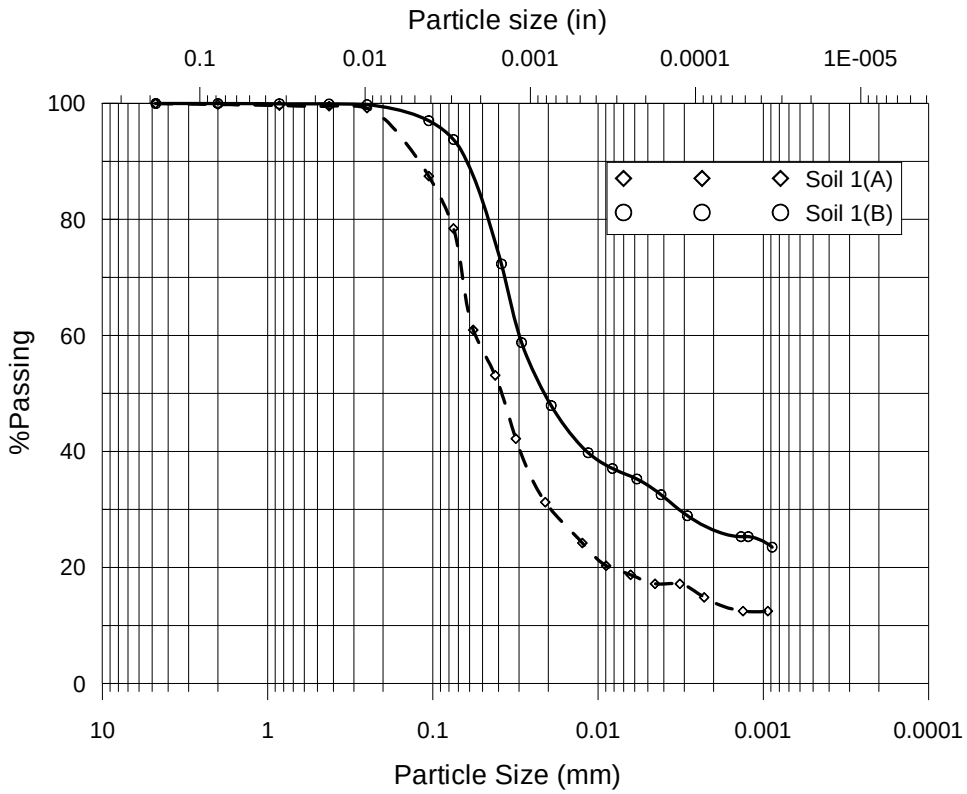

Figure 2.20 Particle Size Distribution of Soil 1

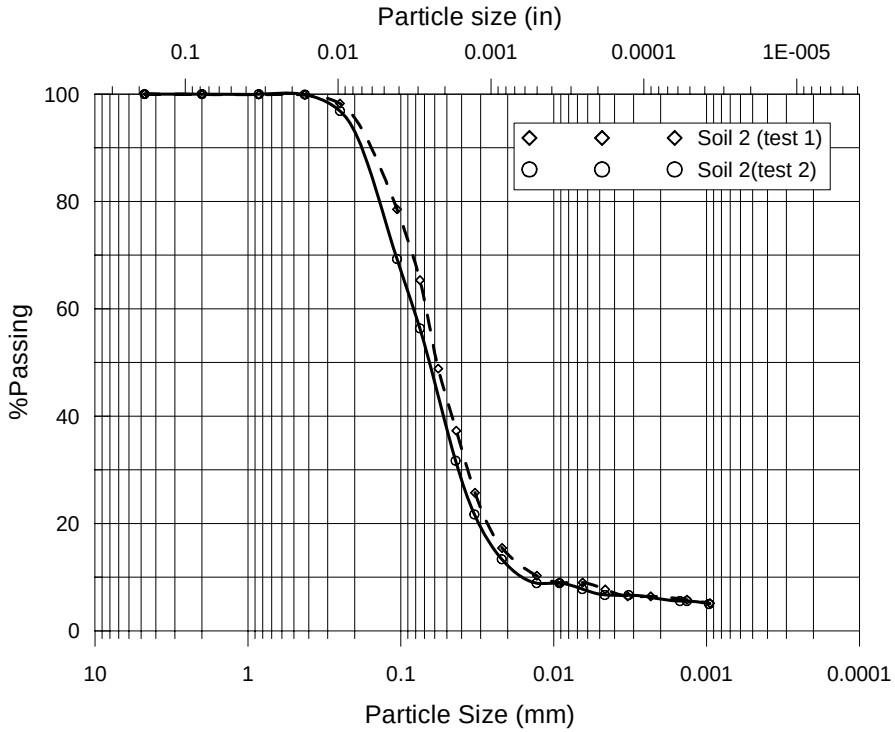

Figure 2.21 Particle Size Distribution of Soil 2

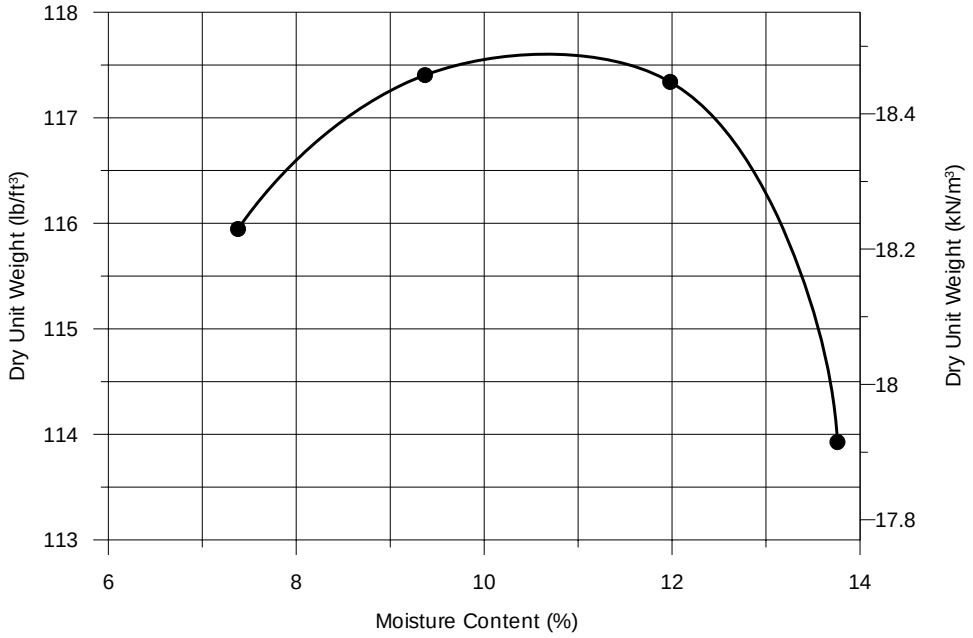

Test 1

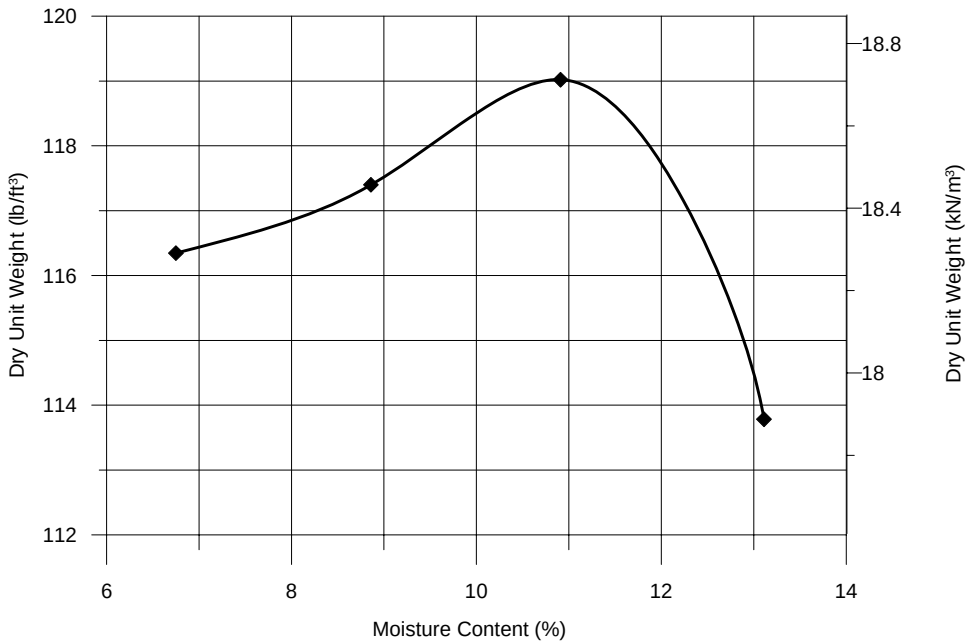

Test 2

Figure 2.22 Compaction Curve for Soil 2

Table 2.11 Results of the Repeated Load Triaxial Test on Subgrade Soil 1A

Test Sequence	σ_c (kPa)	Test #1				Test #2			
		σ_d (kPa)	M_r (MPa)	M_r Standard Deviation	M_r COV (%)	σ_d (kPa)	M_r (MPa)	M_r Standard Deviation	M_r COV (%)
1	41.4	13.0	74.88	0.61	0.82	12.9	73.07	6.25	8.56
2		25.6	73.79	0.76	1.02	25.2	70.89	0.54	0.77
3		38.0	71.69	0.48	0.66	37.5	65.40	0.25	0.39
4		50.1	66.01	0.26	0.39	49.3	58.65	0.15	0.25
5		61.6	61.91	0.20	0.32	61.2	55.93	0.09	0.16
6	27.6	12.8	62.78	6.20	9.87	12.5	62.79	0.48	0.76
7		25.1	59.29	0.51	0.86	24.7	55.03	0.46	0.83
8		37.0	56.33	0.27	0.47	36.6	51.24	0.16	0.32
9		49.0	54.24	0.18	0.33	48.5	48.79	0.16	0.34
10		60.7	52.68	0.16	0.30	60.2	47.05	0.09	0.19
11	13.8	12.4	55.77	0.69	1.23	12.2	50.55	0.37	0.74
12		24.2	74.85	0.58	1.21	33.8	42.94	0.27	0.62
13		35.7	45.05	0.29	0.65	35.3	39.97	0.13	0.34
14		47.5	43.48	0.18	0.42	47.0	38.34	0.09	0.23
15		58.9	42.29	0.16	0.38	58.2	36.96	0.09	0.25

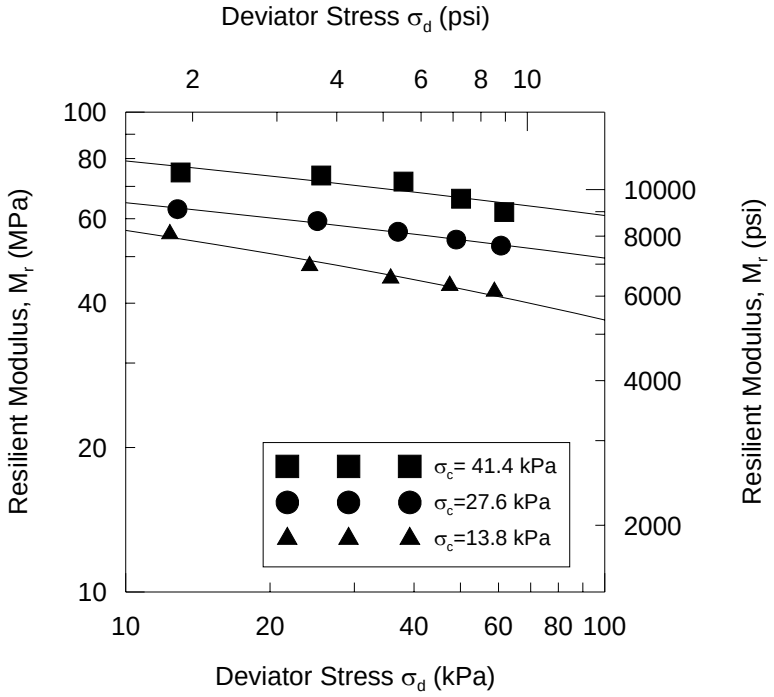

(a) Test 1

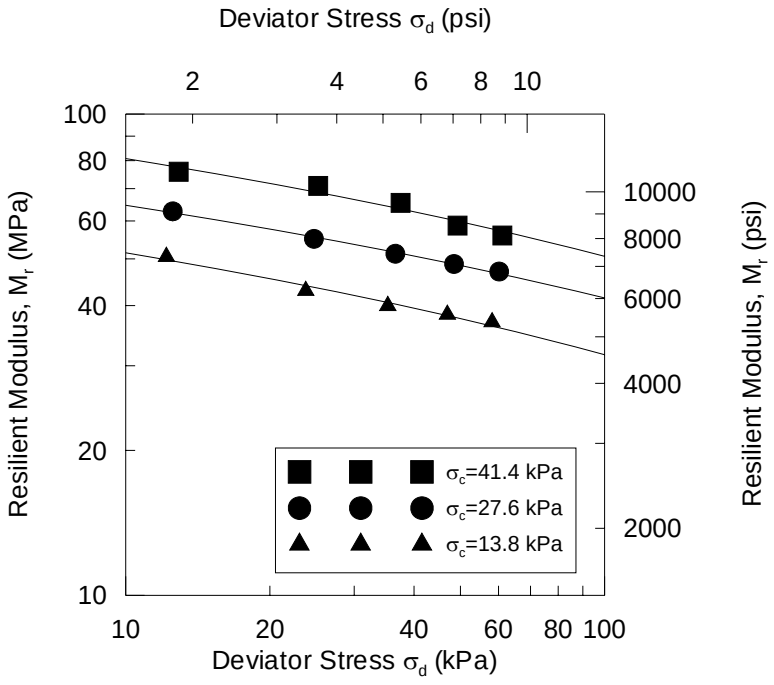

(b) Test 2

Figure 2.23 Results of Repeated Load Triaxial Test on Soil 1A

Table 2.12 Results of the Repeated Load Triaxial Test on Subgrade Soil 1B

Test Sequence	σ_c (kPa)	Test #1				Test #2			
		σ_d (kPa)	M_r (MPa)	M_r Standard Deviation	M_r COV (%)	σ_d (kPa)	M_r (MPa)	M_r Standard Deviation	M_r COV (%)
1	41.4	13.0	99.12	1.10	1.11	12.0	100.16	0.97	0.96
2		26.0	100.76	0.77	0.76	25.5	105.52	0.81	0.77
3		38.6	100.99	0.88	0.87	37.9	107.38	0.69	0.64
4		50.8	98.85	0.03	0.03	50.4	107.30	0.30	0.28
5		63.0	97.31	0.51	0.52	62.7	109.96	0.24	0.22
6	27.6	13.1	93.20	1.15	1.23	12.1	91.36	1.48	1.62
7		25.9	91.33	1.31	1.44	24.9	92.35	0.22	0.23
8		38.3	90.57	0.50	0.55	37.1	94.62	0.28	0.29
9		50.5	90.34	0.79	0.88	49.9	97.31	0.35	0.36
10		62.7	90.59	0.77	0.85	62.1	100.57	0.29	0.29
11	13.8	12.7	76.42	10.05	13.15	12.1	81.37	0.86	1.06
12		25.5	78.19	0.64	0.82	24.3	79.82	0.75	0.93
13		37.5	76.26	2.72	3.57	37.0	81.72	1.46	1.79
14		49.8	77.80	0.22	0.28	49.2	84.26	0.15	0.18
15		62.4	79.89	0.13	0.165	61.5	87.43	0.28	0.32

Table 2.13 Results of the Repeated Load Triaxial Test on Subgrade Soil 2

Test Sequence	σ_c (kPa)	Test #1				Test #2			
		σ_d (kPa)	M_r (MPa)	M_r Standard Deviation	M_r COV (%)	σ_d (kPa)	M_r (MPa)	M_r Standard Deviation	M_r COV (%)
1	41.4	12.6	63.32	1.18	1.87	12.8	67.33	1.64	2.44
2		25.4	60.32	2.43	4.02	25.6	62.66	0.27	0.44
3		37.9	58.58	0.13	0.23	38.1	59.86	0.37	0.62
4		50.3	56.92	0.19	0.34	50.3	57.47	0.20	0.35
5		62.8	58.85	0.35	0.68	62.7	58.17	0.17	0.29
6	27.6	12.3	51.89	0.35	0.68	12.3	52.70	0.09	0.16
7		24.8	46.43	0.28	0.61	25.4	46.14	0.35	0.77
8		37.2	45.68	0.12	0.26	38.0	45.10	0.11	0.25
9		49.7	46.40	0.20	0.44	50.7	45.88	0.20	0.44
10		62.1	47.82	0.05	0.09	63.0	46.82	0.06	0.14
11	13.8	12.5	37.36	2.85	7.64	13.1	37.95	0.38	1.00
12		24.9	33.55	0.15	0.45	25.5	32.79	0.19	0.59
13		37.8	34.37	0.15	0.43	38.3	33.36	0.17	0.50
14		49.9	34.85	0.06	0.18	50.4	33.77	0.15	0.43
15		62.6	35.89	0.12	0.35	63.0	35.00	0.09	0.26

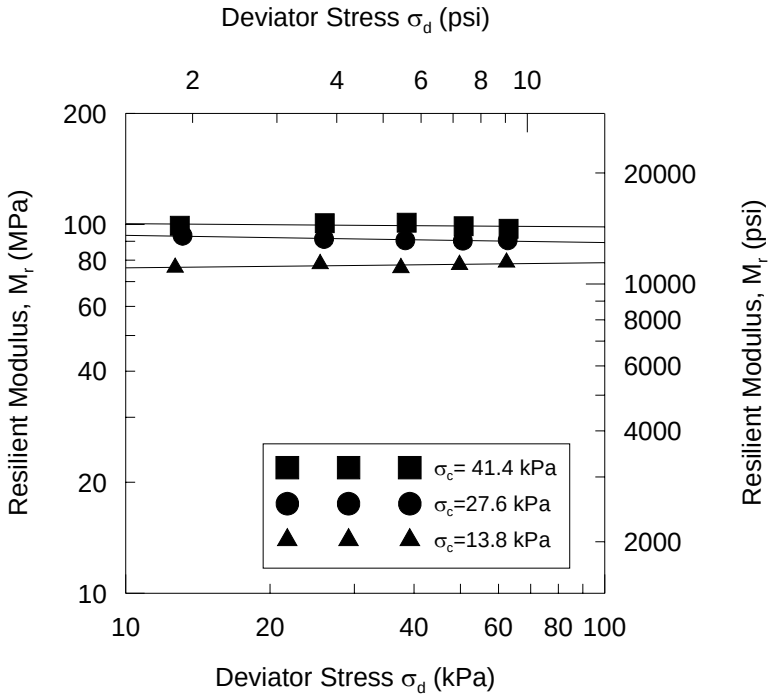

(a) Test 1

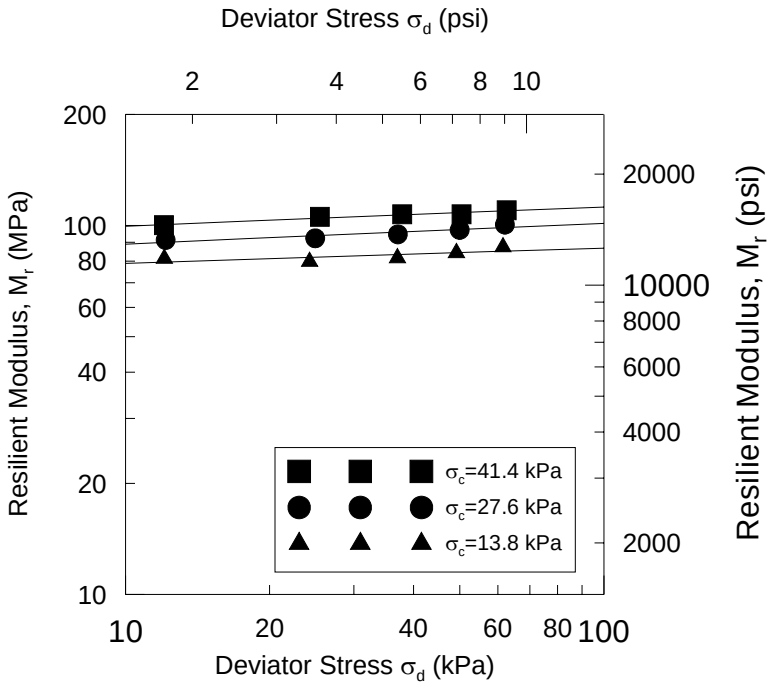

(b) Test 2

Figure 2.24 Results of Repeated Load Triaxial Test on Soil 1B

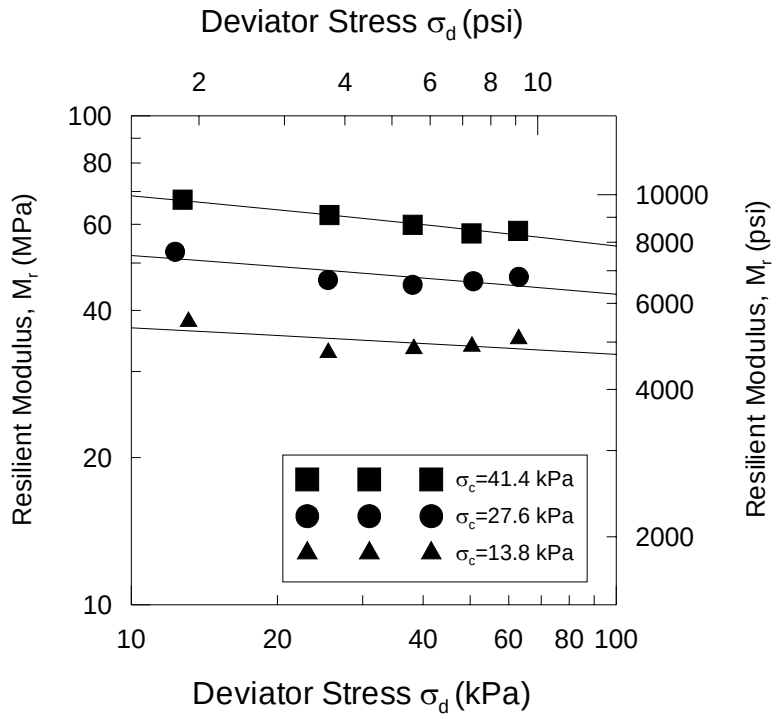

(a) Test 1

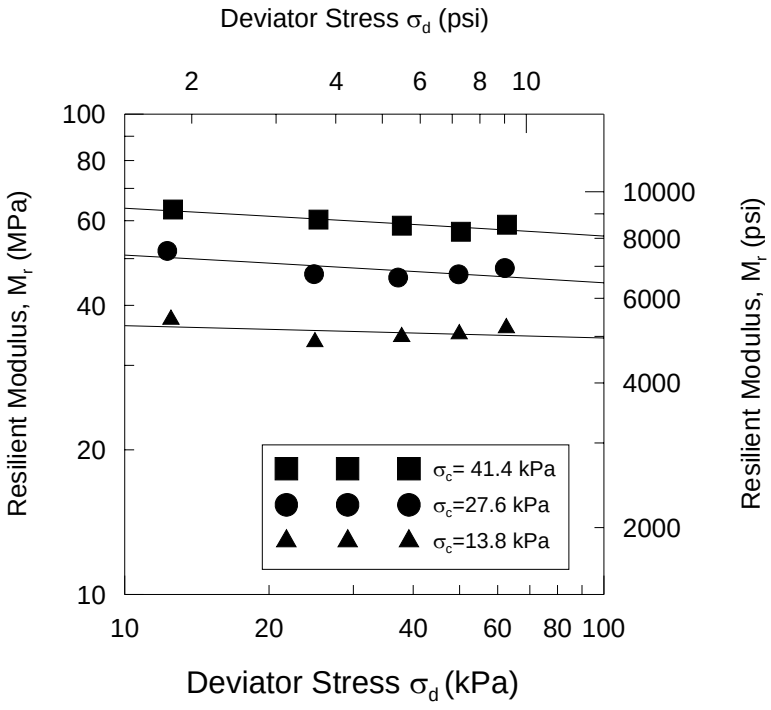

(b) Test 2

Figure 2.25 Results of Repeated Load Triaxial Test on Soil 2

Table 2.14 Results of the Falling Head Permeability Tests on Subgrade Soils

Subgrade Soil	Coefficient of Permeability k (cm/sec)
Soil 1A – Test 1	5.71×10^{-6}
Soil 1B – Test 1	1.409×10^{-6}
Soil 2 – Test 1	1.755×10^{-5}
Soil 2 – Test 2	1.750×10^{-5}

2.4.6 Laboratory Testing of Aggregates

Collected aggregates were subjected to standard laboratory tests to determine their physical properties, permeability, and compaction characteristics. Aggregate testing consisted of the following: moisture content, grain size distribution, specific gravity (G_s), absorption, and permeability. Aggregates were also subjected to compaction test to determine the optimum moisture content ($w_{opt.}$) and maximum dry unit weight (γ_{dmax}).

Repeated load triaxial test was conducted, to determine the resilient modulus of the investigated aggregates, following AASHTO T 307*: Standard Method of Test for Determining the Resilient Modulus of Soils and Aggregate Materials*. The test was conducted on compacted specimens at optimum moisture content ($w_{opt.}$) and maximum dry unit weight (γ_{dmax}). It should be noted that several test trials were attempted on aggregate specimens and difficulties were encountered during testing, especially with the open graded aggregates. It was difficult to keep the open grade aggregate standing inside the triaxial chamber under very low confining pressure. Therefore three plastic straps were used around the membrane to provide support while minimizing confinement on the specimen. Figure 2.26 depicts pictures of aggregate samples preparation and testing.

2.4.7 Results of Testing Program on Aggregates

The results of laboratory tests conducted to evaluate aggregate properties are presented in Table 2.15. The data on aggregate properties consists of moisture content; particle size analysis; specific gravity; absorption; maximum dry unit weight and optimum moisture content; and classification using the Unified Soil Classification System (USCS).

Figures 2.27 and 2.28 show the particle size distribution curves for the open graded and dense graded aggregates, respectively.

The results of the repeated load triaxial test on the dense graded and open graded aggregates are summarized in Tables 2.16 and 2.17, respectively. For dense graded aggregates, the resilient modulus showed increasing trend with the increase of bulk stress (σ_b). The coefficient of variation for the resilient modulus values shows very low values (0.09 to 0.52) indicating consistent test results. The variation of the resilient modulus

values with bulk stress for dense graded and open graded aggregates are shown in Figures 2.29 and 2.30, respectively.

Figure 2.26 Sample Preparation and Testing of Aggregates

Table 2.15 Properties of Aggregates

Aggregate Type	Moisture Content (%)	% Passing										Bulk Specific Gravity (SSD)	Apparent Specific Gravity	Absorption (%)	Unified Soil Classification System (USCS)
		1" Sieve	¾ " Sieve	3/8 " Sieve	Sieve #4	Sieve #10	Sieve #20	Sieve #40	Sieve #60	Sieve #140	Sieve #200				
Open Graded	0.178	100	97.7	62.1	26.7	3.8	3.1	3	2.8	2.6	2.4	2.743	2.809	1.34	GP Poorly Graded Gravel with Sand
Dense Graded	7.245	99.5	90.2	64.5	35.8	22.2	13.9	8.2	4.8	2.3	1.7	2.396	2.594	5.47	Well-Graded Gravel with Sand

Aggregate Type	Optimum Moisture Content W_{opt} (%)	Maximum Dry Unit Weight, γ_{dmax} (pcf)
Open Graded	3.52	128.4
Dense Graded	11.22	121.1

	Open graded aggregate	Dense graded aggregate
D_{10}	2.75	0.55
D_{30}	5	3.6
D_{60}	9	8.5
C_u	3.27	15.45
C_c	1.01	2.77

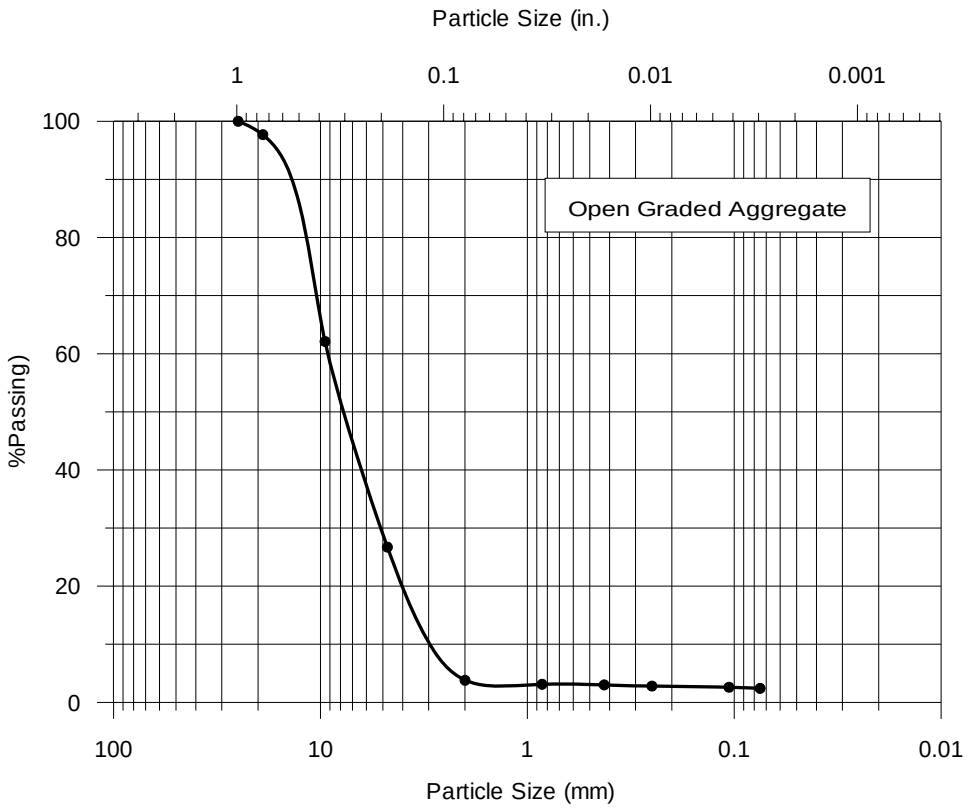

Figure 2.27 Particle Size Distribution Curve - Open Graded Aggregate

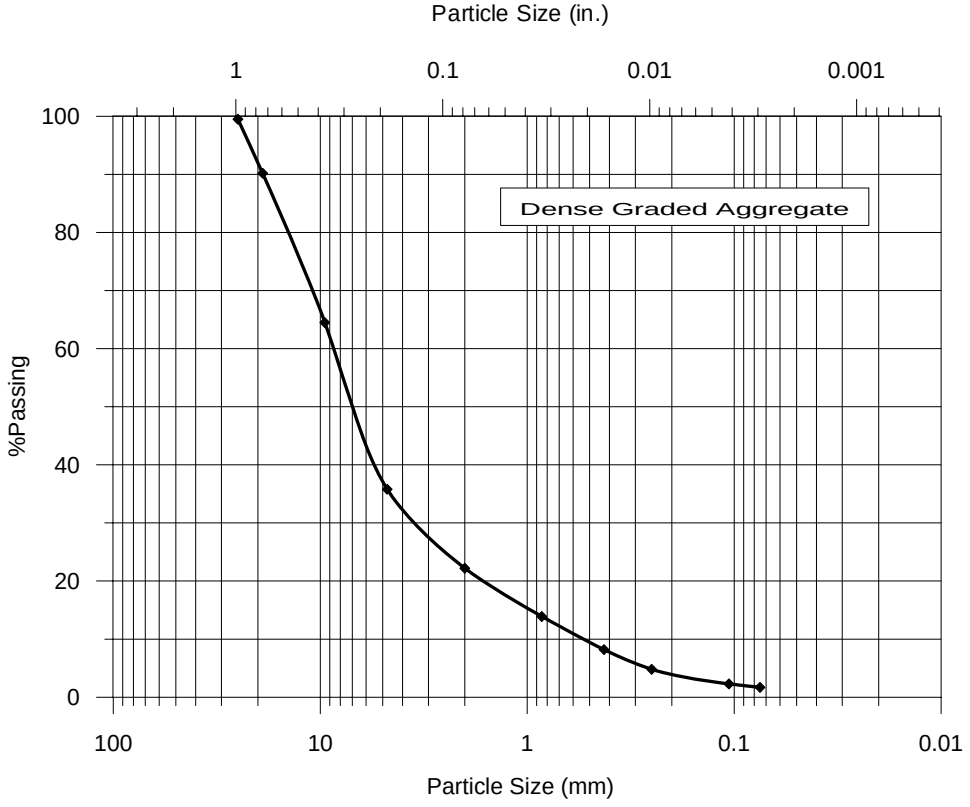

Figure 2.28 Particle Size Distribution Curve - Dense Graded Aggregate

Table 2.16 Repeated Load Triaxial Test Results on Dense Graded Aggregate

Test Sequence	σ_c (kPa)	Test #1				
		σ_d (kPa)	σ_b (kPa)	M_r (MPa)	M_r Standard Deviation	M_r COV (%)
1	20.7	18.4	80.5	79.91	0.41	0.52
2	20.7	36.8	98.9	96.56	0.24	0.25
3	20.7	56.3	118.4	119.90	0.22	0.19
4	34.5	30.7	134.2	91.28	0.21	0.23
5	34.5	62.8	166.3	129.16	0.25	0.20
6	34.5	94.2	197.7	165.06	0.23	0.14
7	68.9	62.7	269.4	129.54	0.26	0.20
8	68.9	123.9	330.6	183.60	0.24	0.13
9	68.9	185.4	392.1	203.06	0.18	0.09
10	103.4	61.6	371.8	104.86	0.11	0.11
11	103.4	93.8	404.0	136.99	0.16	0.11
12	103.4	187.4	497.6	212.14	0.23	0.11
13	137.9	93.4	507.1	135.53	0.29	0.21

Table 2.17 Repeated Load Triaxial Test Results on Open Graded Aggregate

Test Sequence	σ_c (kPa)	Test #2				
		σ_d (kPa)	σ_b (kPa)	M_r (MPa)	M_r Standard Deviation	M_r COV (%)
1	20.7	19.0	81.1	22.75	0.11	0.49
2	20.7	37.3	99.4	31.16	0.10	0.31
3	20.7	57.2	119.3	44.51	0.11	0.25
4	34.5	31.4	134.9	27.21	0.14	0.50
5	34.5	63.6	167.1	50.58	0.23	0.45
6	34.5	93.8	197.3	71.79	0.14	0.19
7	68.9	63.8	270.5	48.65	0.11	0.23
8	68.9	125.0	331.7	80.97	0.07	0.09
9	68.9	186.2	392.9	82.18	0.19	0.23
10	103.4	62.9	373.1	36.80	0.11	0.29
11	103.4	93.3	403.5	55.71	0.08	0.14
12	103.4	188.0	498.2	85.91	0.06	0.07
13	137.9	95.4	509.1	50.99	0.13	0.26

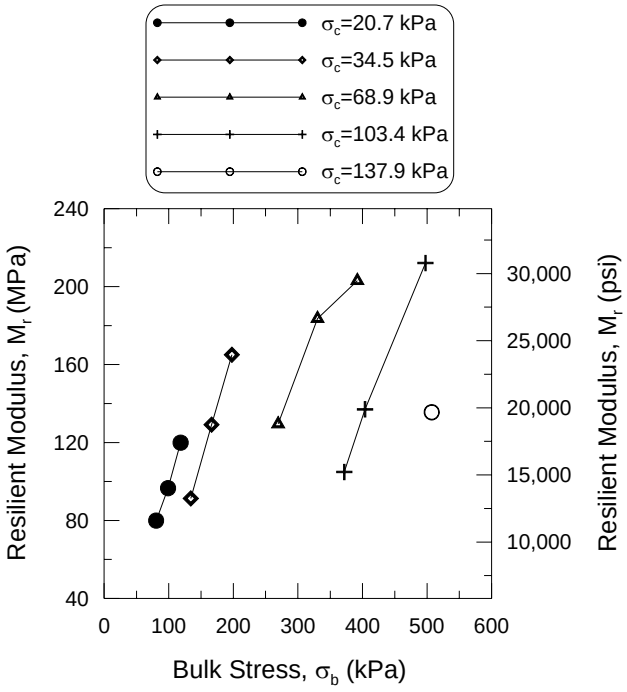

Figure 2.29 Triaxial Test Results - Dense Graded Aggregate Base

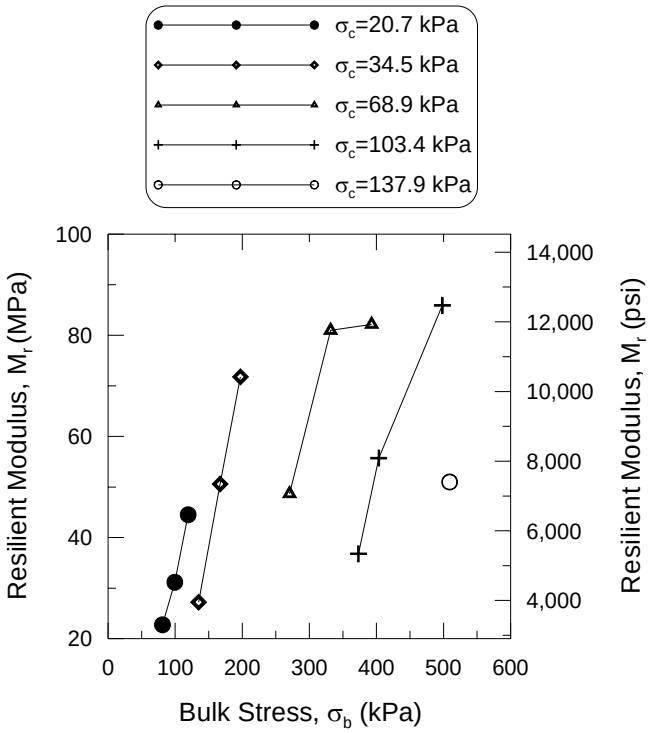

Figure 2.30 Triaxial Test Results - Open Graded Aggregate Base

CHAPTER 3.0
PERFORMANCE ANALYSIS

3.1 Introduction

A performance analysis of the HMA perpetual pavement was conducted to estimate the ride quality and levels of cracking and rutting after 50 years of trafficking. The mechanistic-empirical pavement design guide version 1.003 (MEPDG v1.003), which was developed under NCHRP Projects 1-37A and 1-40D, was utilized to provide baseline damage/cracking estimates. The stand-alone software programs KENLAYER and EVERSTRESS were also used to compute critical tensile strains in the HMA layer, which were then used to estimate the 50-year damage due to bottom-up fatigue cracking. Results of the laboratory testing described in Chapter 2 were used in conjunction with field data obtained with pavement sensors to provide necessary inputs for program executions.

3.2 MEPDG v1.003 Input Data Generation

The primary focus of the laboratory testing was the development of material characterization inputs for the mechanistic-empirical appraisal of projected pavement performance. Data provided from these tests were further analyzed to establish specific data inputs as required by each software package. A detailed analysis of weigh-in-motion (WIM) data obtained through pavement instrumentations was completed to establish the axle loading spectra data necessary for a thorough pavement analysis.

3.2.1. HMA Dynamic Modulus

The HMA dynamic modulus was determined at three temperatures and nine test frequencies for each of the three HMA mixtures used within the HMA perpetual pavement structure. Mixture-specific master curves for were developed in the general form of:

$$Log(E^*) = \delta + \frac{\alpha}{1 + e^{(\beta + \gamma \log t_r)}} \quad (3.1)$$

$$\log t_r = \log t - c(\log \eta - \log \eta_{TR}) \quad (3.2)$$

Where E* = HMA dynamic modulus, psi
δ = minimum value of E*
$\delta+\alpha$ = maximum value of E*
β,γ = parameters describing the shape of the sigmoidal function
t_r = time of loading at the reference temperature
t = time of loading, sec
c = regression constant
n = viscosity at test temperature, centiPoise
nTR = viscosity at reference temperature, centiPoise

All test data was entered into an Excel spreadsheet and the Solver function of Excel was utilized to determine the parameters δ, α, β, γ and c through nonlinear optimization. Table 3.1 provides the outputs of the optimization.

Table 3.1 Master Curve Parameters for HMA Mixtures

HMA Mixture	Optimization Parameters				
	δ	α	β	γ	c
SMA Surface Layer	4.1560	2.4244	-0.3918	0.4794	1.6996
E30x Middle Layer	2.5566	4.2125	-1.5623	0.3937	1.6214
C2 Bottom Layer	1.6841	5.1418	-1.7168	0.3650	1.6905

Figure 3.1 illustrates the master curves for each HMA mixture, plotted as a function of the reduced test time. For use within the MEPDG v1.003, dynamic modulus values must be provided for a minimum of 5 test temperatures for Level 1 analyses. The master curves developed for each mixture were used to generate additional E* values at test temperatures of 10F and 130F. Figure 3.2 illustrates these additional data points. Tables 3.2 through 3.4 provide a summary of the E* input values used for MEPDG v1.003 program executions. As shown, this data represents E* values at five temperatures and six loading frequencies. A maximum E* input value of 5,000,000 psi was utilized per MEPDG v1.003 restrictions.

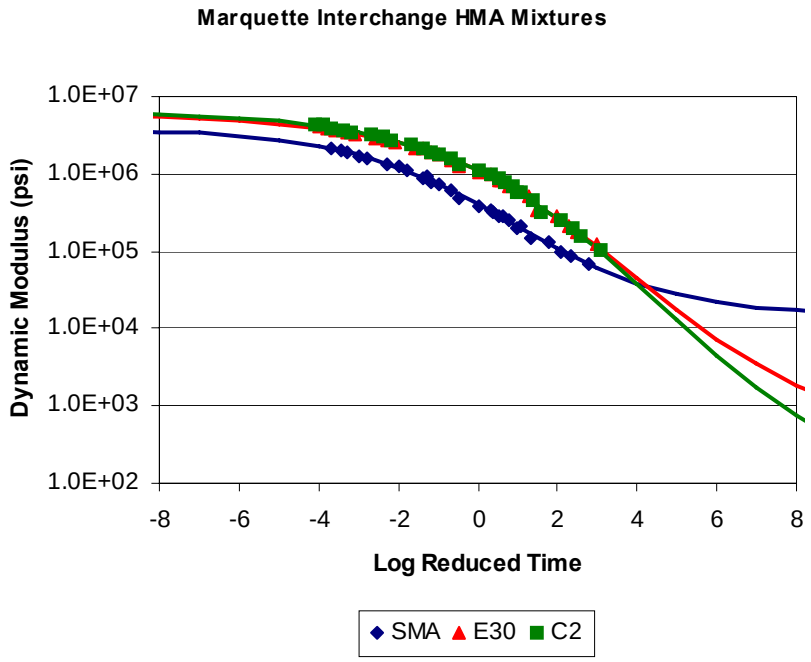

Figure 3.1 HMA Master Curves and Test E* Data

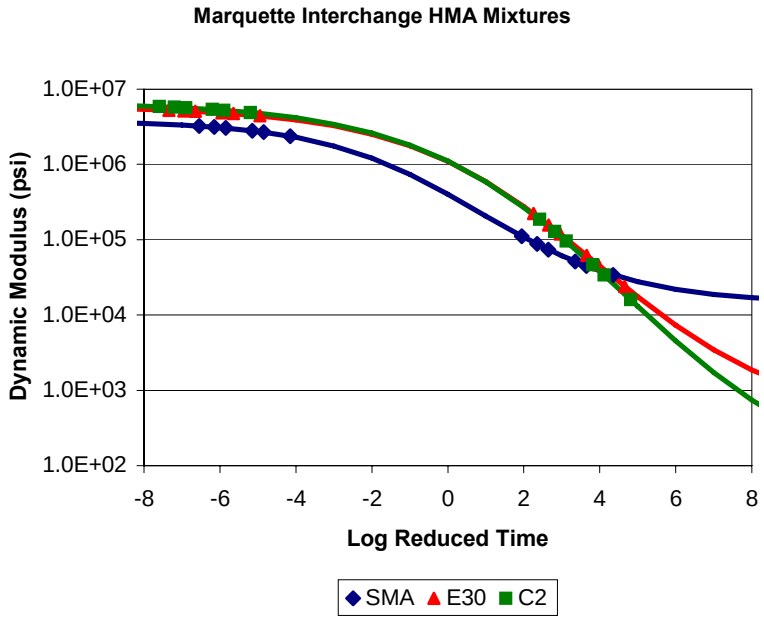

Figure 3.2 HMA Master Curves and Generated E* Data

Table 3.2 E* Input Values for SMA Surface Layer

Temperature °F	Loading Frequency, Hz					
	0.1	**0.5**	**1**	**5**	**10**	**25**
10*	2,373,081	2,692,045	2,813,119	3,055,455	3,143,740	3,246,704
40	907,700	1,241,200	1,363,000	1,728,400	1,887,900	2,154,700
70	200,100	330,600	382,800	617,700	725,000	893,200
99	69,600	98,600	133,400	211,700	249,400	321,900
130*	34,120	44,910	51,492	73,787	87,628	111,481

Table 3.3 E* Input Values for E30x Middle Layer

Temperature °F	Loading Frequency, Hz					
	0.1	**0.5**	**1**	**5**	**10**	**25**
10*	4,433,494	4,737,227	4,850,366	5,000,000	5,000,000	5,000,000
40	2,177,900	2,749,200	2,937,700	3,424,900	3,645,300	4,106,400
70	603,200	959,000	1,075,900	1,537,000	1,769,000	2,093,800
99	121,800	214,600	281,300	501,700	620,600	829,400
130*	23,959	46,506	61,965	119,299	156,712	221,943

Table 3.4 E* Input Values for C2 Bottom Layer

Temperature °F	Loading Frequency, Hz					
	0.1	**0.5**	**1**	**5**	**10**	**25**
10*	4,910,131	5,000,000	5,000,000	5,000,000	5,000,000	5,000,000
40	2,360,600	2,981,200	3,175,500	3,672,125	3,938,200	4,280,400
70	591,600	968,600	1,084,600	1,557,300	1,774,800	2,109,750
99	104,400	194,300	252,300	464,000	591,600	785,900
130*	16,005	33,970	46,746	95,729	128,499	186,556

Note: E* values shown for 10F and 130F were generated from master curves.

3.2.2. Binder Data

The primary HMA binder data used for Level 1 analyses includes the complex shear modulus, G*, and the phase angle, δ, determined after rolling thin film oven (RTFO) short-term. A minimum of 3 test temperatures are required for Level 1 analysis. Tables 3.5 and 3.6 provide MEPDG v1.003 input data for the PG 70-22 and PG 64-22 binders used for the HMA perpetual pavements.

Table 3.5 G* and δ Input Values for PG 70-22 within SMA Surface Layer

Temperature °F	Angular frequency = 10 rad/sec	
	G*, psi	Delta (°)
136	4,308	61.90
147	2,449	63.37
158	1,436	65.35

Table 3.6 G* and δ Input Values for PG 64-22 within E30x and C2 Layers

Temperature °F	Angular frequency = 10 rad/sec	
	G*, psi	Delta (°)
136	6,277	83.38
147	2,681	85.98
158	1,236	88.75

3.2.3. Unbound Aggregate Data

MEPDG v1.003 currently recommends the use of Level 3 analysis for unbound aggregates. The primary input data for Level 3 analyses includes the gradation, plasticity and compaction properties of each aggregate layer. Table 3.7 provides input values used for the unbound open graded, dense graded, and select crushed material aggregate layers.

Table 3.7 Input Data for Unbound Aggregates

Property	Open Graded	Dense Graded	Select Crushed
Plasticity Index	0	0	0
Liquid Limit	0	0	0
Max Dry Unit Weight, pcf	128.4	121.1	125.0
Optimum Moisture, %	3.5	11.2	5.0
Percent Passing			
3-1/2”			97.6
1-1/2”		100	35.0
1”	100	99.5	
¾”	97.7	90.2	
3/8”	62.1	64.5	
No. 4	26.7	35.8	
No. 10	3.8	22.2	10.0
No. 20	3.1	13.9	
No. 40	3.0	8.2	
No. 200	2.4	1.7	2.0

3.2.4. Soils Data

MEPDG v1.003 currently recommends the use of Level 3 analysis for soils. The primary input data for Level 3 analyses includes the gradation, plasticity, compaction properties and hydraulic conductivity of each soil layer. Table 3.8 provides input values used for the two soil layers.

Table 3.8 Primary Input Data for Soil Layers

Property	Top 12”	Remaining
AASHTO Class	A-4	A-4
Plasticity Index	4	7
Liquid Limit	17	24
Max Dry Unit Weight, pcf	127.5	119.0
Optimum Moisture, %	10.0	12.5
Sat Hydraulic Conductivity, ft/hr	6.7 E-4	1.7 E-4
Percent Passing		
No. 40	100	100
No. 200	78	94
20 μm	31	48
2 μm	14	26
1 μm	12	24

3.2.4. Traffic Data

The primary traffic data for Level 1 analyses includes general traffic factors such as the initial two-way annual average daily truck traffic (AADTT), directional factor (DF), lane distribution factor (LDF), annual growth factor (r) as well specific loading factors such as the distribution of truck traffic by class, the hourly distribution of truck traffic, the average axles per truck class, and axle load spectra for each axle type. Pavement design data was used to generate the general traffic factors, which are summarized in Table 3.9. Data collected from the on-site WIM system was used to generate the specific loading factors. Tables 3.10 through 3.16 provide the specific truck loading input data.

Table 3.9 General Traffic Inputs Developed From Pavement Design Data

Traffic Factor	Input Value
1999 ADT	138,800
2025 ADT	152,700
% Trucks	11
Average Annual Growth Rate, %	0.4
2006 2-way AADTT	15,950
Directional Factor, %	55
No. of Lanes in Design Direction	4
Lane Distribution Factor, %	50
Operational Speed	55

Table 3.10 Truck Traffic Distribution by Class Developed From WIM Data

FHWA Vehicle Class	% of Total Trucks
4	19.6
5	30.3
6	5.5
7	4.6
8	3.0
9	35.9
10	0.7
11	0.3
12	0.1
Total	100

Table 3.11 Hourly Truck Traffic Distribution Developed From WIM Data

Hour Beginning	% of All Trucks	Hour Beginning	% of All Trucks
Midnight	1.1%	Noon	7.6%
1:00 am	1.0%	1:00 pm	6.0%
2:00 am	0.9%	2:00 pm	4.9%
3:00 am	1.2%	3:00 pm	5.7%
4:00 am	2.1%	4:00 pm	3.1%
5:00 am	4.8%	5:00 pm	2.2%
6:00 am	8.0%	6:00 pm	2.5%
7:00 am	10.4%	7:00 pm	2.3%
8:00 am	6.8%	8:00 pm	2.0%
9:00 am	6.7%	9:00 pm	1.2%
10:00 am	8.9%	10:00 pm	1.2%
11:00 am	8.2%	11:00 pm	1.2%

Table 3.12 Average Axles per Truck Developed From WIM Data

FHWA Class	Single Axle	Tandem Axle	Tridem Axle	Quad Axle
4	1.82	0.18	0.00	0.00
5	2.00	0.00	0.00	0.00
6	1.00	1.00	0.00	0.00
7	1.00	0.00	0.14	0.86
8	3.00	0.00	0.00	0.00
9	1.00	2.00	0.00	0.00
10	1.00	1.00	1.00	0.00
11	5.00	0.00	0.00	0.00
12	4.00	1.00	0.00	0.00

Table 3.13 Single Axle Load Spectra Developed From WIM Data

Axle Load, kips	FHWA Vehicle Classification								
	4	5	6	7	8	9	10	11	12
3	0.22	1.02	0.00	0.23	3.38	0.21	0.00	3.18	0.00
4	0.54	13.01	0.64	0.16	0.97	0.21	0.00	2.45	0.00
5	0.63	11.43	0.43	0.17	0.52	0.12	0.00	4.66	3.82
6	3.13	8.07	0.36	0.16	2.47	0.20	1.37	2.16	4.79
7	8.25	12.19	2.32	0.17	5.08	0.29	1.96	1.73	8.66
8	15.68	15.12	3.76	1.53	11.87	2.54	1.96	3.46	6.75
9	14.29	10.82	13.79	3.33	15.25	9.94	5.37	8.83	8.30
10	6.62	7.94	17.04	3.08	18.93	20.43	29.34	11.76	8.23
11	7.31	7.46	19.55	1.70	9.70	30.26	23.33	5.88	6.60
12	7.90	3.63	13.16	4.01	4.14	26.67	26.67	10.30	5.69
13	7.32	2.26	7.64	3.86	4.52	7.68	6.00	5.70	8.06
14	5.81	1.84	4.76	9.05	3.67	1.17	4.00	2.24	11.82
15	2.67	1.37	9.40	8.00	1.98	0.24	0.00	6.76	7.00
16	3.36	0.69	2.38	8.18	2.83	0.04	0.00	3.68	12.06
17	3.80	1.23	0.78	8.64	1.97	0.00	0.00	4.41	2.94
18	2.07	0.75	0.75	11.13	0.85	0.00	0.00	4.08	2.93
19	1.45	0.41	1.13	10.23	3.96	0.00	0.00	5.06	2.35
20	1.98	0.23	0.23	13.94	3.95	0.00	0.00	4.83	0.00
21	4.18	0.25	0.22	6.97	0.51	0.00	0.00	8.83	0.00
22	1.58	0.03	0.28	2.91	2.32	0.00	0.00	0.00	0.00
23	0.68	0.02	0.45	2.09	0.95	0.00	0.00	0.00	0.00
24	0.24	0.19	0.58	0.46	0.18	0.00	0.00	0.00	0.00
25	0.19	0.04	0.35	0.00	0.00	0.00	0.00	0.00	0.00
26	0.03	0.00	0.00	0.00	0.00	0.00	0.00	0.00	0.00
27	0.03	0.00	0.00	0.00	0.00	0.00	0.00	0.00	0.00
28	0.04	0.00	0.00	0.00	0.00	0.00	0.00	0.00	0.00
Total	100	100	100	100	100	100	100	100	100

Table 3.14 Tandem Axle Load Spectra Developed From WIM Data

Axle Load, kips	FHWA Vehicle Classification								
	4	5	6	7	8	9	10	11	12
6	0.00	n.a.	0.00	n.a.	0.00	0.24	0.00	n.a.	0.00
8	0.00	n.a.	0.45	n.a.	0.00	0.45	0.00	n.a.	0.00
10	0.00	n.a.	16.84	n.a.	3.04	2.94	0.00	n.a.	0.00
12	0.00	n.a.	24.56	n.a.	15.87	8.43	0.22	n.a.	0.00
14	1.36	n.a.	2.33	n.a.	21.90	11.30	4.44	n.a.	4.31
16	3.28	n.a.	7.51	n.a.	9.86	10.28	14.31	n.a.	17.24
18	4.63	n.a.	5.82	n.a.	18.69	8.36	6.74	n.a.	17.24
20	2.64	n.a.	10.91	n.a.	7.66	6.35	2.81	n.a.	18.07
22	14.94	n.a.	3.63	n.a.	12.53	4.39	2.19	n.a.	19.61
24	5.07	n.a.	4.42	n.a.	2.64	4.50	2.18	n.a.	19.60
26	7.11	n.a.	3.98	n.a.	5.31	4.04	5.08	n.a.	3.93
28	15.18	n.a.	2.55	n.a.	0.59	2.94	3.76	n.a.	0.00
30	11.88	n.a.	1.82	n.a.	0.60	4.44	2.67	n.a.	0.00
32	11.01	n.a.	2.99	n.a.	0.59	4.33	6.26	n.a.	0.00
34	10.97	n.a.	7.08	n.a.	0.60	4.90	16.00	n.a.	0.00
36	3.94	n.a.	0.72	n.a.	0.12	7.68	20.00	n.a.	0.00
38	1.58	n.a.	0.28	n.a.	0.00	6.69	7.82	n.a.	0.00
40	1.67	n.a.	0.28	n.a.	0.00	4.79	2.30	n.a.	0.00
42	2.38	n.a.	0.56	n.a.	0.00	2.14	2.30	n.a.	0.00
44	0.33	n.a.	0.44	n.a.	0.00	0.51	0.92	n.a.	0.00
46	0.33	n.a.	0.30	n.a.	0.00	0.13	0.00	n.a.	0.00
48	0.34	n.a.	0.32	n.a.	0.00	0.05	0.00	n.a.	0.00
50	0.49	n.a.	0.52	n.a.	0.00	0.02	0.00	n.a.	0.00
52	0.62	n.a.	0.88	n.a.	0.00	0.03	0.00	n.a.	0.00
54	0.25	n.a.	0.30	n.a.	0.00	0.03	0.00	n.a.	0.00
56	0.00	n.a.	0.25	n.a.	0.00	0.02	0.00	n.a.	0.00
58	0.00	n.a.	0.26	n.a.	0.00	0.02	0.00	n.a.	0.00
Total	100	n.a.	100	n.a.	100	100	100	n.a.	100

Table 3.15 Tridem Axle Load Spectra Developed From WIM Data

Axle Load, kips	FHWA Vehicle Classification								
	4	5	6	7	8	9	10	11	12
12	n.a.	n.a.	n.a.	0.00	n.a.	n.a.	7.16	n.a.	n.a.
15	n.a.	n.a.	n.a.	0.00	n.a.	n.a.	13.31	n.a.	n.a.
18	n.a.	n.a.	n.a.	0.00	n.a.	n.a.	7.26	n.a.	n.a.
21	n.a.	n.a.	n.a.	0.00	n.a.	n.a.	7.27	n.a.	n.a.
24	n.a.	n.a.	n.a.	1.64	n.a.	n.a.	5.21	n.a.	n.a.
27	n.a.	n.a.	n.a.	2.47	n.a.	n.a.	2.20	n.a.	n.a.
30	n.a.	n.a.	n.a.	2.47	n.a.	n.a.	2.20	n.a.	n.a.
33	n.a.	n.a.	n.a.	9.15	n.a.	n.a.	9.32	n.a.	n.a.
36	n.a.	n.a.	n.a.	7.28	n.a.	n.a.	8.63	n.a.	n.a.
39	n.a.	n.a.	n.a.	10.32	n.a.	n.a.	5.56	n.a.	n.a.
42	n.a.	n.a.	n.a.	2.13	n.a.	n.a.	3.13	n.a.	n.a.
45	n.a.	n.a.	n.a.	2.12	n.a.	n.a.	16.46	n.a.	n.a.
48	n.a.	n.a.	n.a.	2.13	n.a.	n.a.	10.80	n.a.	n.a.
51	n.a.	n.a.	n.a.	20.29	n.a.	n.a.	1.49	n.a.	n.a.
54	n.a.	n.a.	n.a.	20.00	n.a.	n.a.	0.00	n.a.	n.a.
57	n.a.	n.a.	n.a.	16.19	n.a.	n.a.	0.00	n.a.	n.a.
60	n.a.	n.a.	n.a.	3.81	n.a.	n.a.	0.00	n.a.	n.a.
Total	n.a.	n.a.	n.a.	100	n.a.	n.a.	100	n.a.	n.a.

Table 3.16 Quad Axle Load Spectra Developed From WIM Data

Axle Load, kips	FHWA Vehicle Classification								
	4	5	6	7	8	9	10	11	12
33	n.a.	n.a.	n.a.	0.00	n.a.	n.a.	n.a.	n.a.	n.a.
36	n.a.	n.a.	n.a.	2.63	n.a.	n.a.	n.a.	n.a.	n.a.
39	n.a.	n.a.	n.a.	0.98	n.a.	n.a.	n.a.	n.a.	n.a.
42	n.a.	n.a.	n.a.	0.64	n.a.	n.a.	n.a.	n.a.	n.a.
45	n.a.	n.a.	n.a.	1.43	n.a.	n.a.	n.a.	n.a.	n.a.
48	n.a.	n.a.	n.a.	2.92	n.a.	n.a.	n.a.	n.a.	n.a.
51	n.a.	n.a.	n.a.	4.69	n.a.	n.a.	n.a.	n.a.	n.a.
54	n.a.	n.a.	n.a.	4.79	n.a.	n.a.	n.a.	n.a.	n.a.
57	n.a.	n.a.	n.a.	10.28	n.a.	n.a.	n.a.	n.a.	n.a.
60	n.a.	n.a.	n.a.	12.06	n.a.	n.a.	n.a.	n.a.	n.a.
63	n.a.	n.a.	n.a.	23.25	n.a.	n.a.	n.a.	n.a.	n.a.
66	n.a.	n.a.	n.a.	15.05	n.a.	n.a.	n.a.	n.a.	n.a.
69	n.a.	n.a.	n.a.	8.98	n.a.	n.a.	n.a.	n.a.	n.a.
72	n.a.	n.a.	n.a.	5.91	n.a.	n.a.	n.a.	n.a.	n.a.
75	n.a.	n.a.	n.a.	4.53	n.a.	n.a.	n.a.	n.a.	n.a.
78	n.a.	n.a.	n.a.	0.82	n.a.	n.a.	n.a.	n.a.	n.a.
81	n.a.	n.a.	n.a.	0.76	n.a.	n.a.	n.a.	n.a.	n.a.
84	n.a.	n.a.	n.a.	0.28	n.a.	n.a.	n.a.	n.a.	n.a.
Total	n.a.	n.a.	n.a.	100	n.a.	n.a.	n.a.	n.a.	n.a.

3.2.5. Environmental Data

The primary environmental data for site-specific performance analyses includes air and pavement temperatures, precipitation, wind speed, % sunshine and frost penetration. The enhanced integrated climatic model (EICM) included within MEPDG v1.003 was utilized to compute monthly average values based on the previous nine years of environmental data available for the Milwaukee area. Tables 3.17 to 3.19 provide general site information used for environmental data computations. The estimated monthly air and pavement layer temperatures are provided in Tables 3.20 to 3.23.

Table 3.17 General Site Information for Project Analysis

Project Location	Milwaukee, WI
Latitude (degrees.minutes)	42.57 N
Longitude (degrees.minutes)	87.54 W
Elevation, ft	687
Depth of Water Table, ft	12
Mean Annual Air Temperature, F	48.6
Mean Annual Rainfall, in	30.9
Freezing Index (F-days)	756.5
Average Number of Freeze-Thaw Cycles	52

Table 3.18 Rainfall Statistics for Project Analysis

Month	**Mean Rainfall (in)**	**Std. Dev. (in)**
January	1.65	0.87
February	1.67	1.13
March	3.24	1.39
April	4.22	2.39
May	3.88	1.85
June	3.22	1.19
July	3.3	1.65
August	2.93	1.71
September	1.93	1.1
October	1.73	1.09
November	1.32	0.59

Table 3.19 Selected Monthly Data for 1997-1998

Month	Min. Temp. (ºF)	Max. Temp. (ºF)	Average Temp. (ºF)	Max. Range (ºF)	Precip. (in.)	Average Wind (mph)	Average Sun (%)	Number Wet Days	Max. Frost (in.)
1/1997	-8	59	20.3	27.5	1.27	10.3	49	19	50
2/1997	12	51.1	28.9	26.1	2.38	9.1	44.2	15	50.4
3/1997	10.9	73.9	35.8	30.9	0.67	9.7	52.4	19	40.3
4/1997	19.9	78.1	43.3	31.2	1.98	9.6	59.8	18	5.2
5/1997	34	72	49.1	27.9	1.95	10	29.9	16	0
6/1997	46	90	64.6	34	7.48	7.2	42.4	12	0
7/1997	52	91.9	69.2	24	3.59	8	41.7	15	0
8/1997	54	88	66.6	21	3.95	7.4	35.4	14	0
9/1997	42.1	82	61.6	26	2.92	8.1	47.5	14	0
10/1997	26.1	87.1	51.8	36	1.11	8.6	44.9	11	3
11/1997	14	55.9	35.1	21.1	1.03	8.5	28	20	16.3
12/1997	10	48	30.4	18	0.78	8.7	20.6	17	24.4
1/1998	-4	54	27.7	26	1.94	9.2	13.3	24	32.8
2/1998	24.1	50	34.8	18	2.03	7.9	13.5	17	22.7
3/1998	10	75	36	33	3.15	11.2	22.7	18	27.1
4/1998	28	70	45.8	25	4.16	8.7	34.3	16	0.5
5/1998	45	88	60.1	27	2.48	8.8	45.2	15	0
6/1998	43	93.9	66.2	27	2.83	7.5	38.2	15	0
7/1998	55.9	90	72.6	23.1	1.79	7.5	50.5	12	0
8/1998	57.9	89.1	72.6	21.9	4.34	6.9	46.1	15	0
9/1998	46	90	67.2	27	2.17	7.2	58.6	12	0
10/1998	34	72	54	22.8	2.47	8.4	43.4	12	0
11/1998	25	66	42.9	36	2.69	10.5	36.4	12	2.8
12/1998	-3	64	32.2	34	0.88	8.8	49	9	26.9

Table 3.20 Estimated Monthly Temperature Data - Pavement Surface

Month	1st Quintile (ºF)	2nd Quintile (ºF)	3rd Quintile (ºF)	4th Quintile (ºF)	5th Quintile (ºF)	Mean Temp. (ºF)	Std. Dev. (ºF)
January	11.3	21.1	26.9	31.7	40	26.2	10.2
February	19.9	28.1	32.9	37.4	45.4	32.7	9.1
March	25.3	33	38.4	45.2	57.6	39.9	11.7
April	36.2	43.6	50	58.8	74.3	52.6	13.8
May	46.4	53.9	60.7	68.9	82.6	62.5	13
June	56.3	66.1	73.5	83.3	96.1	75.1	14.3
July	64	71.6	78.6	87.8	99.2	80.3	12.7
August	63.1	69.4	75.8	84.9	96.4	77.9	12.1
September	53.3	61.6	68.1	76.2	90.4	69.9	13.3
October	41.3	49	54.8	61.8	74.1	56.2	11.8
November	29.6	37.1	42.3	47.6	56.5	42.7	9.6
December	18.1	25.7	31.3	36.2	43.4	31	9.1

Table 3.21 Estimated Monthly Temperatures - SMA Surface Layer

Month	1st Quintile (ºF)	2nd Quintile (ºF)	3rd Quintile (ºF)	4th Quintile (ºF)	5th Quintile (ºF)	Mean Temp. (ºF)	Std. Dev. (ºF)
January	12.6	21.6	26.9	31.4	39	26.3	9.4
February	21.1	28.5	32.9	36.9	43.9	32.7	8.1
March	26.5	33.6	38.5	44.7	55.7	39.8	10.5
April	37.4	44.5	50.3	58	71.9	52.4	12.4
May	47.8	54.7	60.8	68.1	80.2	62.3	11.6
June	57.6	66.9	73.8	82.1	93.6	74.8	12.8
July	65.7	72.7	78.8	86.6	96.7	80.1	11.1
August	64.8	70.5	76.2	83.8	94	77.9	10.6
September	54.9	62.6	68.6	75.7	88	70	11.8
October	42.6	49.9	55.1	61.6	72.4	56.3	10.7
November	30.9	37.8	42.7	47.5	55.4	42.9	8.8
December	19.4	26.4	31.5	36.1	42.7	31.2	8.4

Table 3.22 Estimated Monthly Temperatures - E30x Middle Layer

Month	1st Quintile (ºF)	2nd Quintile (ºF)	3rd Quintile (ºF)	4th Quintile (ºF)	5th Quintile (ºF)	Mean Temp. (ºF)	Std. Dev. (ºF)
January	16.5	22.9	27.3	30.8	36.5	26.8	7.2
February	24.2	29.5	32.7	35.6	40.2	32.5	5.7
March	29.5	34.8	38.5	43.1	50.6	39.3	7.6
April	40.5	46.5	50.9	56.2	65.7	52	9
May	51.2	56.7	61	65.9	73.9	61.7	8.1
June	60.9	68.5	73.9	79.3	87.1	73.9	9.3
July	70	75.3	79.1	83.4	90	79.6	7.1
August	69	73.3	77	81.2	87.6	77.6	6.7
September	59.2	65.2	69.7	74.4	82	70.1	8.2
October	46.5	51.9	56	60.9	68.4	56.8	7.9
November	34.4	39.6	43.5	47.2	53	43.5	6.7
December	23.1	28	32.2	36	40.9	32.1	6.5

Table 3.23 Estimated Monthly Temperatures - C2 Bottom Layer

Month	1st Quintile (ºF)	2nd Quintile (ºF)	3rd Quintile (ºF)	4th Quintile (ºF)	5th Quintile (ºF)	Mean Temp. (ºF)	Std. Dev. (ºF)
January	23.6	26.3	28.3	30.2	33.7	28.4	3.6
February	28.3	30.2	31.6	33.5	35.9	31.9	2.8
March	32.6	35.3	37.5	40.2	44.7	38.1	4.4
April	43.5	47.3	50.4	53.5	58.7	50.7	5.5
May	54	57.3	59.9	62.6	66.8	60.1	4.6
June	62.9	67.9	71.8	75.4	79.5	71.5	6
July	73.7	76.1	77.9	79.7	82.3	78	3.1
August	73	74.8	76.3	78.3	81.3	76.7	3
September	63.6	67.5	70.3	73.5	76.9	70.3	4.8
October	51	54.4	57.2	61	65.4	57.8	5.2
November	39.2	42.9	45.5	47.7	51.7	45.4	4.5
December	29.7	31.7	34	36.7	39.9	34.4	3.8

3.3 MEPDG v1.003 Performance Prediction

The key outputs of the MEPDG v1.003 analysis are predicted levels of cracking, rutting and roughness. Cracking is predicted based on top-down and bottom-up fatigue cracking as well as top down thermal cracking. Pavement rutting is predicted individually for the HMA, aggregate base and subgrade layers and also as an overall combined total. Surface roughness is predicted as a function of the International Roughness Index (IRI).

3.3.1 – 55 mph Operational Speed

Figures 3.3 through 3.8 provide outputs of the MEPDG v1.003 analysis for an operational speed of 55 mph. As indicated in Figures 3.3 through 3.8, the HMA perpetual pavement constructed within the North-Leg of the Marquette Interchange is expected to perform as expected. The median value for top-down cracking initiated by fatigue damage after 50 years is predicted to be approximately 40 ft/mi at the surface and essentially zero at a depth of 0.5 inches. At the 90% reliability level, the terminal level of 1,000 ft/mi of top-down fatigue cracking is expected around year 16, again being limited to the top 0.5 inches of the pavement. Median values of bottom-up fatigue cracking after 50 years of trafficking is predicted to cover 2.75% of the total lane area, or approximately 5.5% of the loaded wheel paths. At the 90% reliability level, bottom-up fatigue damage is expected over 15% of the total lane area, or 30% of the loaded wheel paths, which are well below typical design limits of 25% and 50%, respectively.

The median values for predicted thermal cracking are essentially zero. At the 90% reliability level, thermal crack lengths of approximately 80 ft/mi are predicted after 50 years, well below typical design limits of 1,000 ft/mi. After 50 years of trafficking, median values for HMA and total rutting are predicted at 0.18 and 0.45 inches, respectively. At the 90% reliability level, total rutting is predicted to be 0.56 inches, which is slightly above the typical design limit of 0.5 inches. The median value for predicted IRI after 50 years is 210 in/mi, which exceeds a typical design limit of 175 in/mi. At the 90% reliability level, the design limit of 175 in/mi is expected to occur in year 27.

The above discussion related various distress measures to typical design limits after 50 years of trafficking, assuming no major rehabilitation efforts occur during that service period. Typical expectations for HMA perpetual pavements in Wisconsin, as presented in WisDOT Facilities Development Manual Procedure 14-15-10 – Life Cycle Computation Parameters, result in an initial service life of 16 – 22 years. At this time a surface mill and overlay, which is the standard rehabilitation option, would effectively remove and correct any top-down cracking and/or pavement rutting. For conservative analysis, the surface mill and overlay rehabilitation is considered to have no effect on the progression of bottom-up fatigue cracking.

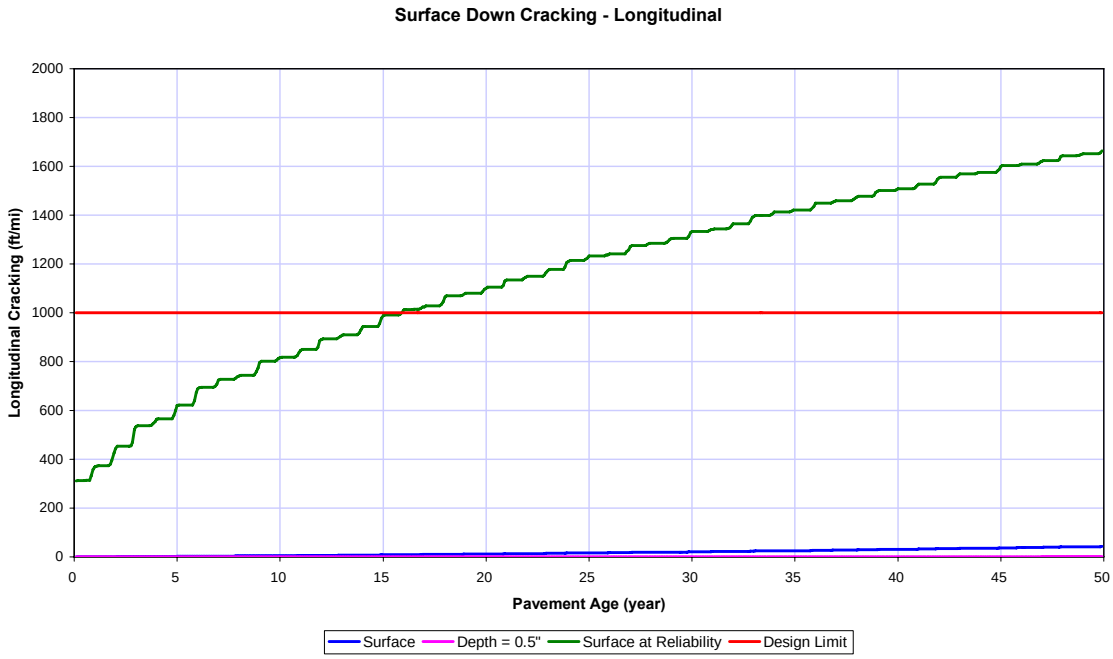

Figure 3.3 Predicted Top-Down Fatigue Cracking - 55 mph Design Speed

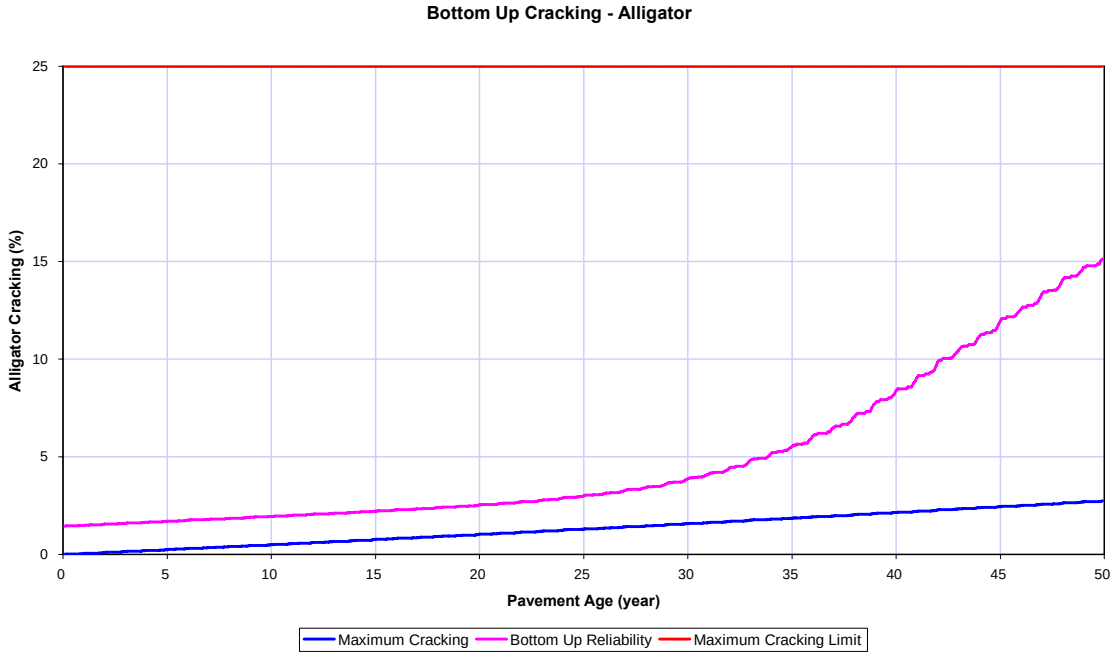

Figure 3.4 Predicted Bottom-Up Fatigue Cracking - 55 mph Design Speed

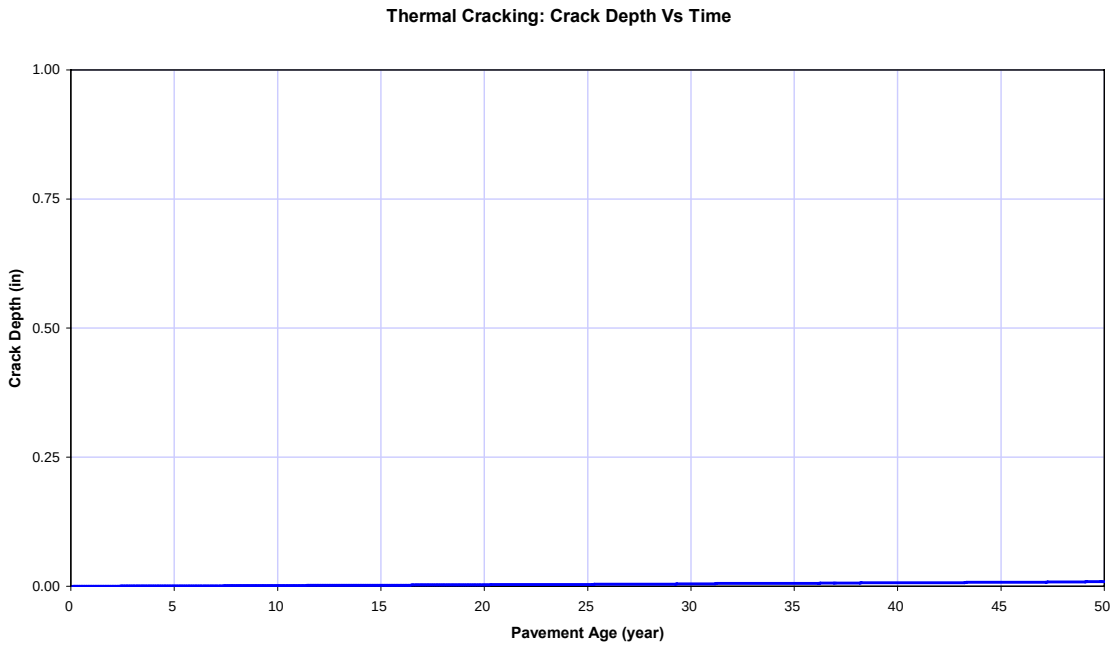

Figure 3.5 Predicted Thermal Crack Depth - 55 mph Design Speed

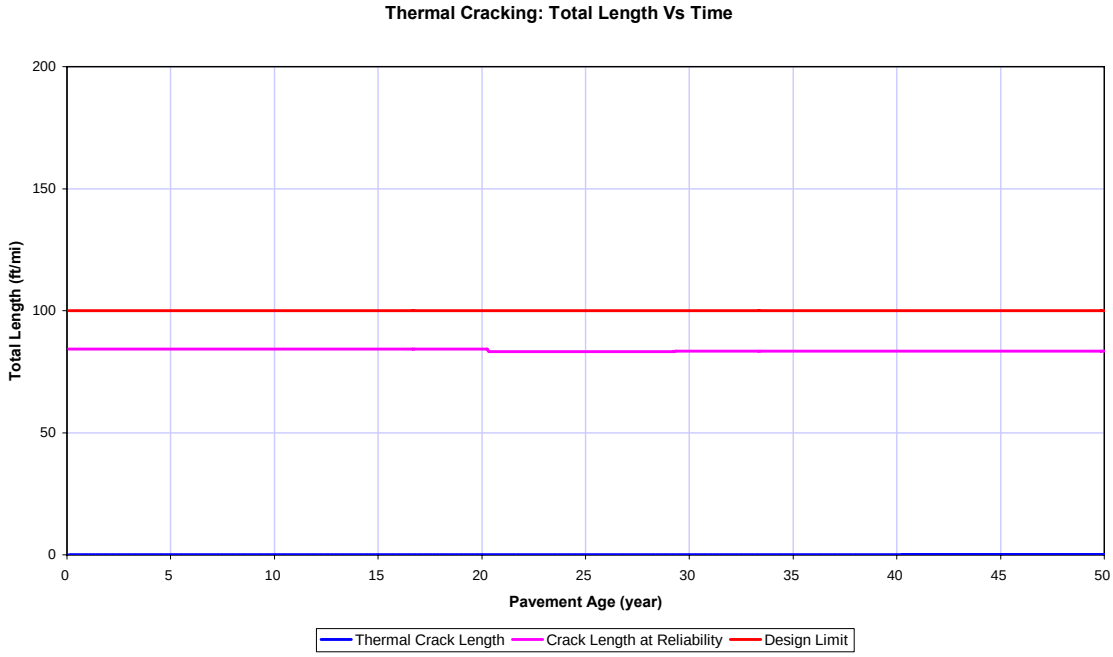

Figure 3.6 Predicted Thermal Crack Length - 55 mph Design Speed

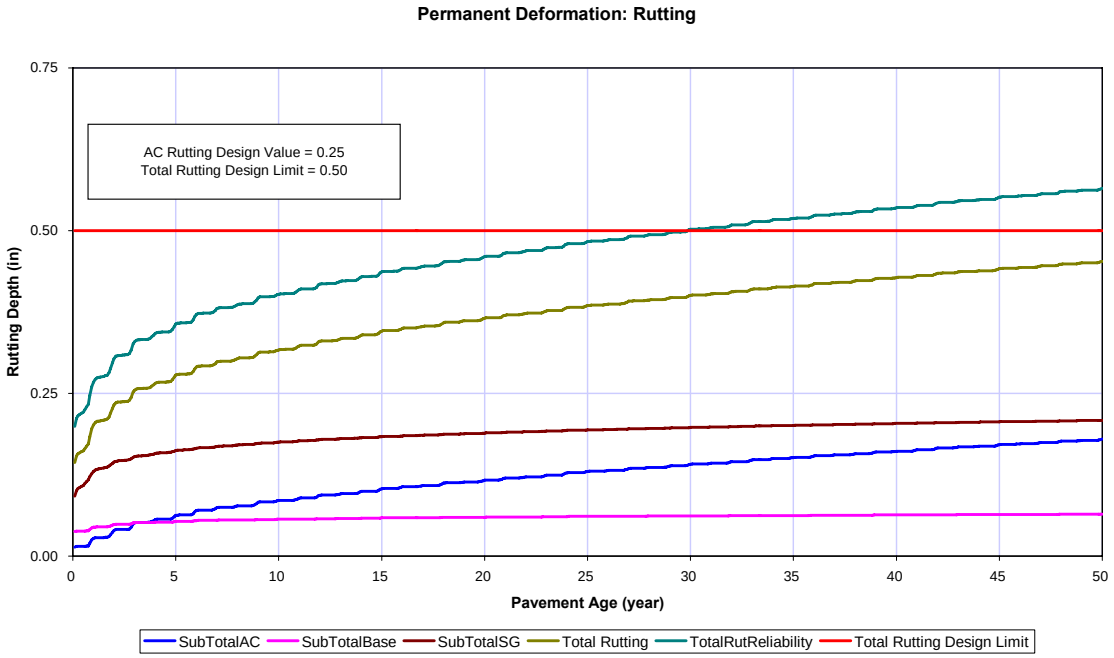

Figure 3.7 Predicted Pavement Rutting - 55 mph Design Speed

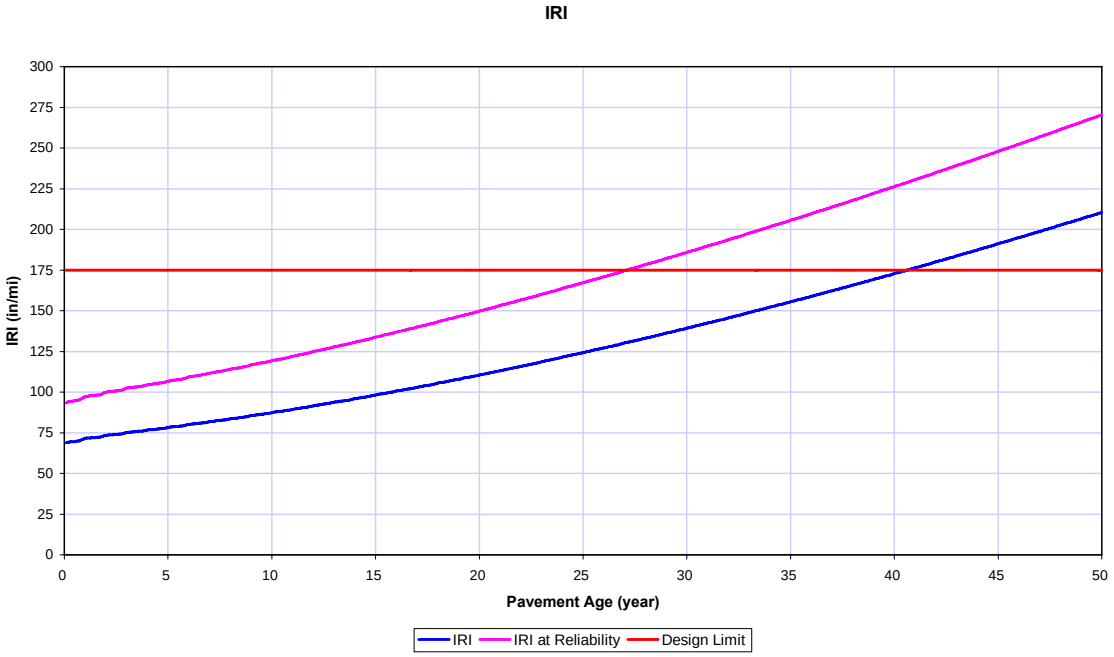

Figure 3.8 Predicted Pavement Roughness - 55 mph Design Speed

Table 3.24 provides a listing of predicted distress levels after 16 and 22 years of trafficking, which coincides with the typical initial service life expectations for HMA perpetual pavements in Wisconsin. As shown, only top-down fatigue cracking is expected to barely exceed typical design limits. As discussed previously, this cracking is expected to be contained within the uppermost 0.5 inches of the pavement surface.

Table 3.24 Predicted Pavement Distress at 90% Reliability - 55 mph Traffic

Pavement Distress	At End of Year 16	At End of Year 22	Design Limit
Top-Down Fatigue Cracking, ft/mi	1,012	1,150	1,000
Bottom-Up Fatigue Cracking, % Area	2.3	2.7	25
Thermal Cracking ft/mi	84	84	1,000
Total Rutting, in	0.44	0.47	0.50
IRI, in/mi	137	156	175

3.3.2 – 15 mph Operational Speed

A comparative analysis was also completed for an operation speed of 15 mph to simulate the effects of congested traffic operations. Typically, traffic congestion results in slower traffic speeds for a period of approximately 1.5 hours per weekday. It must be noted that MEPDG v1.003 assumes the operational speed is consistent for the entire design period. The combined effects of high and slow speed traffic on pavement distress may be roughly approximated by computing the weighted average distress based on the percentage of time each traffic speed is assumed.

Table 3.25 provides predicted pavement distress at the 90% reliability level for an operational speed of 15 mph. As shown, all distress levels expect thermal cracking increase as the operational speed decreases (compare to Table 3.24).

Table 3.25 Predicted Pavement Distress at 90% Reliability - 15 mph Traffic

Pavement Distress	At End of Year 16	At End of Year 22	Design Limit
Top-Down Fatigue Cracking, ft/mi	1,910	2,099	1,000
Bottom-Up Fatigue Cracking, % Area	2.8	4.1	25
Thermal Cracking ft/mi	84	84	1,000
Total Rutting, in	0.51	0.55	0.50
IRI, in/mi	140	160	175

To estimate the combined effects of high and slow speed traffic, the results provided in Tables 3.24 and 3.25 were combined assuming the slow speed traffic occurs for 7.5 hours per week (4.46% of the total weekly traffic). Table 3.26 provides the results of this combined analysis. As indicated, the distress levels are increased slightly over those predicted for the 55 mph operational speed.

Table 3.26 Predicted Pavement Distress at 90% Reliability - Combined Traffic

Pavement Distress	At End of Year 16	At End of Year 22	Design Limit
Top-Down Fatigue Cracking, ft/mi	1,058	1,199	1,000
Bottom-Up Fatigue Cracking, % Area	2.3	2.8	25
Thermal Cracking ft/mi	84.5	84.5	1,000
Total Rutting, in	0.45	0.48	0.50
IRI, in/mi	138	157	175

3.4 KENLAYER Pavement Analysis

A comparative analysis of predicted levels of bottom-up fatigue cracking was completed using the KENPAVE software. KENPAVE includes the KENLAYER computer program which is suitable for the analysis of flexible pavements with no joints or rigid surface layers. KENLAYER allows the pavement to be modeled as a stress-dependent multilayer system and provides detailed outputs of stress, strain and deflection under single or multiple circular wheel loadings. A fatigue damage analysis can me made by dividing each year into a maximum of twelve periods (months), each with a unique set of layer material properties in response to environmental changes in moisture and/or temperature. Load-induced strains were used to compute the fatigue consumption in each period, and then summed to estimate the yearly fatigue damage. In general applications, the time to a fatigue damage level of 1.00 is determined as the expected service life of the pavement.

KENLAYER allows for the pavement structure to be modeled with a maximum of 19 distinct layers. For this analysis, the HMA perpetual pavement was modeled as a 9-layer system, as shown in Figure 3.9, with both linear elastic and nonlinear elastic (stress-dependent) material layers. Twelve design periods were utilized to simulate year-round pavement conditions. Single wheel and dual tandem wheel loadings of varying magnitude and speed were utilized to simulate the loading spectra. Maximum load-induced tensile strains were computed for each combination of loading and design period and used to estimate the resulting fatigue damage.

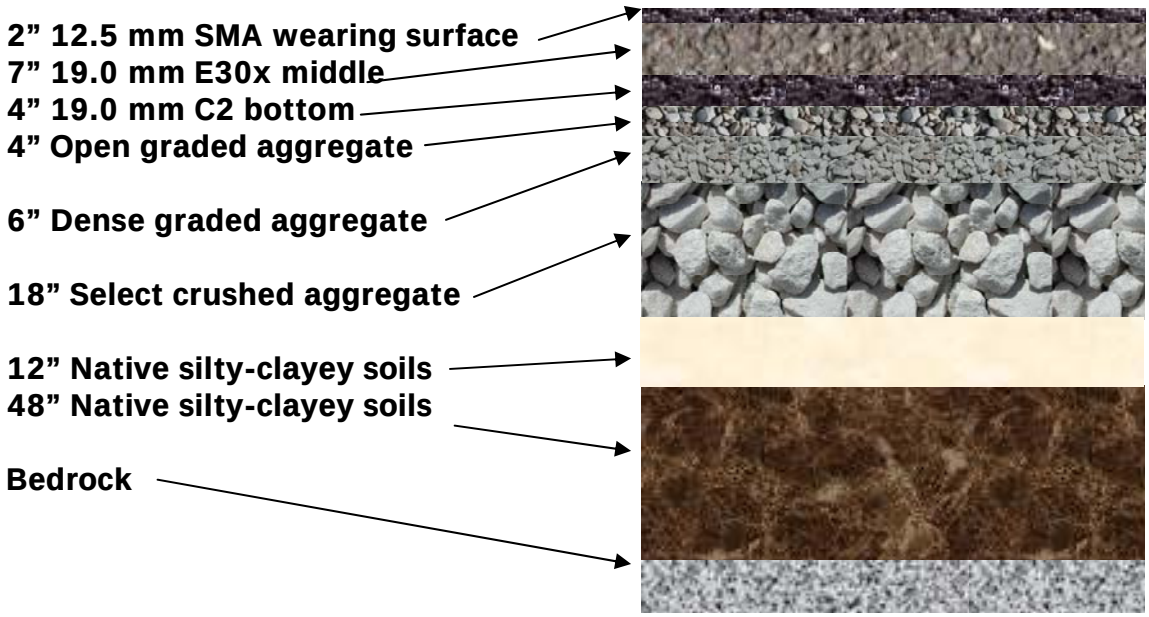

Figure 3,9 KENLAYER Pavement Structure

3.4.1 – HMA Material Properties

For KENLAYER executions, the pavement was modeled with three distinct HMA layers, each assigned as a linear elastic material with elastic moduli dependent on the month and speed of traffic. The E* outputs from previous executions of MEPDG v1.003 were used as representative values for each combination of layer type, design period and traffic speed. Figures 3.10 and 3.11 illustrate the E* variations for this analysis.

3.4.2 – Aggregate Material Properties

For KENLAYER executions, the open graded and dense graded aggregate layers were modeled as stress-dependent materials and the select crushed layer was modeled as a linear elastic material. Unbound aggregates are generally considered as stress-hardening (stress-stiffening) materials, with the resilient modulus dependent on the bulk stress state. KENLAYER uses the following general model to describe materials of this type:

$$M_R = k_1\theta^{k_2} \qquad (3.3)$$

Where M_R = resilient modulus, psi
θ = bulk stress state, psi.
k_1, k_2 = regression constants

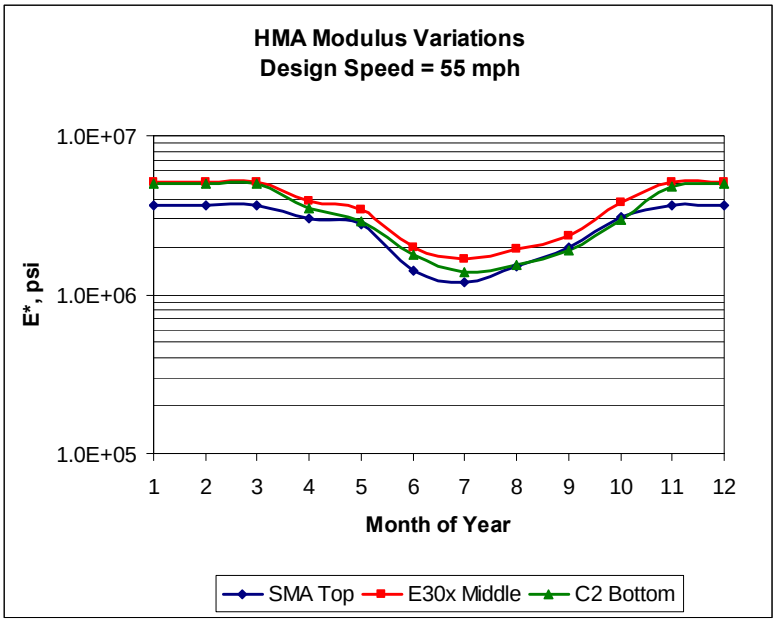

Figure 3.10 E* Variations - 55 mph Traffic

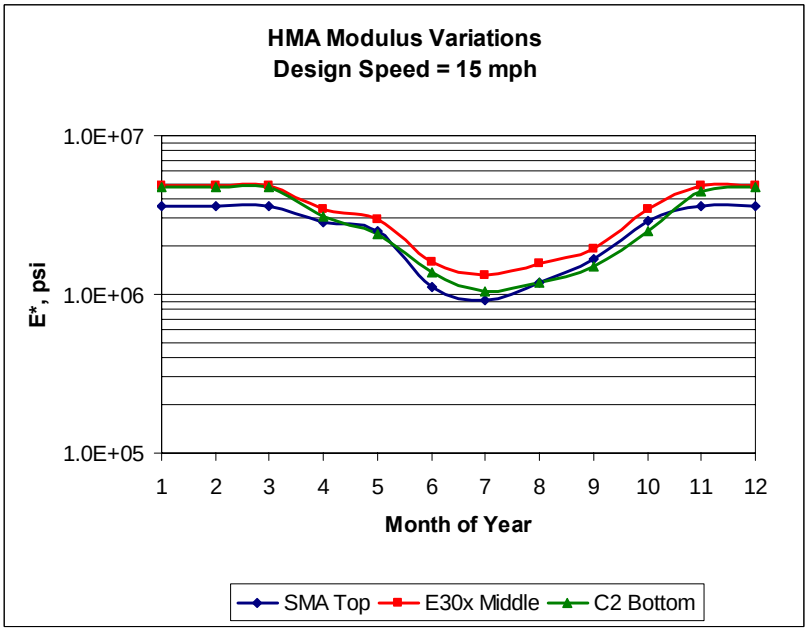

Figure 3.11 E* Variations - 15 mph Traffic

Regression analyses were performed on the UW-M laboratory test data to determine the regression constants k_1 and k_2 for the open graded and dense graded aggregate layers. Figures 3.12 and 3.13 illustrate the data for each aggregate type and the resulting equations. The select crushed material was modeled as a linear elastic material with an elastic modulus of 30,000 psi to be compatible with previous MEPDG v1.003 analysis.

3.4.3 – Soil Material Properties

For KENLAYER executions, the native subgrade was modeled as two distinct stress-dependent layers. Fine-grained soils may behave as stress-hardening or stress-softening materials depending on the plasticity of the soil. Stress-hardening materials can be described as indicated in Eqn 3.3. For stress-softening materials, the resilient modulus typically decreases in a bi-linear fashion with increases in the deviator stress, as shown in Figure 3.14. The UW-M laboratory data was investigated considering both stress-dependent conditions to determine which model form best fit the data, as shown in Figures 3.15 through 3.18. Based on this review, the stress-hardening models were chosen to best describe the material behavior of each soil layer.

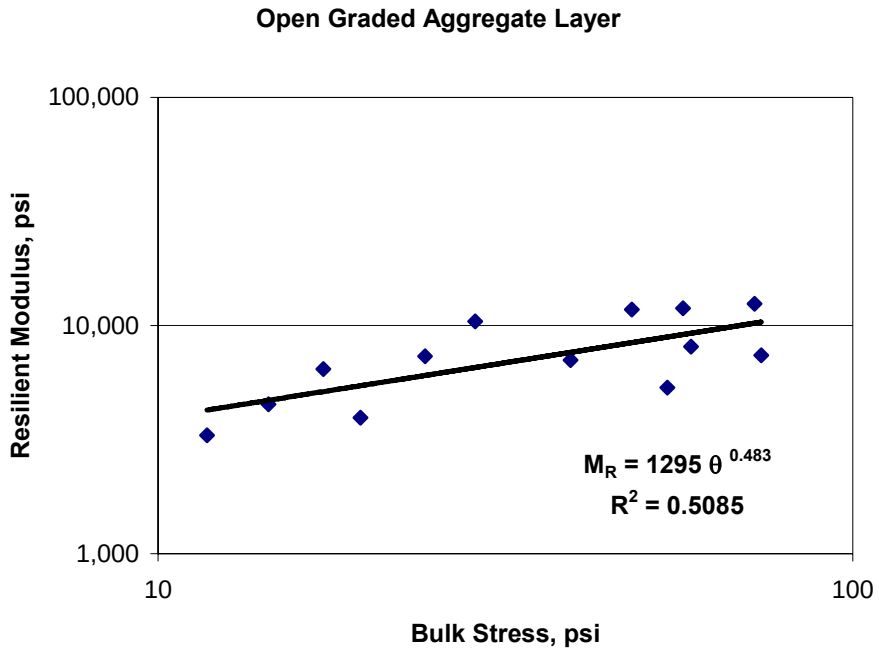

Figure 3.12 Resilient Modulus Data - Open Graded Aggregate Layer

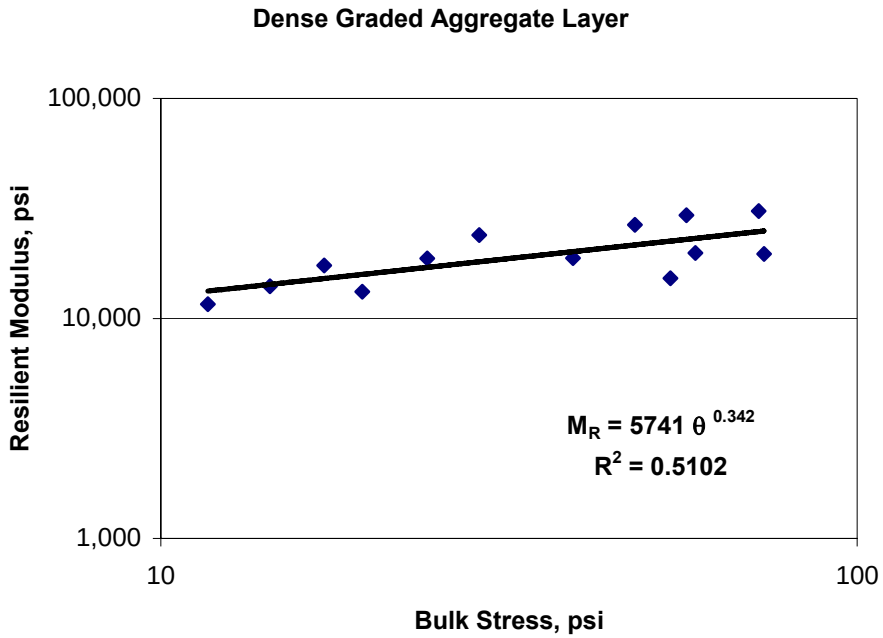

Figure 3.13 Resilient Modulus Data - Dense Graded Aggregate Layer

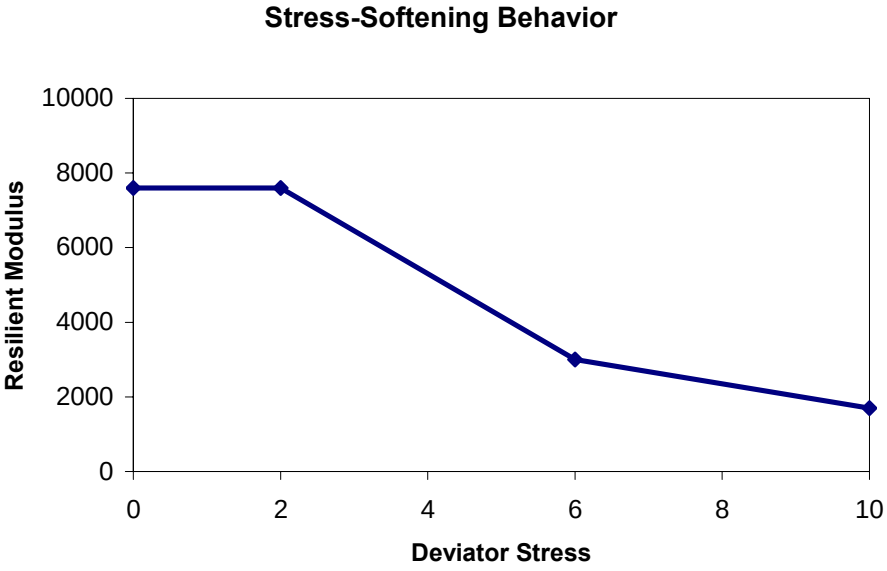

Figure 3.14 Typical Stress-Softening Material Behavior

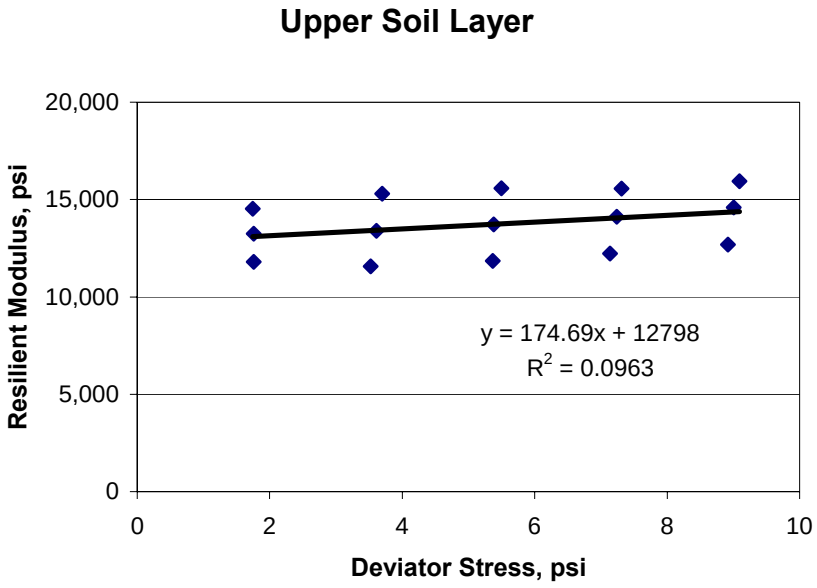

Figure 3.15 Upper Soil Layer as a Stress-Softening Material

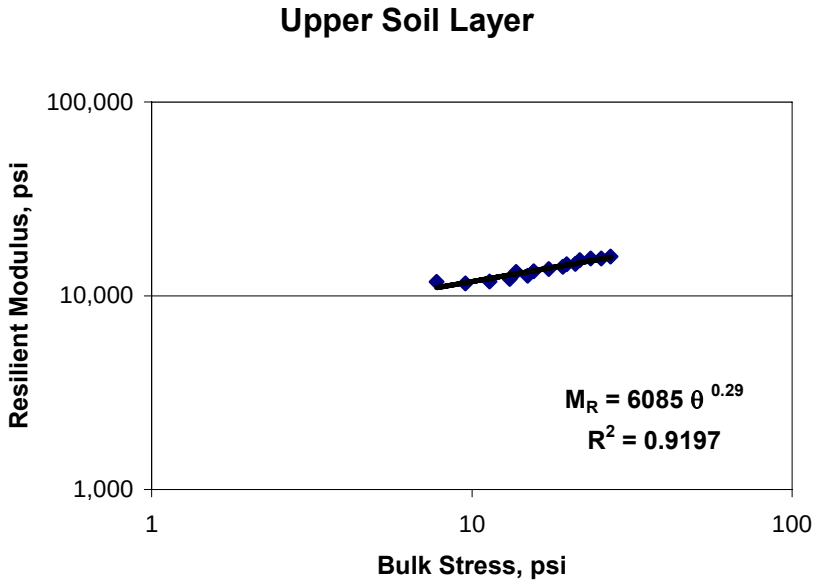

Figure 3.16 Upper Soil Layer as a Stress-Stiffening Material

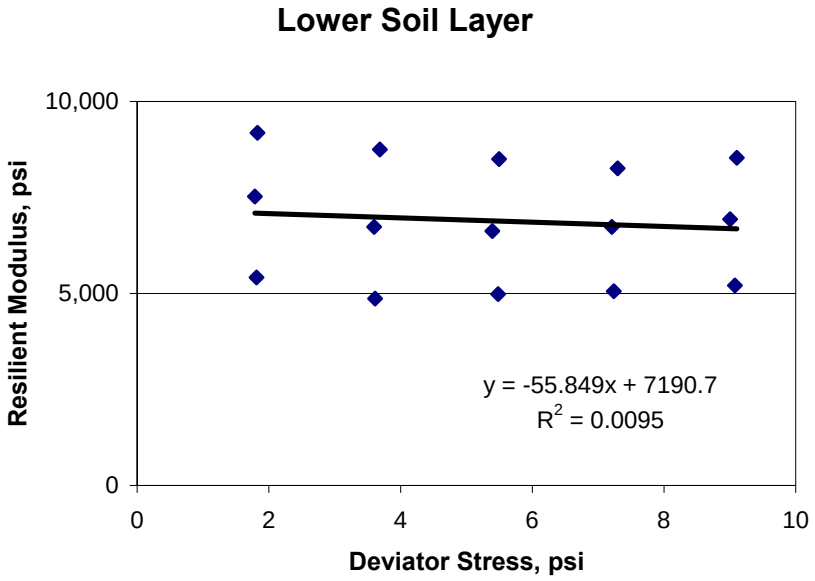

Figure 3.17 Lower Soil Layer as a Stress-Softening Material

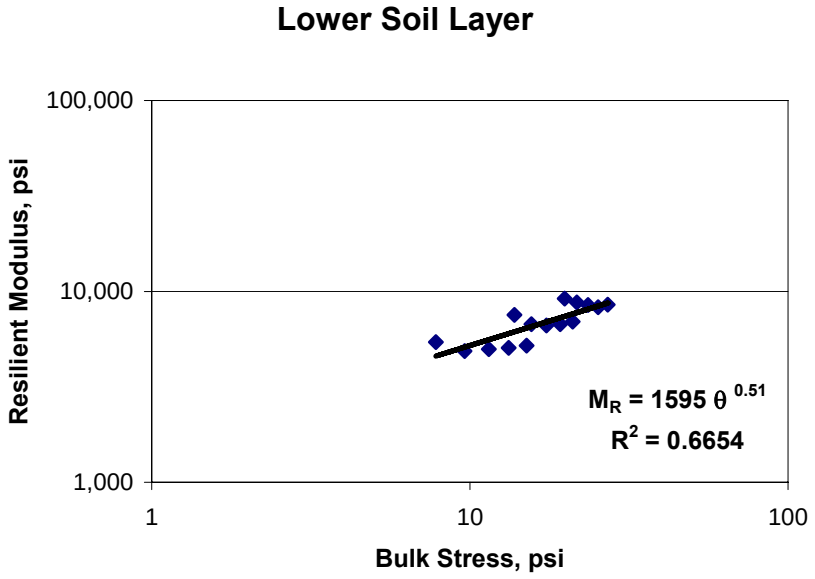

Figure 3.18 Lower Soil Layer as a Stress-Stiffening Material

3.4.4 – Traffic Characteristics

For KENLAYER executions, the traffic data obtained with the on-site WIM system was analyzed to establish the dominant loading types for analysis. Table 3.27 provides a summary of the representative number of weekly axle loading types registered by the WIM system. As indicated, the dominant loading types are the single and tandem axle loadings.

Table 3.27 Representative Weekly Axle Loadings from WIM Data

FHWA Class	No. of Vehicles	% of Total	Single Axles	Tandem Axles	Tridem Axles	Quad Axles
4	473	19.6	861	85	0	0
5	731	30.3	1,462	0	0	0
6	134	5.6	134	134	0	0
7	111	4.6	111	0	15	95
8	72	3.0	216	0	0	0
9	867	35.9	867	1,734	0	0
10	16	0.7	16	16	16	0
11	7	0.3	35	0	0	0
12	3	0.1	12	3	0	0
Total	2,414	100	3,714	1,972	31	95

Load spectra for the single and tandem axle loadings are presented in Figure 3.19. From this data, the representative weekly wheel loadings for KENLAYER were developed as indicated in Table 3.28, assuming a tire inflation pressure of 100 psi for all loadings. The monthly reps of each loading type were determined by apportioning the total number of vehicles in Table 3.27 to the design number of weekly trucks of 131,587 and assuming 40% of the total traffic acts over the critical center-of-wheelpath location.

Table 3.28 KENLAYER Wheel Loadings Used for Analysis

Axle Type	Axle Load, kips	Wheel Load, kips	% of Total	Monthly Reps	Load Radius	Tire Spacing
Single	9	4.5	35%	28,342	3.78	n.a.
	15	7.5	46%	37,249	4.89	
	24	12	19%	15,385	6.18	
Tandem	16	2	35%	15,051	2.52	18” Dual 51” Tandem
	32	4	39%	16,770	3.57	
	44	5.5	26%	11,180	4.18	

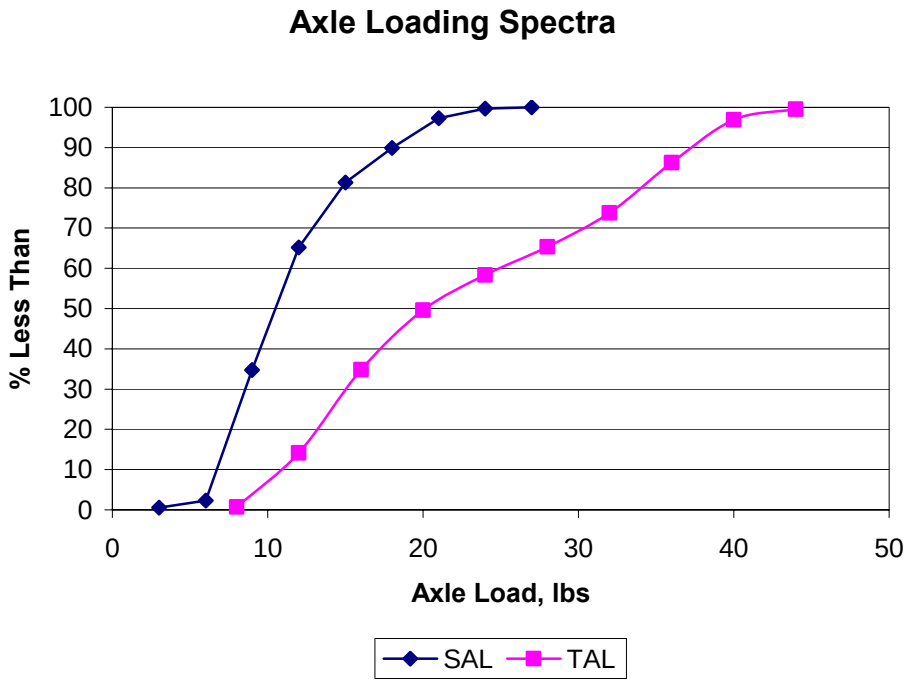

Figure 3.19 Single and Tandem Axle Loading Spectra

3.4.5 – KENLAYER Performance Prediction

The outputs of the KENLAYER program runs were utilized to estimate the fatigue life for bottom-up cracking based on the cumulative damage approach, which is consistent with state-of-the-practice for mechanistic-empirical pavement analyses. The overall analysis can be considered as a step by step approach as follows:

Step 1 – The critical tensile strain at the bottom of the C2 HMA layer is computed by KENLAYER for a given combination of design period, load type and load speed.

Step 2 - The allowable number of loadings to fatigue failure is determined based on a selected fatigue transfer function using the critical strain computed in Step 1.

Step 3 – The load induced damage is computed as the ratio of applied loadings to allowable loadings computed in Step 2.

Step 4 – The sequence of Steps 1 – 3 is repeated for every possible combination of design period (12), loading type (6) and load speed (2).

Step 5 – The yearly damage is computed as the summation of individual damage values computed in Step 4.

Step 6 – The estimated fatigue life of the pavement is computed based on the projected yearly increase in traffic applications.

For this analysis, the percentage of time for congested traffic operations (speed = 15 mph) was varied from 0 to 20%, which represents a range from 0 to 6.7 hours per weekday. The projected yearly increase in traffic was varied from the design value of 0.4% to a high of 2.0%. To be consistent with MEPDG v1.003 performance predictions, the nationally calibrated NCHRP 1-37A fatigue model was employed, which is described as follows:

$$N_f = .007566\varepsilon_t^{-3.9492} \mid E^* \mid^{-1.281} \qquad (3.4)$$

where: N_f = number of load applications to fatigue failure (damage = 1.0)
ε_t = critical tensile strain at the bottom of the HMA layer
E* = dynamic HMA modulus, psi

For illustrative purposes, Figure 3.20 presents the monthly damage computed for both selected design speeds, assuming ALL traffic operated at this speed. As shown, monthly damage is highest during the warmer periods (June – Sep) and increases for the slower travels speed.

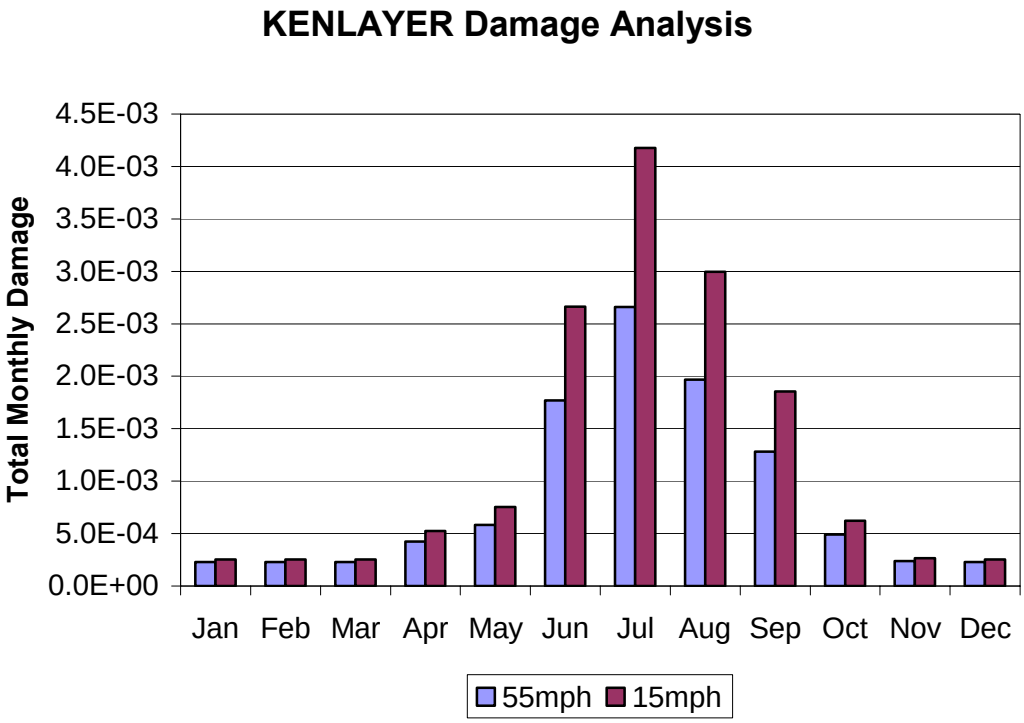

Figure 3.20 Monthly Damage Estimated Based on Traffic Speed

The monthly damage estimates shown in Figure 3.20 were used to compute the estimated fatigue life of the pavement (Damage = 100%) assuming yearly traffic growth rates of 0.4% to 2.0% and traffic congestion percentages of 0% to 20%. Figure 3.21 illustrates the results of this analysis. As shown for the design growth rate of 0.4% and assumed congestion percentage of 5-10%, the estimated fatigue life is approximately 80 years. For these same conditions of growth and congestion, the estimated time to a fatigue damage level of 45% (approximately 25% cracked area) is 39 years, which is more conservative that estimated produced during the MEPDG v1.003 analysis (damage = 15% after 50 years).

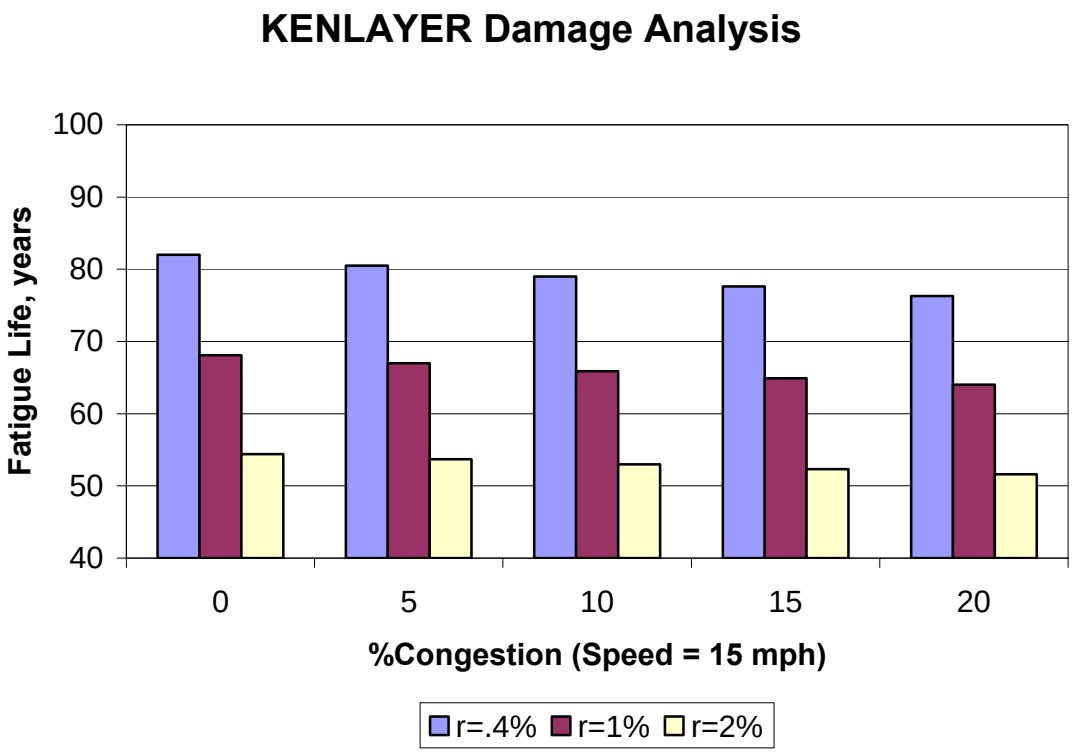

Figure 3.21 Fatigue Life Estimates Based on Traffic Growth and Congestion

3.5 EVERSTRESS Pavement Analysis

A comparative analysis of predicted levels of critical tensile strains during July conditions was completed using the EVERSTRESS software. EVERSTRESS allows the pavement to be modeled as a 5- layer stress-dependent system and provides detailed outputs of stress, strain and deflection under single or multiple circular wheel loadings. To satisfy software constraints, the 9-layer pavement system utilized for KENLAY executions was reduced to a 5-layer system by combining HMA layers, aggregate layers, and all layers below the select crushed material, as shown in Figure 3.22.

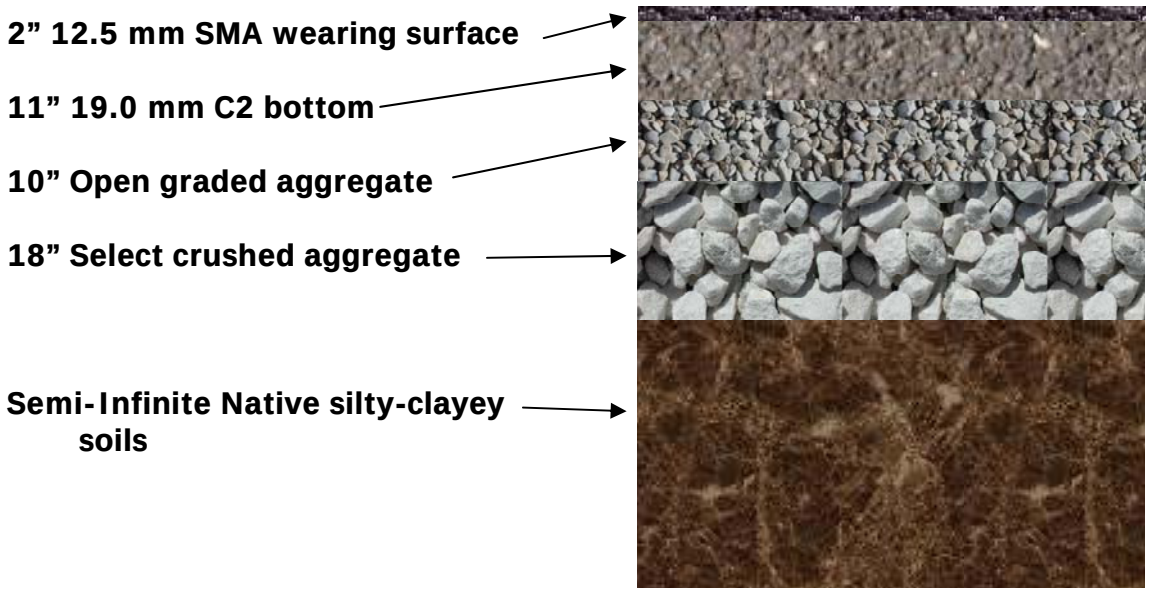

Figure 3.22 Pavement Structure Used for EVERSTRESS Analysis

For the combined layers, material properties were assigned as appropriate to yield conservative output results.

3.5.1 – HMA Material Properties

For EVERSTRESS executions, the pavement was modeled with two distinct HMA layers. The upper 2-inch SMA layer was left intact while lower two HMA layers (E30x and C2) were combined into a single 11-inch C2 layer. The E* outputs for July conditions produced by MEPDG v1.003 were used as representative values for each layer.

3.5.2 – Aggregate Material Properties

For EVERSTRESS executions, the open graded and dense graded aggregate layers were combined and modeled as a stress-stiffening material. The select crushed layer was left

intact and modeled as a linear elastic material (E = 30ksi). EVERSTRESS uses the following general model to describe stress-stiffening materials:

$$M_R = k_1\left(\frac{\theta}{P_a}\right)^{k_2} \quad (3.5)$$

Where M_R = resilient modulus, psi
θ = bulk stress state, psi
Pa = atmospheric pressure, psi
k_1, k_2 = regression constants

For this analysis, properties of the open graded layer were utilized, producing the following relation:

$$M_R = 4,746\left(\frac{\theta}{P_a}\right)^{0.483} \quad (3.6)$$

3.5.3 – Soil Material Properties

For EVERSTRESS executions, the native subgrade was modeled as a single stress-stiffening layer with properties of the upper soil layer used for the KENLAYER analysis, producing the following relation:

$$M_R = 13,231\left(\frac{\theta}{P_a}\right)^{0.29} \quad (3.7)$$

3.5.4 – Traffic Characteristics

For EVERSTRESS executions, the single and tandem axle loadings were modeled exactly as utilized for the KENLAYER analysis.

3.5.5 – EVERSTRESS Critical Strain Comparison

The critical load-induced tensile strains at the bottom of the C2 HMA layer computed by EVERSTRESS were compared to those values produced by KENLAYER to determine if reasonable agreement was achieved, as illustrated in Figure 3.23. As shown, the critical strains computed by both programs are in close agreement, providing an independent verification of the previously described KENLAYER results.

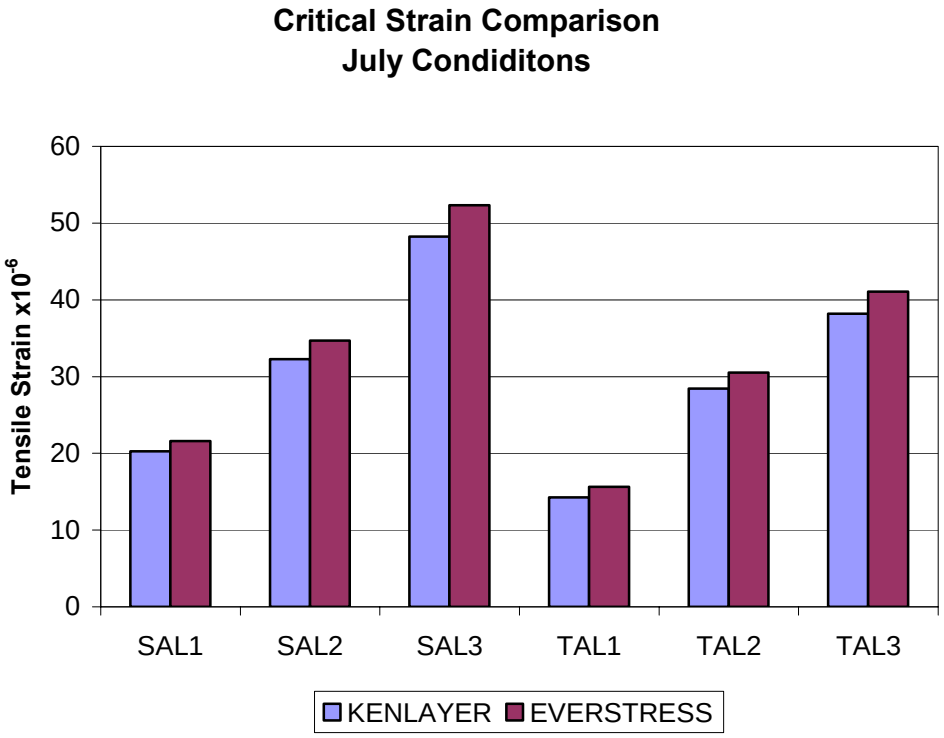

Figure 3.23 Critical Strain Comparison

CHAPTER 4.0
SUMMARY & RECOMMENDATIONS

4.1 Summary

This report presents the results of laboratory testing and mechanistic-empirical analyses completed for the Hot Mix Asphalt (HMA) perpetual pavement constructed within the North leg of the Marquette Interchange project. This project serves as a supplement to Wisconsin Highway Research Program (WHRP) Study 0092-06-01 Perpetual Pavement Instrumentation for the Marquette Interchange Project.

The HMA perpetual pavement structure is located in a heavily trafficked urban corridor and was designed and constructed to provide a service life in excess of 48 years before reconstruction may be required. As part of the life cycle of this pavement, rehabilitation operations including a mill and relay of the SMA surface layer may occur at intervals of approximately 16 and 32 years after initial construction. These rehabilitation operations are expected to take place during night-time lane closures, resulting in minimal disruptions to normal traffic flows.

The laboratory testing completed at UW-Milwaukee and Iowa State University using paving materials obtained during construction. This lab testing provided valuable data to characterize the HMA, unbound aggregate and unbound soil pavement layers. This data was used to develop Level 1 HMA inputs to the current version of the Mechanistic-Empirical Pavement Design Guide (MEPDG v1.003) and to better characterize the unbound aggregates and soils during Level 3 analysis. At the time of this report, Level 1 analysis of unbound aggregates and soils is not recommended for MEPDG v1.003. Weigh-In-Motion (WIM) data obtained as part of WHRP Project 0092-06-01 was analyzed to develop site-specific inputs for the heavy axle loading spectra.

Pavement performance predictions were developed using the MEPDG v1.003 and stand-alone KENPAVE software. For both analyses, the baseline material properties determined via laboratory testing were used to estimate monthly variations in response to changes in environmental conditions (i.e., temperature, moisture). Critical pavement stresses and strains resulting from applied traffic loadings were used to develop estimates of accumulated cracking, rutting and roughness over time. Consideration was given to both free flow (55 mph) and congested (15 mph) traffic conditions. Using a combined traffic approach, pavement distress at the 90% reliability level were projected after 16 and 22 years of trafficking as follows:

Pavement Distress 90% Reliability Level	At End of Year 16	At End of Year 22	Design Limit
Heavy Truck Applications	26.4 million	36.8 million	n.a.
Top-Down Fatigue Cracking, ft/mi	1,058	1,199	1,000
Bottom-Up Fatigue Cracking, % Area	2.3	2.8	25
Thermal Cracking ft/mi	84.5	84.5	1,000
Total Rutting, in	0.45	0.48	0.50
IRI, in/mi	138	157	175

The predicted distress levels after 16 and 22 years of trafficking were selected to coincide with the typical initial service life expectations for HMA perpetual pavements in Wisconsin. As shown, only top-down fatigue cracking, which is confined within the uppermost 0.5 inches of the pavement surface, is projected to exceed typical design limits. This projected distress will easily be corrected using the standard practice of mill and relay. Furthermore, after 50 years of service the 90% reliability level for bottom-up fatigue damage is expected over 15% of the total lane area, or 30% of the loaded wheel paths, which is well below typical design limits of 25% and 50%, respectively. All analysis results indicate the constructed HMA perpetual pavement should meet or exceed performance expectations.

4.2 Recommendations

The pavement analyses conducted for the Marquette Interchange HMA perpetual pavement, using the MEPDG v.1003 and KENPAVE programs, yielded acceptable long-term performance expectations. This pavement was constructed in September, 2006 and to date, there is insufficient field performance data available to confirm or deny these expectations (i.e., no pavement distress measured to date). To augment these results, it is recommended that the monitoring of pavement performance be continued through at least the first 10 years to provide comparative values of measured versus predicted pavement distress. This will provide valuable data for calibrating mechanistic-empirical performance models for local conditions.

Furthermore, analyses of this type should be extended to existing aged HMA pavement structures in Wisconsin, preferably built using paving materials and construction practices which reflect current conditions. For practical applications, this will likely include pavements constructed from 1996 – 2002. Comparative analyses between the field performance data of these pavements to MEPDG predicted levels of distress will further validate the use of the MEPDG for designing HMA pavements in Wisconsin.